Charge Pumping with Human Capacitance for Body Energy Harvesting

Alyssa Zhou

Charge Pumping with Human Capacitance for Body Energy Harvesting

by

Alyssa Y. Zhou

A dissertation submitted in partial satisfaction of the

requirements for the degree of

Doctor of Philosophy

in

Electrical Engineering and Computer Sciences

in the

Graduate Division

of the

University of California, Berkeley

Committee in charge:

Professor Michel M. Maharbiz, Chair
Professor Jan M. Rabaey
Professor Dorian Liepmann

Summer 2020

Charge Pumping with Human Capacitance for Body Energy Harvesting

Abstract

Charge Pumping with Human Capacitance for Body Energy Harvesting

by

Alyssa Y. Zhou

Doctor of Philosophy in Electrical Engineering and Computer Sciences

University of California, Berkeley

Professor Michel M. Maharbiz, Chair

The proliferation of Internet-of-Things (IoT) systems and human body sensors is rapidly transforming the way we interact with our surroundings. As these devices increase in number and longevity, there grows a critical need to find sustainable and convenient power sources. Shrinking consumer electronics have generated a demand for battery-less power sources for some applications. Significant interest in studying energy harvesting techniques exists as a solution to power these devices. In particular for interactive electronics meant to exist on and around the human body, kinetic energy of human movement is a popular energy scavenging source.

This dissertation presents an electrostatic, charge-pumping energy harvesting system capable of scavenging energy from capacitive changes induced by the human body. As is well known for touchscreen devices, the proximity of a finger alters the effective value of small capacitances. These capacitance changes drive a current which is rectified to charge an energy storage component. This technology is fabricated in a standard CMOS process, and is also compatible with other mediums such as printed circuit boards, conductive fabrics, and paper. These systems transduce the kinetic energy of a human finger tap to electrical energy in the range of pico- to nano- joules, depending on the size, material, and design of the capacitive touch-sensing electrodes. We highlight the harvester's ability to power low-power applications such as light-emitting diodes and ring oscillators. This system illustrates one solution for powering the growing number of electronic devices with on-demand, user-generated interactive human movement.

To my friends and family.

Contents

List of Figures

List of Tables

Acknowledgments

Thanking all the people who have helped me throughout this journey would be a complete thesis in itself. I will try to do it justice with an abbreviated version.

Thank you...

To my undergraduate mentors, David D'Argenio, Satsuki Takahashi, and John Choma, without whom I would not be in graduate school. They instilled in me an interest in research and encouraged me to pursue a higher degree. John Choma in particular became a dear friend and had steadfast faith in my ability to change departments and study Electrical Engineering. The last time we chatted he promised he would only be a phone call away if I ever had any circuits questions. The news of his passing came one week before I started my graduate studies in 2014. This work is written in his memory.

To my advisor, Michel Maharbiz, for helping me navigate grad school and creating a supportive and productive environment. When incoming students ask me what Michel is like, "crazy mad scientist" comes to mind, but in an exciting way. When they ask me what his advising style is like, I describe it as "whatever you need it to be." Thank you for always being there when I have questions and need a sounding board, but also for giving me the space to develop my own critical thinking and problem solving skills. Even while balancing numerous other responsibilities, Michel's dedication to his students is clear and he is always one slack message away. Outside of research, Michel is the most amazing Argentinian BBQ master and I will miss our group dinners and retreats. Thank you for being an inspiration to us all and for fostering the group I called home for the past six years.

To my dissertation committee: Jan Rabaey for sparking my interest in low-power energy harvesting from the human body when I took his course, EE290, and for continuing to be involved in this project over the years. And Dorian Liepmann for giving me the opportunity to be a graduate student instructor for BioE Ethics, which I thoroughly enjoyed, and for being a great mentor and supporter when I was in tough situations. Special shout-out to Bodie because he is a good boy and makes everyone smile.

To Kris Pister for serving on my qualifying exam committee. Kris was also an amazing mentor and helped me find a home when I first arrived here. He introduced me to Michel and also the field of MEMS. None of this work would be possible without the technical foundation I developed in his classes.

To Tom Zajdel, Michaela TerAvest, Moshe Baruch, and Caroline Ajo-Franklin who taught me great research habits and helped me settle into my own project space when I first arrived here. Although our collaborative work is not the main subject of this dissertation, the lessons they taught me are invaluable. I'll never forget our "summit" lunches.

To the rest of the Maharbiz group who I have had the privilege of working with: DJ Seo, Travis Massey, Camilo Diaz-Botia, Amy Liao, Monica Lin, Stefanie Garcia, Bochao Lu, Konlin Shen, Soner Sonmezoglu, Wei Li, David Piech, Arda Ozilgen, KyoungTae Lee, Oliver Chen, Mauricio Bustamante, Wentian Mi, and Jordan Edmunds. Thank you for all the conversations and good times over the years. You all made coming into lab fun and I look forward to maintaining our friendships over the years to come.

Chapter 1

Introduction

> The internet of things has the
> potential to change the world,
> just as the internet did, maybe
> more so.
>
> *Kevin Ashton*

1.1 Motivation: Internet of Things and Wearables

The "Internet of Things (IoT)" was first termed by Kevin Ashton in a Procter & Gamble report from 1998, when the phrase mainly referred to RFID tags on commercial products to help aid in tracking inventory. Since then, the revolution of IoT has found its way into numerous applications including smart homes, environmental monitoring, transportation, commercial goods, lifestyle tracking, and healthcare [55, 41, 66]. IoT devices have proliferated in recent years and reports predict the industry to continue to grow reaching 75 billion connected devices in 2025 [28]. The importance of these devices is further supported by a predicted 25% compound annual growth rate in revenue, with the industry reaching an estimated global market size of US$1.1 trillion by 2026 [65]. Figure 1.1 illustrates this growing trend and the significant impact these devices will have on our economy and everyday lives. This boom has been fueled by technological advances, allowing for significant reductions in cost, size, and power consumption of electronics [108], coupled with increasing decentralizaiton of sensing and computer systems [157].

A perennial obstacle to realizing the deployment of these devices is power. As a significant subset of IoT devices move towards wearables and portable electronics, wiring all nodes to the power grid becomes cost prohibitive and functionally inconvenient[66]. As such, many existing IoT devices are designed to be run off of batteries, but there are limitations associated with relying on batteries alone [105]. For many years, electronics followed Moore's Law by doubling in number of components on a chip about every two years. This allowed devices
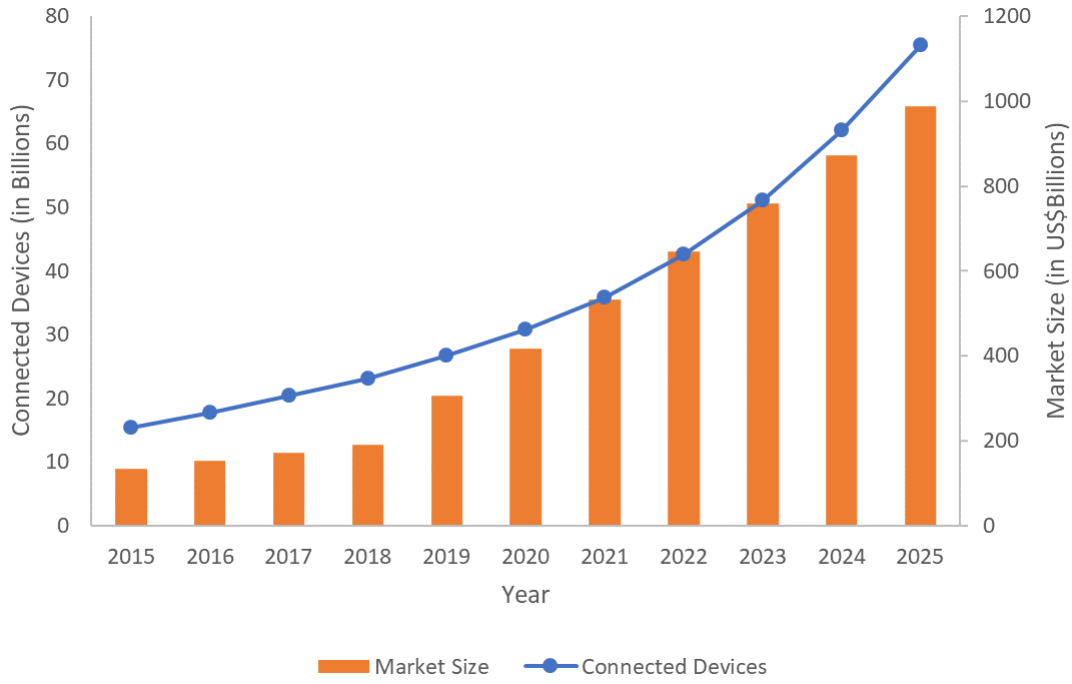
Figure 1.1: Global IoT trend forecast from 2015 to 2025 for number of devices and market size. (Adapted from [28, 65])

such as sensors, actuators, and wireless nodes to grow in complexity while decreasing in size and cost. However, battery densities during this time lagged substantially, only doubling approximately every ten years [138]. Although new and innovative battery chemistries are improving power densities, there still exists limits to a battery's capacity, longevity, and size. Figure 1.2 shows a brief survey of current energy density for a variety of common battery chemistries. This figure offers general guidance of how large a battery would need to be to provide a certain amount of energy for a device. As IoT devices trend smaller in size, especially in the application space of healthcare trackers and implants, batteries will begin to become the limiting size factor [179]. Researchers are investigating more energy dense chemistries, such as the Lithium-Air battery which has the highest theoretical specific energy (3.5 Wh/g), but has stability concerns which limit cyclability [8], and therefore is not currently dependable for long-lasting IoT devices. In addition to having a limited number of charging cycles, self-discharge reduces battery lifetimes, even if they are not in use [13]. This results in batteries needing to be recharged or replaced, which can be cost prohibitive and also generates significant electronic waste. In some cases, batteries can be safety hazards due to material leeching, chemical leakages, or unintentional shorts [183, 50, 80]. To mitigate these concerns, there is research into new battery chemistries, configurations, and manufacturing
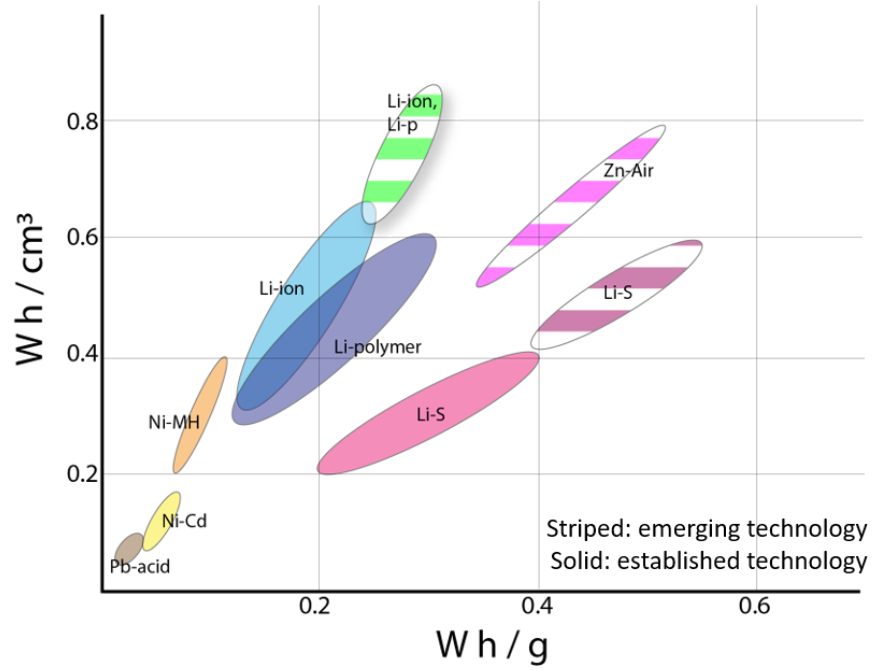
Figure 1.2: Typical battery energy densities for various chemistry families. (Adapted from [6])

techniques, such as printed [159], nanofabricated [169], and flexible batteries [193], but there may be cost, resource, and material limitations for a subset of applications. In many of these cases, the power constraints and battery requirements can be relaxed or, in some cases, completely replaced with the integration of energy harvesters.

1.2   Power from Energy Harvesting

To address the challenge of powering billions of IoT devices, there has been increasing interest in developing energy harvesting technologies. These methods can either help improve the longevity of existing battery-powered devices or replace the need for batteries in systems altogether. An energy harvester generates useful electric energy from its surroundings. The main sources of energy devices can scavenge from is kinetic, thermal, chemical, and electromagnetic radiation [82, 118, 106]. Many of these energies come from natural environmental sources such as solar radiation, wind, water, and geothermal activity. Others can be man-made, such as RF sources and vibration from machinery. Humans themselves can also be a source of chemical, kinetic, and thermal energy. Table 1.1 summarizes these categories of energy sources and Figure 1.3 illustrates how the interest in these areas have grown over time. Although this is not a comprehensive record of all published papers on the

Table 1.1: Common sources for energy harvesting

energy type	natural source	artificial source	human source
kinetic	wind flow [94] water motion [167]	infrastructure vibrations (bridges [44], buildings [5]) machinery vibrations (automobiles [207], blenders [12])	walking and running [185] pushing and typing [162] arterial [119] and heart movement [91]
thermal	geothermal activity [126]	car engines [140] machines dissipating heat [181]	body heat [168]
chemical	salinity gradients [73, 116] electrogenic microbes [90]		blood glucose [70, 153] sweat lactate [67, 40]
EM radiation	solar [57, 54]	RF transmitters [172, 165] IR lasers [117, 52]	
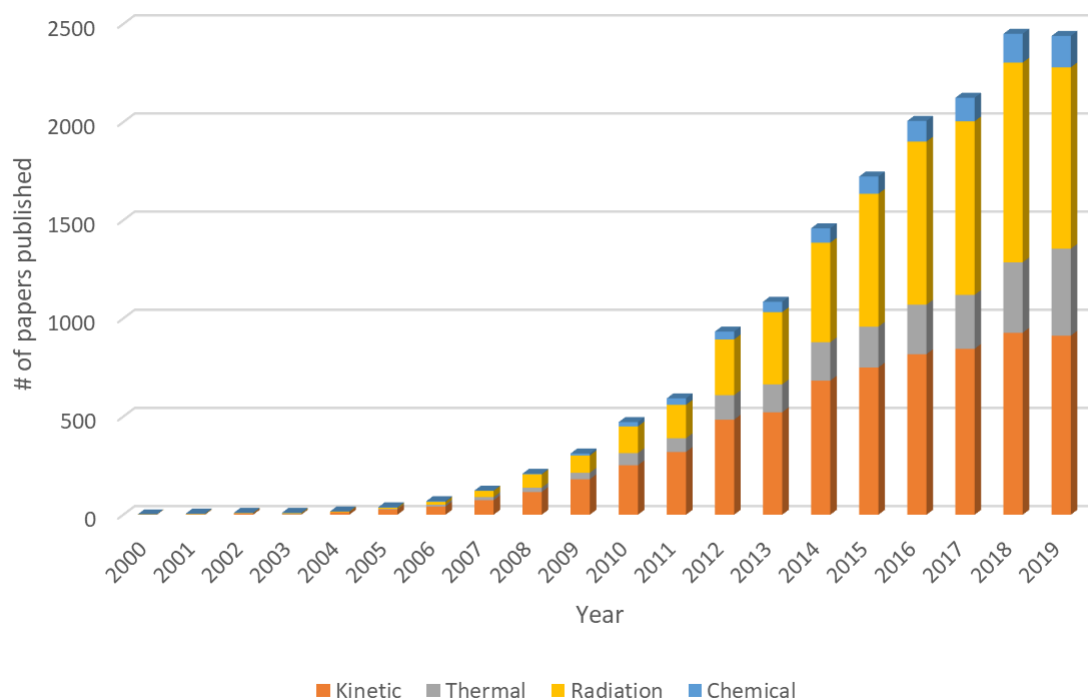
Figure 1.3: Number of papers on the topic of energy harvesting archived on Web of Science for years 2010-2019, presented by energy type.

topic of energy harvesting for the past two decades, the growth of research in these areas in recent years provides evidence that there is an interest and demand in these technologies as a solution for powering emerging electronic devices.

The numerous types of energies and sources suggest that there is no one-type-fits-all solution, and each application should be individually analyzed to determine the most relevant and effective harvesting source for its expected operating environment. Solar energy, for

example, has a power density of 100 mW/cm^2 under direct outdoor sunlight [130]. Therefore, if the application is outdoors and is active during the day, or has an option to store energy, then this can be a very desirable power source. However, this power density drops off once indoors (100 µW/cm^2 [130]), and as size of devices continue to shrink, it becomes more difficult to ensure the limited area has unobstructed access to light. Vibrational energy is also very location specific and harvesters should be designed to be match the vibration's amplitude and frequency. This can be useful for devices which are meant to be stationary with a constant vibrational source, but will not be the best option for a portable device. Similar arguments can be made for the environmental availability of wind, water, RF, and chemical sources for specific applications. Thermal energy is an interesting option to consider because many electronics naturally dissipate heat and these temperature gradients can be converted back to electricity through materials known as thermoelectrics. However, it is difficult to find reliable temperature gradients over small volumes, especially if there is no forced convection of the environmental medium [124].

Similar to other environmentally dependent energies, human power is only useful for applications where electronics remain on or around the human body, such as wearables, implants, and interactive devices. Human power comes in two forms: active and passive [106]. Passive power is scavenged from already existing sources (i.e. biobattery from the catalysis of glucose or routine activities like walking), and active power requires the user to perform additional activities to generate power (i.e. wind-up radios or shake-activated flashlights). One main consideration for scavenging human energy is minimizing user effort where possible, since most users would not prefer the inconvenience of having to physically exert additional energy to power their devices [152]. Although human power is not feasible for sparse and remote wireless sensor IoT applications, such as environmental monitoring, scavenging human energy is a useful option to ensure users can provide on-demand power to devices such as wearables and interactive, smart commercial goods. Additionally, it would be convenient to harvest energy from gestures already commonly used to interface with devices, such as tapping, typing, and swiping [174]. In this way, users would be able to power their devices while using them without having to exert additional energy. Towards this end, this research will focus on investigating kinetic energy harvesting from human gestures. In general, devices do not have to rely on one single harvesting technique and energy source. Although fabrication and assembly of harvesters becomes more complicated, some applications may be best suited for integration of multiple energy conversion methods [177].

1.3 Thesis Organization

The primary goal of this work is to demonstrate a unique energy harvesting system that scavenges energy from human gestures, focusing on a finger tap. Some important considerations for the design of this system include (1) a small form factor for more inconspicuous integration with existing devices and other smart goods and (2) a convenient integration

plan with electronics to simplify fabrication and processing.

Chapter 2 gives an overview of kinetic energy conversion methods and discusses the merits of electromagnetic, piezoelectric, electrostatic, and triboelectric converters. It also provides a survey of current harvesters and their applications. Chapter 3 will further pursue electrostatic energy transduction and discuss the circuit architecture for this conversion method in more detail. Simulation results of these circuits are presented as well.

Chapter 4 discusses the development of a commercialized-off-the-shelf (COTS) version of the electrostatic harvester. The system design, assembly, and characterization are discussed. The performance of the harvester is presented in response to human finger tapping, with an example application of powering a light-emitting diode (LED).

Chapter 5 presents an custom application specific integrated circuit (ASIC) chip with an electrostatic energy harvesting module fabricated on the same bulk silicon die. Here, all components of the ASIC are discussed, simulated, and characterized in detail.

Chapter 6 discusses the full system assembly and presents the test results of the ASIC in response to human finger tapping. This harvested energy powers a ring oscillator (RO) as a stand-in for a low-power circuit application. Energy harvesting from conductive fabrics and smart paper electronics are also posited as potential applications for this technology.

This work culminates in Chapter 7, which summarizes the achievements of this project, with discussion on limitations of this technology and suggested directions.

Chapter 2

Kinetic Energy Harvesting

As batteries become more limited in their application scope due to size, cost, and maintenance requirements, energy harvesting becomes an attractive alternative power option. In particular, the human body expends significant amounts of kinetic energy from performing routine activities [162]. Most literature which discusses human body kinetic energy harvesting focuses on large movements. Some ballpark estimates for exerted power by these movements are presented in Table 2.1. These values vary widely depending on the size of the human, which affects the weight and distance of limb movement. Only fractions of this exerted energy can be converted without adding noticeable burden to the user.

Although these limb movements are the largest source of kinetic energy from the human body, it can be inconvenient to harvest from them in some applications. For example, in a classroom, office, or other movement-restrictive environment, a user would not want to have to walk around the room to power electronics. Even if the user was free to move around, some would prefer not to be forced to exert additional energy in this way. Although users could carry larger energy storage devices on their body throughout the day to harvest energy passively, this increases the size and weight of some applications. Alternatively, many users are comfortable using smaller gestures to interact with their devices. Tapping, typing, clicking, and swiping are already very common, natural motions used to interact with devices [174]. The energy exerted during these actions are estimated here. Throughout this section, force, work, and power will be calculated with the following equations where m is mass, a is acceleration, d is distance traveled, and t is time.

$$F = ma \tag{2.1}$$

$$W = F \times d \tag{2.2}$$

$$P = \frac{\Delta W}{\Delta t} \tag{2.3}$$

For a single tap on a flat surface, like a glass capacitive touchscreen, we can estimate the work a finger performs. If we assume the tip of a finger is one cubic centimeter and is the

Table 2.1: Exerted power for select human body activities. (Data calculated from [161, 143, 180])

Activity	Conditions	Power
Walking (heels)	3.5 mph 68 kg human	67 W
Walking (ankles)	3.5 mph 68 kg human	57 W
Walking (knees)	3.5 mph 68 kg human	31 W
Walking (hips)	3.5 mph 68 kg human	32 W
Walking (shoulders)	3.5 mph 68 kg human	1.8 W
Walking (elbows)	3.5 mph 68 kg human	1.8 W
Bicep curl	1 sec per curl 1 arm	6 W
Overhead arm lift	2 sec per lift 1 arm	11 W

same density as water, the weight of this fingertip is ~ 1 g. If this finger travels a distance of 1 cm, taps at a frequency of 1 Hz, and we assume simple linear motion, then the power is

$$W = (1g)\left(\frac{9.8kg}{m^2}\right)(1cm) = 98\mu J$$

$$P = (98\mu J)\left(\frac{1tap}{sec}\right) = 98\mu W$$

For larger interactive devices, such as a smart screen or interactive children's books, a whole hand may touch the screen. In this case, the hand is estimated at 0.575% of the total body weight [178], and therefore 0.4 kg for a 68 kg person. Assuming the same 1 cm travel distance and 1 Hz speed, the power is

$$W = (0.4kg)\left(\frac{9.8kg}{m^2}\right)(1cm) = 39mJ$$

$$P = (39mJ)\left(\frac{1tap}{sec}\right) = 39mW$$

Buttons are a very common input mechanism for devices. Alexander et al. studied 1515 electronic push buttons in 11 typical household rooms [2]. The average travel distance was 1.48±1.04 mm and the average required force to trigger a button was 326±447.2 g. If we again assume a 1 Hz button pressing speed, the power is

$$W = (326g) \left(\frac{9.8kg}{m^2} \right) (1.48mm) = 4.7mJ$$

$$P = (4.7J) \left(\frac{1tap}{sec} \right) = 4.7mW$$

Keyboards can also be a convenient way to interface with a device. The total travel required for keys typically range from 4 mm (Cherry MX) to 1 mm (2020 MacBook Pro with Magic Keyboard). The force required to depress these keys is around 60 cN [97]. Assuming an average typing speed of 40 words per minute and 6 keys per word (5 characters + 1 space), the power is

$$W = (60cN)(2.5mm) = 15pJ$$

$$P = (15pJ) \left(\frac{40words}{min} \right) \left(\frac{6keys}{word} \right) \left(\frac{1min}{60sec} \right) = 60pW$$

Finally, swiping is a very familiar gesture for interfacing with electronics, especially those with touchscreens. The sliding friction and contact mechanics of this gesture were investigated by Ayyilidiz et al. [9]. They reported the nominal contact pressure is between 3-20 kPa (mid-point=11.5 kPa), and the friction coefficient for a grounded touchscreen is approximately μ_k=0.25. If we again use the 1 cm^3 approximation of a human fingertip, then the contact area is 1 cm^2. In reality, the contact area will be much less than the entire pad of the finger and depends on applied pressure. Empirically, a finger moves a distance of approximately 2 cm at 0.5 Hz when scrolling through a page on a mobile device. Assuming constant speed and disregarding the force required to initiate the swipe and overcome the static friction, the power of swiping is

$$W = (0.25) \left(\frac{11.5kN}{m^2} \right) \left(1cm^2 \right) (2cm) = 5.8mJ$$

$$P = (5.8mJ) \left(\frac{0.5swipe}{sec} \right) = 2.9mW$$

These results are summarized in Table 2.2. Although these power values are orders of magnitude smaller than the large limb motions previously summarized, it is still worthwhile to investigate these gestures as potential energy harvesting sources. As devices continue to shrink in size and power consumption, these small energy sources can help power electronics. More importantly, utilizing gestures already commonly used with devices lowers user effort and accelerates adoption into existing interactive devices.

There are four main methods of converting the energy from these physical gestures into usable electrical energy. These are piezoelectric, electromagnetic, electrostatic, and triboelectric [205]. The remainder of this chapter will review the fundamental physics of these transducers and survey published converters, with a focus on human energy harvesters. A comparison of the advantages and disadvantages of these four methods will also be discussed.

Table 2.2: Exerted power for gestures

Activity	Conditions	Power
Fingertip tap	1 Hz	98 µW
Hand tap	1 Hz	39 mW
Button (average)	1 Hz	4.7 mW
Keyboard	40 words/min	60 pW
Swiping	2 cm 0.5 Hz	2.9 mW

2.1   Piezoelectric Transduction

Piezoelectric energy conversion relies on unique piezoelectric materials, which respond to mechanical deformation with separation of charge, resulting in a generated voltage. These materials are capable of both converting mechanical force to electricity (direct piezoelectric effect), and converting electricity to mechanical actuation (converse piezoelectric effect) [98]. Although this second ability is useful in the application of actuators and motors, energy generation relies on the direct piezoelectric effect.

In inorganic piezoelectric materials, the piezoelectric effect is the result of the internal polarization of the crystal changing with applied force [26]. Piezoelectricity is first introduced by poling the material (applying a large electric field often at elevated temperatures), which aligns the previously randomly oriented dipoles. As the material undergoes compressive and tensile stress, there is an unbalanced shift of ions which creates a dipole and an electric field develops across the material. Figure 2.1 illusrates this mechanism for aluminum nitride (AlN). Organic piezoelectric polymers have also become a popular material choice for energy harvesting due to their flexible qualities [98]. In these materials, the piezoelectric effect is a result of the molecular structure and orientation of the polymer. These organic materials often have weaker piezoelectricity so there have been recent developments in organic-inorganic hybrid nanogenerators that leverage the benefits of both materials [26].

The piezoelectric effect is governed by the constitutive equation 2.4. From this we can derive the equation for the direct piezoelectric effect (Equation 2.5).

$$\begin{bmatrix} \delta \\ D \end{bmatrix} = \begin{bmatrix} s^E & d \\ d & \varepsilon^T \end{bmatrix} \begin{bmatrix} \sigma \\ E \end{bmatrix} \tag{2.4}$$

$$D = d\sigma + \varepsilon^T E \tag{2.5}$$

In these equations, δ is mechanical strain, σ is mechanical stress [N/m^2], D is electric displacement [C/m^2], E is electric field [V/m = N/C], s is elastic compliance [m^2/N], ε is dielectric constant [F/m], and d is piezoelectric strain coefficient [C/N]. Superscripts ^{E} and ^{T} denote under constant electric field and constant stress, respectively. Because most piezoelectric materials have a defined polar axis, the direction the force is applied (parallel or orthogonal) has different effects of piezoelectricity. Conventions define the polar axis the
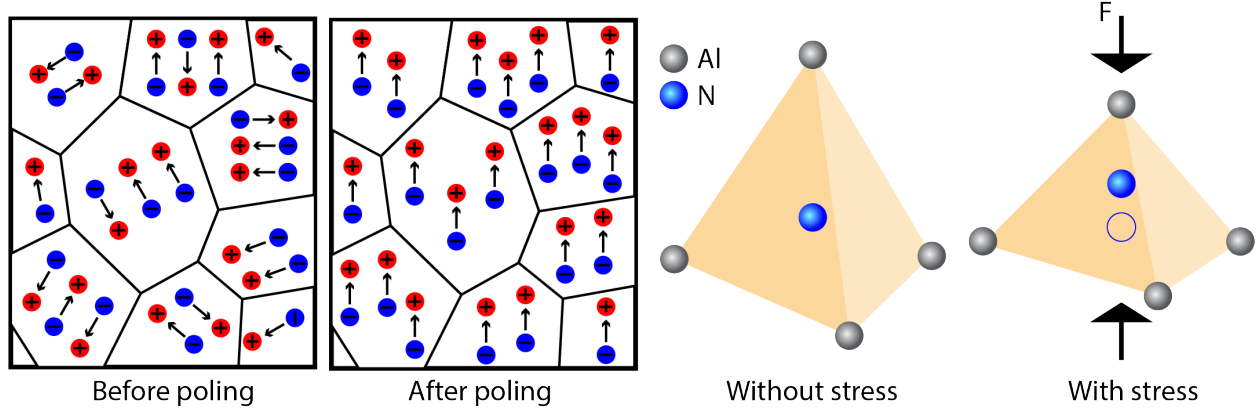
Figure 2.1: Mechanism of piezoelectricity (for AlN). (Adapted from [26])

Table 2.3:   Common piezoelectric materials

Material	Piezoelectric constant d [pC/N]	Dielectric constant $\varepsilon_r = \varepsilon/\varepsilon_0$	Reference
PZT-5H	$d_{33} = 593$, $d_{31} = -274$	3400	[71]
AlN (bulk)	$d_{33} = 5.6$, $d_{31} = -2.8$	9.14	[58, 27]
Quartz	$d_{33} = 2.3$, $d_{31} = 0.09$	5	[71]
ZnO	$d_{33} = 12$, $d_{31} = -4.7$	10.9	[64, 158]
BaTiO$_3$ (ceramic)	$d_{33} = 191$, $d_{31} = -79$	1680	[46]
LiNbO$_3$	$d_{33} = 7.9$, $d_{31} = -1$	29.4	[20]
GaN (bulk)	$d_{33} = 3.7$, $d_{31} = -1.9$	8.9	[58, 16]
PVDF	$d_{33} = -33$, $d_{31} = -23$	13	[158]
Graphene (single layer)	$d_{33} = 1400$	6.9	[43, 34]

"3" direction, and the orthogonal directions the "1" direction. Therefore, the piezoelectric strain coefficient is often reported as d_{ij} where i refers to the direction the force is applied, and j refers to the direction the generated voltage is measured. Table 2.3 summarizes the piezoelectric strain coefficient for common materials.

Generated power can be estimated using these material property values. The induced voltage and output power is determined by the following equations

$$V = g \times \frac{F \times t}{A} \tag{2.6}$$

$$g = \frac{d}{\varepsilon_0 \varepsilon_r} \tag{2.7}$$

$$C = \frac{\varepsilon_0 \varepsilon_r A}{t} \tag{2.8}$$

$$P = \frac{1}{2}CV^2 \cdot f = \frac{1}{2} \cdot g \cdot d \cdot F^2 \cdot \frac{t}{A} \cdot f \qquad (2.9)$$

where g is the piezoelectric voltage constant [Cm/NF], d is the piezoelectric constant [C/N], F is applied force [N], f is frequency [Hz], C is capacitance [F], t is thickness [m], and A is area [m^2] of the piezoelectric material. If we assume the kinetic energy of a tap with 1 cm^2 fingertip area on an 635 μm thick sheet of AlN (industrial standard thickness, good biocompatibility, and thin-film fabrication methods [62]), then the expected output voltage and power is

$$V = \left(\frac{5.6pC/N}{(9.14)(8.85pF/m)} \right) \left(\frac{(1g)(9.8kg/m^2)(635\mu m)}{1cm^2} \right) = 4.3mV$$

$$P = \frac{1}{2} \left(\frac{(9.14)(8.85pF/m)(1cm^2)}{635\mu m} \right) (4.3mV)^2 (1Hz) = 0.12fW$$

Since the piezoelectric effect requires a mechanical deformation, a light tap without applied force does not generate much power. A more realistic scenario might be using the force of an average button press, which would result in the following voltage and power

$$V = \left(\frac{5.6pC/N}{(9.14)(8.85pF/m)} \right) \left(\frac{(0.326kg)(9.8kg/m^2)(635\mu m)}{1cm^2} \right) = 1.4V$$

$$P = \frac{1}{2} \left(\frac{(9.14)(8.85pF/m)(1cm^2)}{635\mu m} \right) (1.4V)^2 (1Hz) = 12pW$$

In both these scenarios, the piezoelectric is operating in the d_{33} working mode, but there are many geometries to improve energy harvested. For example, stacking of multiple layers of piezoelectric material can increase the thickness, t, and overall voltage and power output [35]. It is also common for piezoelectric films to be fabricated as cantilevers allowing operation in d_{31} mode, resulting in designs including the unimorphs, bimorphs, cymbals, diaphragm [205, 98, 88]. With improvements in nanotechnology and nanofabrication, there is also an emergence of piezoelectric nanowires, which improves flexibility, and has been a popular material choice for implanted energy harvesters [187]. Table 2.4 compares some of the published piezoelectric harvesters.

Piezoelectric energy conversion is a growing area and researchers continue to look for ways to improve the efficiency, power density, and area density of these devices. In general, piezoelectric harvesters exhibit high induced voltages and relatively high power outputs. Continued development of this technology from bulk materials to thin-films and nanowires demonstrates the versatility of this conversion method and offers a wide array of relevant application spaces.

2.2 Electromagnetic Transduction

Electromagnetic energy conversion is based on Faraday's law of induction, which defines the interaction between a magnetic field and an electric circuit, which produces an elec-

Table 2.4: Survey of piezoelectric energy harvesters focused on low-frequency human body energy harvesting

Reference	Material & Geometry	Energy Source	Power	Size
Granstrom et al. 2007 [53]	PVDF	Backpack straps	45.6 mW	1.2 m × 51 mm × 52 μm (x4)
Galchev et al. 2010 [45]	Spiral PZT bimorph	9.8 m/s² 10 Hz	3.25 uW	1.2 cm³
Lee et al. 2013 [86]	ZnO nanowires	Wrinkling on face	0.2V, 2nA	5 mm × 13 mm × 25 μm
Yang et al. 2009 [187]	ZnO nanowire	Finger oscillation	25 mV, 150 pA	diameter = 100-800 nm length = 100-500 μm
Li et al. 2010 [95]	ZnO nanowire	Rat diaphragm	2 mV, 4 pA	diameter = 100-800 nm length = 100-500 μm
Qin et al. 2008 [137]	ZnO nanowires	Integrated with fabric	4-16 mW/m²	diameter = 50-200 nm length = 3.5 μm pitch = ~100 nm
Lee et al. 2012 [85]	ZnO nanowires & PVDF	Human elbow	0.1 V, 10 nA/cm²	diameter = 200 μm length = 2 cm support thickness = 6 mm
Dagdeviren et al. 2014 [35]	PZT nanoribbon	Bovine heart	0.12-0.18 μW/cm²	~1.7 cm x 2.4 cm [a]
Sun et al. 2011 [164]	PVDF microbelt	Human respiration (lung simulator)	0.4-0.5 V, 2 nW [b]	20 mm × 2 mm × 17 μm
Platt et al. 2005 [132]	PZT ceramics	Knee replacement implant	0.85 mW	5 mm × 4 mm × 7 mm [c]
Kim et al. 2017 [72]	PMN-PZT	Porcine heart	17.8 V, 1.74 μA	3.5 cm × 7 cm × 75 μm
Park et al. 2010 [131]	thin-film BaTiO₃	Finger pushing	1 V, 0.19 μA/cm² 7 mW/cm³	1 cm × 1 cm × 550 nm
Qian et al. 2018 [135]	PZT stack	Walking 3 mph (heel)	9mW/shoe	7 mm × 7 mm × 30 mm (x6)
Guido et al. 2016 [56]	AlN thin-film	Finger bending (knuckle)	0.7V, 0.2 μW	4 mm × 6 mm × 25 μm
Algier et al. 2018 [3]	AlN thin-film	Linear bending system	1.57 μW	14 mm × 9.6 mm × 25 μm
Almouahed et al. 2017 [4]	Multilayer NCE51F (NAC 2021, Noliac, Inc.)	Knee implants	59.4 mW	7 mm × 7 mm × 8 mm (x4)
Kuang and Zhu 2016 [81]	PZT bimorphs	Knee 0.9 Hz	3.5 mW	diameter = 12 cm height = 2 cm

[a]Approximated from figure
[b]Derived from storage capacitance energy and respiratory rate
[c]Approximated from figure

tromotive force. These generators consist of a conductive coil and permanent magnet, and electrical energy is generated as these two parts move relative to one another. For a tightly wound coil of N identical turns, induced electromotive force ε is defined by the following equations.

$$\varepsilon = -N\frac{d\Phi_B}{dt} \tag{2.10}$$

$$\Phi_B = \iint_A \boldsymbol{B} \cdot dA \tag{2.11}$$

$$\varepsilon = -N\frac{d}{dt}\iint_A \boldsymbol{B} \cdot dA \tag{2.12}$$

In these equations, ε is the electromotive force [V], N is the number of coils, Φ_B is the magnetic flux [Tm^2], $\boldsymbol{B}$ is the magnetic field [T = Vs/m^2], and dA is an element of the surface of A [m^2]. As illustrated by these equations, in order to induce an electromotive force, either the magnetic field, $\boldsymbol{B}$, or the effective area, A, of the magnetic flux must change. In electromagnetic generators, this leads to the two commonly seen configurations illustrated in figure 2.2. On the left, the movement is orthogonal to the magnetic field, and therefore the magnetic field remains relatively uniform. The flux varies with the relative "overlap" between the magnet and coil, as one moves up and down, in the z-direction. In this case, the electromotive force simplifies to

$$\varepsilon = -N \cdot l \cdot B \cdot \frac{dz}{dt} \tag{2.13}$$

where l is the diameter [m] of the coil. On the right is the second case where the direction of movement is parallel to the magnetic field and the field varies as a response to the distance between the magnet and coil. In this case, the electromotive force simplifies to

$$\varepsilon = -N \cdot A \cdot \frac{dB}{dz} \cdot \frac{dz}{dt} \tag{2.14}$$

where A is the cross-sectional area [m^2] of the coil orthogonal to the magnetic field. From these equations, it is clear that the electromotive force is proportional to the linear velocity of the moving component, so this value should be maximized. In both of these modes, either the magnet or coil can be fixed (or moving), but typically a fixed coil (and moving magnet) is preferred since it is easier to assemble fixed electrical wires [106]. In addition, as evidenced by N and A in the previous equations, the coil geometry can greatly affect the induced voltage. Increasing the number of coils, N, and increasing the cross-sectional area of flux, A, both increase harvested energy. However, as devices continue to decrease in size, maintaining these large coil values becomes problematic. Using nano- and micro- fabrication techniques will generally require coils to be fabricated with a 2D planar technology which not only limits the number of coils that can be fabricated, but also limits the dimensions (spacing,
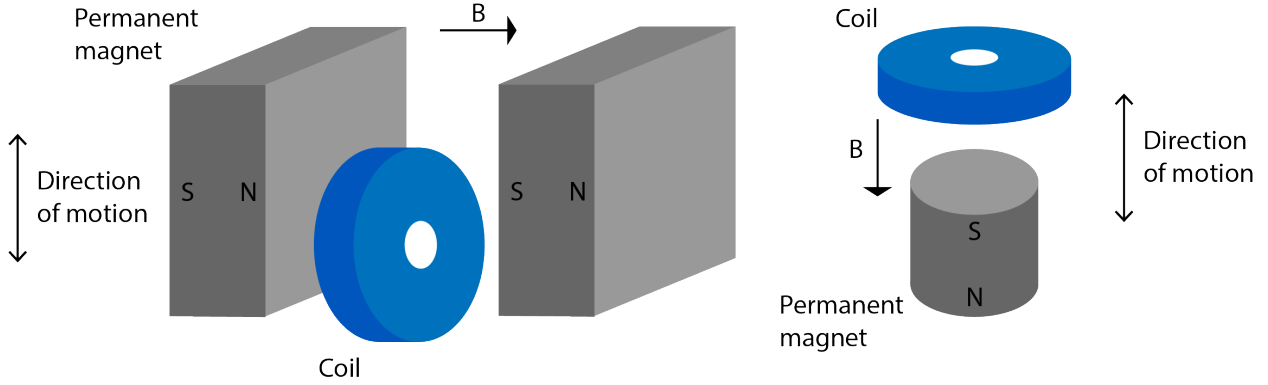
Figure 2.2: Two common modes of electromagnetic generators. (Adapted from [11])

width, thickness), which affects coil resistance [10]. Unfortunately, these miniaturization constraints limit the usefulness of electromagnetic energy conversion in many applications.

In the case that a new fabrication technology emerges and overcomes these challenges, the voltage and current induced by a fingertap can be estimated. Assuming a cylindrical magnet adhered to the finger tapping on a coil (similar to mode on the right in Figure 2.2), the magnetic field and its derivative is given by

$$B = \frac{B_r}{2} \left(\frac{D+z}{\sqrt{R^2 + (D+z)^2}} - \frac{z}{\sqrt{R^2 + z^2}} \right)$$

$$\frac{dB}{dz} = \frac{B_r}{2} \left(\frac{1}{\sqrt{(D+z)^2 + R^2}} - \frac{(D+z)^2}{((D+z)^2 + R^2)^{3/2}} + \frac{z^2}{(R^2 + z^2)^{3/2}} - \frac{1}{\sqrt{R^2 + z^2}} \right)$$

where B_r is the remanence field of the magnet [T], z is the distance from the face of the cylinder [m], D is the height of the cylinder [m], and R is the radius of the cylinder [m]. The last term in equation 2.14 is the derivative of position, or velocity, given as

$$z = z_0 + v_0 t + \frac{1}{2} a t^2$$

$$\frac{dz}{dt} = v = v_0 + at$$

where z_0 is the initial position [m], v_0 is the initial velocity [m/s], a is acceleration [m/s^2], and t is time [s]. Assuming the finger starts with zero velocity, the v_0 terms can be removed. We will also assume constant gravitational acceleration and ignore the opposite damping forces (i.e. assume finger muscle force compensates for the damping and maintains constant acceleration). These expressions can be plugged into equation 2.14 to express electromotive

force, or induced voltage, as a function of time, t.

$$\varepsilon = -N \cdot A \cdot \left[\frac{B_r}{2} \left(\frac{1}{\sqrt{(D + (z_0 + \frac{1}{2}gt^2))^2 + R^2}} - \frac{(D + (z_0 + \frac{1}{2}gt^2))^2}{\left((D + (z_0 + \frac{1}{2}gt^2))^2 + R^2\right)^{3/2}} \right. \right.$$

$$\left. \left. + \frac{(z_0 + \frac{1}{2}gt^2)^2}{\left(R^2 + (z_0 + \frac{1}{2}gt^2)^2\right)^{3/2}} - \frac{1}{\sqrt{R^2 + (z_0 + \frac{1}{2}gt^2)^2}} \right) \right] \cdot (gt)$$

If we assume a N42-grade NdFeB magnet ($Br = 1.32$ T [22]) with a thickness of 1 mm and a diameter of 1 cm ($R = 5$ mm) and a coil with $N = 10$ turns and the same diameter (r = 5 mm, ignore edge effects), then the induced voltage can be plotted as a function of time for a single tap motion. Assuming, similar to before, that the finger begins its motion at zero velocity at a height of 1 cm above the coil, then a single downward tap will occur between $0 < t < 45$ ms. The induced voltage is plotted as a function of time for this range in Figure 2.3. The highest voltage of 7 mV occurs at 41 ms, which corresponds to 1.7 mm above the coil. The current can be solved for by deriving the resistance of the coil and applying ohms law. Using current, standard, multi-layer PCB capabilities as a guideline (manufacturer: BayAreaCircuits), copper traces are $\sim$1.4 mils (0.036 mm) with a resistivity of $\rho \sim 1.7 \times 10^{-8}$ Ωm, and traces must be >5 mils (0.127 mm). If we approximate the width of the copper trace as 0.5 mm and know the radius is 5 mm with 10 turns, we can approximate the resistance of the coil as follows

$$R = \frac{\rho \cdot l}{A}$$

$$R = \frac{(17 n\Omega m)(10(2 \cdot \pi \cdot 5mm))}{0.036mm \cdot 0.5mm} = 0.30\Omega$$

Therefore, the maximum current and instantaneous power can be calculated.

$$I = \frac{V}{R} = \frac{7mV}{0.30\Omega} = 23mA$$

$$P = IV = (23mA)(7mV) = 160\mu W$$

These results highlight some of the advantages and disadvantages of electromagnetic energy harvesting. Typically, these generators cannot produce very high voltages and will require electronic converters to boost the voltage to a useful range; however, they can generate high instantaneous currents if care is taken to keep resistances low. Despite difficulties in miniaturization, there has still been significant research produced on electromagnetic generators, but typically at a larger scale. Table 2.5 summarizes some of these developments, focused in the area of human energy harvesting.

    The published research in electromagnetic energy harvesting has presented innovative solutions to overcoming its challenges. For example, gears provide effective up-converting of linear motions to faster rotational motions, and electronic boost converters help step-up

Table 2.5: Survey of electromagnetic energy harvesters focused on low-frequency human body energy harvesting

Reference	Energy Source	Power	Size	Notes
Delnavaz et al. 2012 [37]	Respiration	25 mV, 3.1 µW	diameter = 12.7 mm, height = 49.5 mm	Breathing through tube moves levitated magnet through coil
Li et al. 2009 [92]	Walking 1.5 m/s (knee)	4.8 W	15 cm × 6 cm × 5 cm [a]	Gear train transfers high torque to speed for rotary magnetic generator
Saha et al. 2008 [147]	Walking 2 Hz (backpack)	300 µW	diameter = 18 mm, height = 55 mm	Magnet moving through coil
Chamanian et al. 2016 [19]	Walking (simulated)	125 µW	diameter = 25 mm, height = 60 mm	NdFeB magnet moving through coil
Romero et al. 2009 [145]	Walking (ankle)	59.4 mV, 44 µW	diameter = 25 mm, height = 3 mm	NdFeB eccentric mass rotor and planar coil stator
Liu et al. 2018 [99]	Handshake 8 Hz (wrist)	0.8 V, 10.4 mW	diameter = 65 mm, height = 18 mm	NdFeB magnet asymmetrically rotating over coils
Halim et al. 2017 [59]	Walking (wrist) simulated arm swing 25° rotation 1.25 Hz	270 mV, 55 µW	diameter = 30 mm, height = 12 mm	two eccentric NdFeB rotors over PCB coils
Samad et al. 2016 [150]	Shaking 5 Hz	5.185 mW	diameter = 16 mm, height = 210 mm	NdFeB magnet moving through coil in curved tube (R=0.25 m)
Zhang et al. 2014 [195]	Running 3.58 m/s (backpack)	32 mW	2 cm × 3 cm × 20 cm	Magnet array vibrating through coil array
Rahimi et al. 2012 [139]	Shaking 2 Hz	1.6 V, 128 µW	7 cm × 2 cm × 1.5 cm	Magnet triggers coil on cantilever to up-convert ambient frequency
Liu et al. 2015 [100]	Handshaking 6.7 Hz	568.66 µW	diameter = 10 mm, height = 66 mm	NdFeB magnet moving through coil
Niroomand and Foroughi 2016 [120]	Walking (ankle)	150 mV, 416.6 µW	diameter = 5 cm, height = 3 mm	Off-center NdFeB magnet rotate over planar coils
Salauddin and Park 2017 [148]	Manual shaking	600 mV, 2.25 mW	6.5 cm × 2.6 cm × 1.8 cm	Halbach magnet array to enhance magnetic field intensity vibrating around coil
Dai and Liu 2014 [36]	Walking 1.47 m/s (hip)	0.59 V, 99.3 µW	diameter = 80 mm, height = 22 mm, lever: 27 × 3 × 0.2 cm³	Rotary generator with lever arm extended to knee
Shepertycky and Li 2015 [152]	Walking 5.6 km/h (lower limbs)	5.2 W	10 cm × 20 cm × 8 cm [b,c]	Generator carried on lower back with cables to feet for rotary motion into gear train to AC generator
Xie and Cai 2015 [184]	Walking 5 km/h (shoe)	1.39 W	80 mm × 47 mm × 22 mm	Trapezoidal teeth to amplify displacement and gear train to accelerate motion
Goto et al. 1999 [51]	Dog heart 200 beats/min	44 µW [d]	diameter = 27.6 mm, height = 4.2 mm [e]	Rotary generator from SEIKO watch

[a] Approximated from figure and dimensions for EC45 Flat brushless DC motor (Maxon Motors)
[b] Approximated from figure and dimensions for EC-4pole brushless AC motor (Maxon Motors)
[c] Not including cables, foot harness, or backpack frame
[d] Derived from energy per heart beat and heart rate
[e] Dimensions of SEIKO quartz automatic generating system
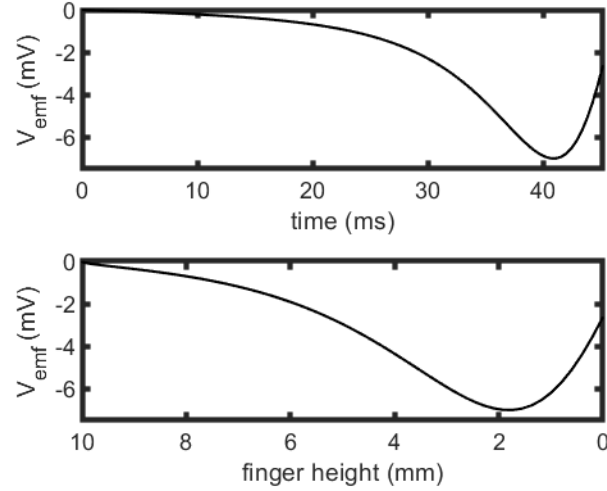
Figure 2.3: Induced voltage by finger tap with neodymium magnet for a single downward stroke.

small voltages to the useful range to power electronic devices. Although there are difficulties involved with microfabricating effective coils and magnetic materials, there exists an application space (macroscale generators) where electromagnetic harvesting can be very effective.

2.3   Electrostatic Transduction

Electrostatic energy conversion depends on mechanical motion influencing a capacitor, creating a variable capacitance. A capacitor is essentially two conductive nodes with a dielectric in between, and it stores electrical energy in its electric field. To illustrate the theory of electrostatic harvesting, a simple parallel plate capacitor can be considered. In this case, the capacitance is defined by equation 2.15.

$$C = \varepsilon \frac{A}{d} \tag{2.15}$$

ε is the electric permittivity of the dielectric [F/m], A is the overlapping area of the parallel plate conductor [m^2], and d is the distance between the plates [m]. From this relationship, it is clear that a change in any of these three variables will affect the capacitance. These three methods of changing capacitance are visualized in Figure 2.4. The top image shows a cartoon of a parallel plate capacitor in its original state, and the bottom three figures depict how capacitance can change. The left mode illustrates moving one electrode in a parallel plane to the other electrode to affect the overlapping area of the capacitor. The center again shows an electrode moving, but this time closer to or away from the other electrode which
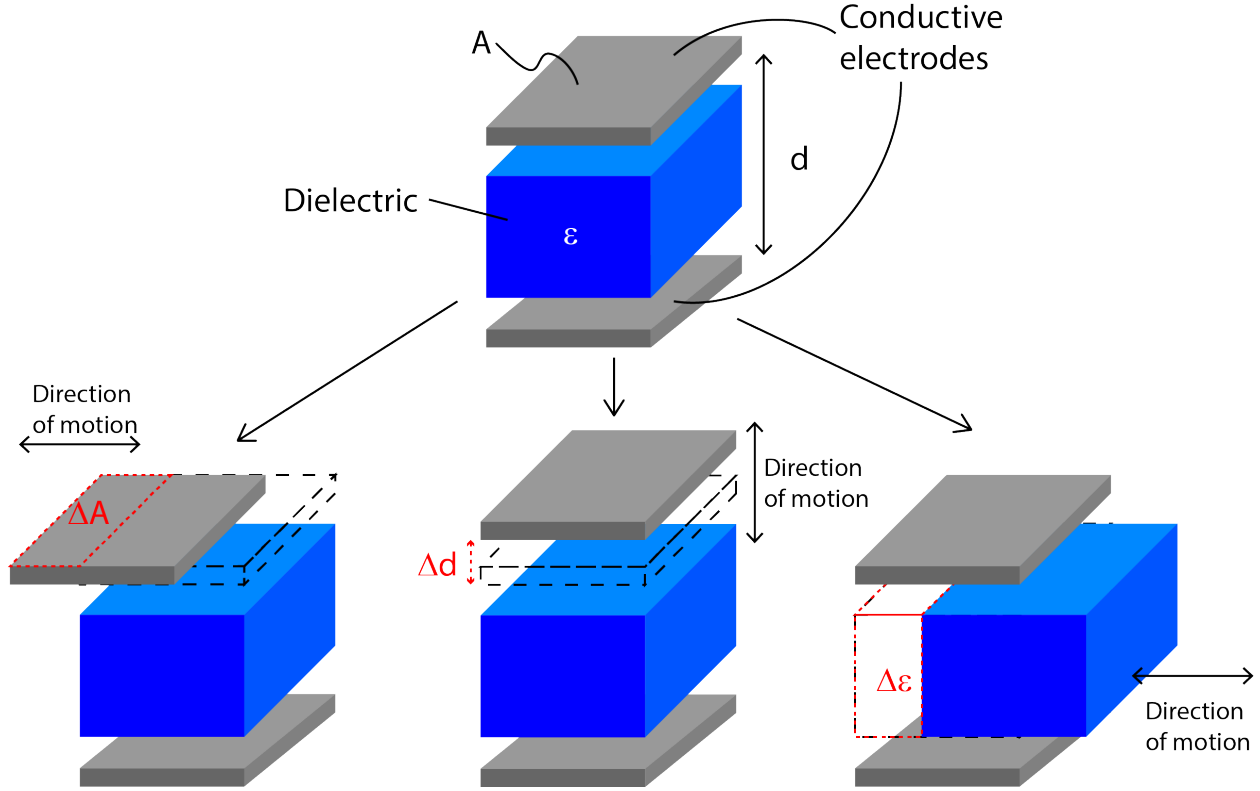
Figure 2.4: Three general methods to change capacitance.

changes the distance between the conductors. Finally the right demonstrates the motion of dielectric between the electrodes, which implies a material of different dielectric constant (air or otherwise) replaces the original dielectric.

Once a variable capacitor is established, energy is harvested in response to how the charge and voltage changes. The charge stored on a capacitor is given by equation 2.16 and the energy stored on a capacitor is given in equation 2.17.

$$Q = CV \tag{2.16}$$

$$E = \frac{1}{2}CV^2 = \frac{1}{2}QV \tag{2.17}$$

Where Q is the charge on the capacitor [C], C is the capacitance [F], and V is the voltage across the capacitor [V]. Energy is stored on a capacitor in the electric field between the two charged plates, and the mechanical forces that change the capacitance do work to redistribute charge. There are two main operational modes for electrostatic energy harvesting: (1) charge constrained mode and (2) voltage constrained mode. Both of these modes can be explained

by looking at the derivative of equation 2.16 with respect to time.

$$\frac{dQ}{dt} = C\frac{dV}{dt} + V\frac{dC}{dt} \tag{2.18}$$

In the charge constrained mode, there is constant charge and thus the dQ/dt term drops out. Therefore the change in voltage is expressed as a function of the variable capacitor.

$$\frac{dV}{dt} = -\frac{V}{C}\left(\frac{dC}{dt}\right)$$

As the capacitance decreases and charge remains constant, the voltage increases. The change in energy in the system can also be solved for in this constant charge state by returning to equation 2.17, where in the following equations subscripts $_f$ and $_i$ stand for the final and initial states.

$$Q = C_iV_i = C_fV_f$$

$$\Delta E = E_f - E_i$$

$$\Delta E = \frac{1}{2}(C_i - C_f)V_iV_f = \frac{1}{2}Q(V_f - V_i)$$

In the voltage constrained mode, voltage remains constant and therefore the dV/dt term is zero. Charge is expressed as a function of the variable capacitor and change in energy a function of the change in charge.

$$\frac{dQ}{dt} = I = V\frac{dC}{dt}$$

Where I is current [A]. In this constant voltage mode, as capacitance increases, the charge increases. Similar equations for energy can also be derived in this mode using equation 2.17 with the same $_f$ and $_i$ subscripts.

$$V = \frac{Q_i}{C_i} = \frac{Q_f}{C_f}$$

$$\Delta E = E_f - E_]$$

$$\Delta E = \frac{1}{2}(C_f - C_i)V^2 = \frac{1}{2}(Q_f - Q_i)V$$

To approximate the power from a fingertap, we can find a change in capacitance assuming the finger is one of the conductive plates and starts at a height of 1 cm. If the other plate of the capacitor is fabricated on a PCB , it can be insulated with a standard soldermask which has thickness of 20 µm and dielectric constant of 3.4. We assume that the remainder of the distance is filled with air with unity dielectric constant and, as before, the area is 1 cm². These two capacitors can be considered in series and the change in capacitance, assuming a simple parallel plate and ignoring fringing fields and other higher order effects, is solved for as follows, where C_{min} is the finger at its maximum 1 cm height and C_{max} is the finger on the PCB.

$$C_{air} = \varepsilon_{air}\frac{A}{d_{air}} = (1)(8.85pF/m)\frac{1cm^2}{1cm - 20\mu m} = 89fF$$

$$C_{soldermask} = \varepsilon_{soldermask}\frac{A}{d_{soldermask}} = (3.4)(8.85pF/m)\frac{1cm^2}{20\mu m} = 150pF$$

$$C_{min} = \frac{C_{air}C_{soldermask}}{C_{air} + C_{soldermask}} = \frac{(89fF)(150pF)}{89fF + 150pF} = 89fF$$

$$C_{max} = C_{soldermask} = 150pF$$

In addition to the change in capacitance, the voltage is also required to approximate the power delivered by this generator. For simplicity, a bias voltage value of 1 V will be assumed, and we will continue to use a tapping frequency of 1 Hz. The energy and power for charge constrained (CC) and voltage constrained (VC) systems are derived below.

$$\Delta E_{cc} = \frac{1}{2}(150pF - 89fF)(1V)\left(\frac{(150pf)(1V)}{89fF}\right) = 0.13\mu J$$

$$P_{cc} = \frac{\Delta E_{cc}}{\Delta T} = \frac{0.13\mu J}{1s} = 0.13\mu W$$

$$\Delta E_{vc} = \frac{1}{2}(150pF - 89fF)(1V)^2 = 75pJ$$

$$P_{vc} = \frac{\Delta E_{vc}}{\Delta T} = \frac{75pJ}{1s} = 75pW$$

In the charge controlled case, it is important to initially charge the system in the C_{max} state since positive energy gain occurs when the variable capacitor changes from $C_{max} \rightarrow C_{min}$ (i.e. when $C_i > C_f$). Conversely, there is positive energy gain in the voltage controlled case when the capacitor varies from $C_{min} \rightarrow C_{max}$ (i.e. when $C_f > C_i$). Therefore, although the charge controlled mode generated more power in this case, it would require a larger initial charging energy to bias a 150 pF capacitor to 1 V as opposed to the 89 fF capacitor.

Due to practical constraints in real-world implementation, such as nonideal voltage sources and charge leakage, most electrostatic transducers will operate somewhere between these two absolute constrained modes. Table 2.6 reports on some of these published innovations in electrostatic energy harvesting, again with a focus on human generated power. One of the biggest limitations of electrostatic energy harvesting is the required initial biasing of the capacitor. The variable capacitor must be precharged for work done on it to generate any energy. There are a number of solutions researchers have developed to address this challenge, such as introducing electrets (permanent charge in the dielectric) [7], using a hybrid-transduction structure that relies on another harvesting technique to create an initial charge [83], or simply periodically connecting it to a power supply [202]. Although this last option will not realize the full benefit of energy harvesting and will still rely on a battery or power supply for charge, integrating electrostatic energy harvesting in these systems can help extend the time between charges and reduce maintenance requirements. There is also growth in the variety of materials and geometries used, such as integration of polymers for enhanced flexibility [200], or addition of liquids between the capacitor electrodes [24] for larger range of variable capacitors.

Table 2.6: Survey of electrostatic energy harvesters focused on low-frequency human body energy harvesting

Reference	Energy Source	Power	Size	Notes
Tashiro et al. 2002 [166]	Canine heart 180 bpm (simulated)	36 µW	90 mm × 100 mm × 5 mm [a]	Honeycomb structured variable capacitor
Arakawa et al. 2004 [7]	Shaking 10 Hz	6 µW	2 cm × 2 cm × 1 mm	Fluorocarbon polymer CYTOP electret dielectric
Tsutsumino et al. 2006 [171]	Shaking 20 Hz	38 µW	10 mm × 20 mm × 0.85 mm	Fluorocarbon polymer CYTOP electret dielectric
Miao et al. 2006 [113]	Shaking 20 Hz	2.4 µW	11 mm × 11 mm × 0.5 mm	Gap-closer
Zhong et al. 2014 [200]	Finger bending	0.91 µW	diameter = 1 mm height = 9 cm	Carbon nanotube and PTFE coated cotton fiber based for power shirt
Choi et al. 2011 [24]	Running 8 km/h (foot)	35.3 µW	1 cm × 1 cm × 1 cm	Conductive ionic liquid in capacitive gap
Bu et al. 2013 [17]	Rotation 1 Hz	2.19 µW	4 cm × 1.5 cm × 3.1 mm	PVDF electret and liquid-based capacitive gap
Lu et al. 2015 [103]	Hand shaken ∼ 5 Hz	0.15 µW	12 mm × 10 mm × 0.38 mm	Small ball free to move in mass to upconvert frequency
Rocha et al. 2010 [144]	Walking 4 steps/s (shoe)	14 µW [b]	4.8 cm × 12 cm × 5 mm [c]	Hybrid piezo generator charges electrostatic capacitance
Cornogolub et al. 2016 [31]	Stretching 1 Hz	114 µW	4 cm × 10 cm × 100 µm	Hybrid piezo compensates charge loss in dielectric polymer
McKay et al. 2010 [110]	Pressing 3 Hz		diameter = 11 cm height = 2 cm	Self-priming dielectric elastomer diaphragm
Vu-Cong et al. 2013 [30]	Stretching 1 Hz	33 µW	10 cm × 2.5 cm × 0.6 mm	Electret combined with dielectric elastomer
Lagomarsini et al. 2019 [83]	Stretching 1 Hz	0.45 µW	8 cm × 3 cm × 1 cm	Hybrid PVDF piezo generator biases dielectric elastomer
Kiziroglou et al. 2008 [77]	Rolling 1 Hz	< 8 µW	10 mm × 10 mm × 2 mm	Rolling rod over electrode

[a]Estimated from unit cell dimension and array size of honeycomb
[b]Derived from energy per step and step rate
[c]Approximated from appearance in figure

2.4   Triboelectric Transduction

Triboelectric energy conversion relies on a combination of the triboelectrification effect and electrostatic induction. Triboelectrification describes the effect where charge is transferred between two materials through frictional contact, due to the properties and chemistries of the materials and their relative tendencies to gain or lose electrons [101]. When a force is applied on two materials of opposite charge affinities, causing them to bend into contact, charge of opposite polarities accumulates on the surfaces of the materials. When the force is released, the materials will separate, but maintain their charged states, which creates an electric potential [182]. If an external load is connected, this electric field drives charge and generates current.

Triboelectric generators typically appear in four different operation modes: (1) vertical contact-separation mode, (2) lateral-sliding mode, (3) single-electrode mode, and (4) free-standing triboelectric-layer mode [176]. These four working modes are illustrated in Figure 2.5. The vertical contact-separation mode includes two dissimilar dielectrics with electrode contacts on the backs. The energy harvesting cycle begins when the dielectric films are brought into contact, which creates oppositely charged surfaces. When they are separated, a potential drop appears across the gap and free electrons would flow through a load from one electrode to the other. When the gap is closed, the potential disappears, electrons flow back, and the cycle repeats. The lateral sliding mode has the same structure of two dielectrics with electrodes. However, here the dielectrics slide laterally with respect to one another while keeping their contact, thus inducing a lateral polarization. Charge will again flow from one electrode to the other. This method can be implemented in various forms, including rotational sliding. Many objects and materials naturally carry charge due to contact with other materials throughout routine use. The last two modes leverage natural charge with free-moving dielectrics. The single-electrode mode only has one stand-alone electrode and a free dielectric. As the dielectric moves (in either contact separation or contact-sliding directions), the local electric field around the electrode changes, therefore flowing charge to and from a ground node. The freestanding triboelectric-layer mode similarly uses a free dielectric to vary local electric fields, but in this case between two stand-alone electrodes. Again, as the dielectric moves near the electrodes, electrons flow from one electrode to the other to balance local potential disruptions [176].

Although most materials undergo triboelectrification, the degree to which a material gains or loses electrons depends on its polarity. Table 2.7 lists some commonly used triboelectric materials and their charge affinity. Materials further away from one another on this spectrum will transfer more charge, therefore inducing a larger voltage upon separation. Some of the more commonly used materials include poly tetrafluoroethylene (PTFE) and silicone for a net negative triboelectric charge, and nylon for a net positive charge [182].

An alternative way of viewing this system is by looking at the system as a variable capacitor after the electric potential has been established. From this perspective, and especially for the vertical contact-separation mode, many of the same equations that were presented for electrostatic transduction (Section 2.3) apply. If we assume as we did for electrostatics a
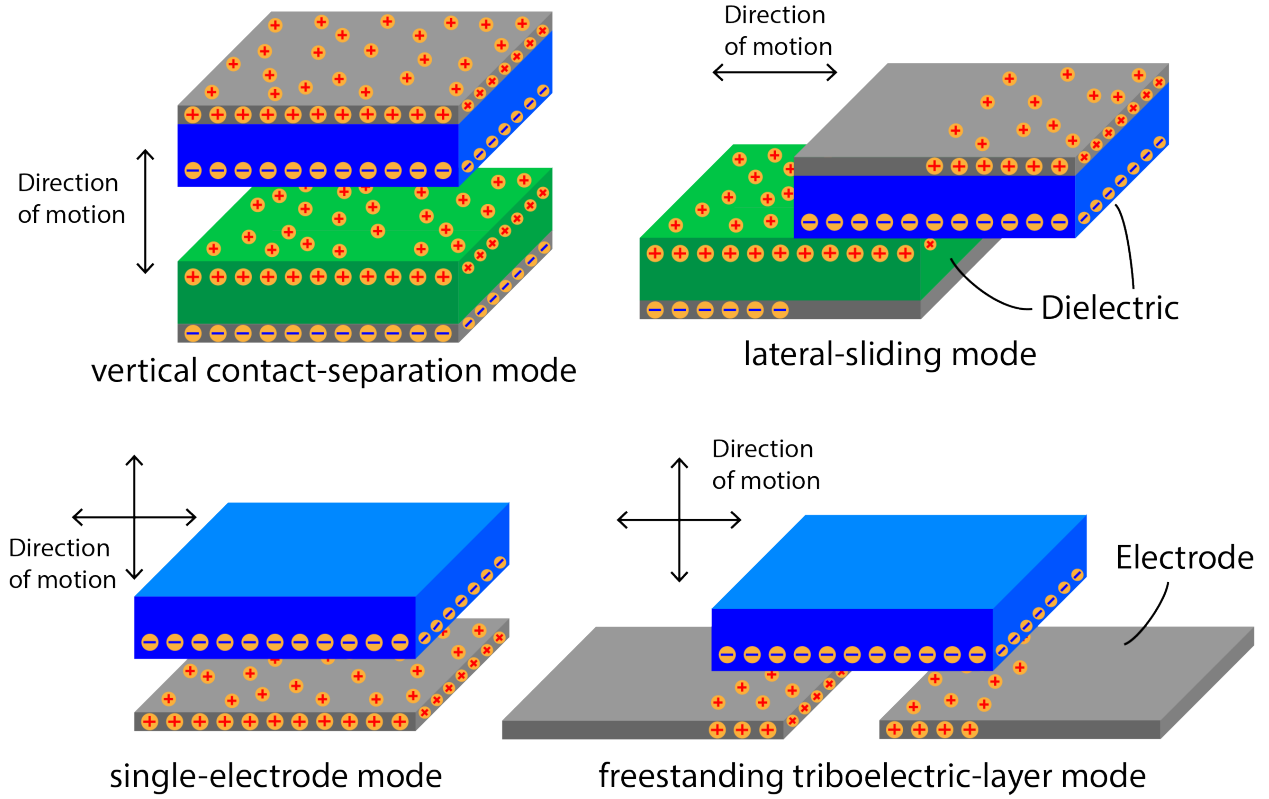
Figure 2.5: Four general modes of tribelectric generation.

parallel-plate capacitance where the area of the electrodes is orders of magnitude larger than their gap, then the total capacitance is three capacitors in series: C_{d1}, C_g, and C_g, where subscripts g is the gap and $d1$ and $d2$ are the dielectric capacitances. Both the polarized triboelectric charges and the electrode charges contribute to the output voltage in equation 2.19

$$V = V_{oc}(z) - \frac{Q}{C(z)} \tag{2.19}$$

$$V_{oc} = \frac{Q_{oc}}{C_{oc}} = \frac{\sigma A}{\varepsilon_g \frac{A}{z(t)}} = \frac{\sigma z(t)}{\varepsilon_g} \tag{2.20}$$

$$C(z) = C_{d1} || C_g || C_{d2} = \frac{1}{\frac{t_{d1}}{\varepsilon_{d1} A} + \frac{z(t)}{\varepsilon_g A} + \frac{t_{d2}}{\varepsilon_{d2} A}} \tag{2.21}$$

$$V = \frac{\sigma z(t)}{\varepsilon_g} - \frac{Q}{A} \left(\frac{t_{d1}}{\varepsilon_{d1}} + \frac{z(t)}{\varepsilon_g} + \frac{t_{d2}}{\varepsilon_{d2}} \right) \tag{2.22}$$

In equation 2.19, V_{oc} is the open circuit voltage between the two electrodes [V], and this is the maximum possible voltage on the system as a function of $z(t)$, which is the displacement

Table 2.7:   Triboelectric charge affinity for select materials (Adapted from [21])

Triboelectric	Charge affinity [nC/J]	
Polyurethane foam	+60	
Hair, oily skin	+45	
Solid polyurethane	+40	
Nylon, dry skin	+30	
Machine oil	+29	
Glass (soda)	+25	
Paper	+10	
Wood (pine)	+7	
Cotton	+5	
Nitrile rubber	+3	
Wool	0	0
Polycarbonate	-5	
Acrylic	-10	
Epoxy	-32	
PET (mylar) solid	-40	
Polystyrene	-70	
Polyimide	-70	
Silicones	-72	
Vinyl: flexible	-75	
Polypropylene	-90	
PVC (rigid vinyl)	-100	
Latex (natural) rubber	-105	
PTFE (teflon)	-190	

or gap distance [m]. The second term accounts for the reduction of electric potential due to charge transfer once a load is connected, as a function of Q, the amount of transferred charge [C], and $C(z)$, the equivalent capacitance of the system [F]. Equation 2.20 defines the open circuit voltage in terms of σ, the charge density from triboelectrification on the dielectric surface [C/m^2] and ε_g, the dielectric permittivity of the gap [F/m]. Equation 2.21 defines the total equivalent capacitance of the three capacitors in series, as a function of their respective thicknesses, t [m], and dielectric constants, ε [F/m]. And finally, equation 2.22 is solving for the voltage equation given in 2.19 as a function of $z(t)$.

At short circuit conditions, the electrodes will be at the same electric potential (i.e. $V = 0$), and the charges transferred will be

$$Q_{sc} = \frac{A\sigma z(t)}{\frac{\varepsilon_g t_{d1}}{\varepsilon_{d1}} + \frac{\varepsilon_g t_{d2}}{\varepsilon_{d2}} + z(t)} \tag{2.23}$$

To make this equation cleaner, a new variable t_d is defined, which can simplify the Q_{sc} and

V equations

$$t_d = \frac{\varepsilon_g t_{d1}}{\varepsilon_{d1}} + \frac{\varepsilon_g t_{d2}}{\varepsilon_{d2}}$$

$$V = \frac{\sigma z(t)}{\varepsilon_g} - \frac{Q}{A\varepsilon_g}(t_d + z(t)) \qquad (2.24)$$

$$Q_{sc} = \frac{A\sigma z(t)}{t_d + z(t)} \qquad (2.25)$$

The short circuit current can be solved for

$$I_{sc} = \frac{dQ_{sc}}{dt} = \left(\frac{dQ_{sc}}{dz}\right)\left(\frac{dz}{dt}\right)$$

$$I_{sc} = \frac{A\sigma t_d}{(t_d + z(t))^2}\frac{dz(t)}{dt} = \frac{A\sigma t_d}{(t_d + z(t))^2}v(t) \qquad (2.26)$$

Here, we have the short circuit current as a function of velocity, $v(t)$ [m/s]. To solve for the current in a general case in between open and short circuit, for example an arbitrary load of resistance R, we can use ohms law and define I as

$$\frac{dQ}{dt} = I = \frac{V}{R}$$

$$\frac{dQ}{dt} = \frac{\sigma z(t)}{\varepsilon_g R} - \frac{Q}{A\varepsilon_g R}(t_d + z(t)) \qquad (2.27)$$

This first-order differential equation can then be solved for Q given known boundary conditions [122]. The current ($I = dQ/dt$) and voltage ($V = IR$) will then follow from that solution.

We can approximate the power from a fingertap to compare this transduction method with the others. We assume a contact-separation mode generator with a nylon pad with attached electrode adhered to a human fingertip and a stationary PTFE dielectric on the opposite electrode. The surface charge density, σ, is dependent on numerous conditions including force, humidity, and temperature. Assuming a linear relationship with force, temperature of 25°C, and 50% humidity, the surface charge density can be extrapolated from data presented by Kleyman et al. [78] to be 0.9 μC/m² at 9.8 mN (F = 1 g · 9.8 m/s²). The thickness of these layers will be 1 mil (25 μm), which is a commercially available thickness of nylon and PTFE films (McMaster Carr). The dielectric constant used for PTFE is 2 [79] and for nylon is 3.6 [33]. Again using the approximations of a 1 cm² area and max travel distance of 1 cm, we can find the open circuit voltage and short circuit current.

$$V_{oc} = \frac{\sigma z}{\varepsilon_g} = \frac{(0.9\mu C/m^2)(1cm)}{8.85pF/m} = 1kV$$

$$t_d = \frac{\varepsilon_g t_{d1}}{\varepsilon_{d1}} + \frac{\varepsilon_g t_{d2}}{\varepsilon_{d2}} = \frac{25\mu m}{2} + \frac{25\mu m}{3.6} = 19\mu m$$

$$I_{sc} = \frac{A\sigma t_d}{(t_d + z(t))^2}v(t) = \frac{(1cm^2)(0.9\mu C/m^2)(19\mu m)}{(19\mu m + 1cm)^2}(9.8m/s^2)(0.045s) = 7.5pA$$

Therefore, the maximum instantaneous power is

$$P = IV = (1kV)(7.5pA) = 7.5nW$$

Although this power could never realistically be achieved, and the device would operate somewhere between open circuit and short circuit conditions, this approximation gives us a reasonable frame of reference to understand the order of magnitude of power that can be generated by triboelectric transduction.

Due to the universal presence of triboelectricity on almost all materials, triboelectric transduction has drawn significant interest in the research community. Being able to build a triboelectric generator from a variety of materials allows for easier energy harvesting integration into most devices. In particular, the flexibility of many triboelectric materials allows for better mechanical impedance matching with the human body. Table 2.8 summarizes some of the recent emerging technologies for triboelectric energy harvesters, with a specific focused on human energy harvesting.

Since the established triboelectric charge is a function of area and charge density, increasing these values improves the power generated from a triboelectric harvester. A significant amount of research has been aimed towards functionalization of the triboelectric surfaces. This includes both physical modifications, such as increasing contact area with microstructures [111], and chemical treatments, such as depositing nanoparticles [75] and introducing dopants [146]. Another interesting feature, which is possible due to the vast selection of triboelectric materials, is the ability to biodegrade, leading to less waste [68]. In general, triboelectric energy harvesting produces extremely high voltages and has an abundant selection of materials to chose from. However, there still exist questions surrounding its long term stability and reliability [25], since it can be dependent on environmental conditions such as humidity. As these uncertainties are researched and better understood, triboelectric energy harvesting can be suitable for many applications.

2.5   Comparison of Transduction Methods

As electronics become increasingly smaller in size and portable in nature, there exist significant efforts to develop alternative energy harvesting. Kinetic energy harvesting from human motion is particularly relevant for interactive electronics as well as wearables and sensors on and around the body. The four main methods of converting this kinetic energy to useful electrical energy are piezoelectric, electromagnetic, electrostatic, and triboelectric. The fundamental theory and a brief literature survey for these energy conversion methods were presented previously in this chapter. Table 2.9 compares the primary advantages and disadvantages of each of these four tranductions methods.

It is important to remember that due to the variety of applications, there is no one transduction method that will always be the best. Instead, developers should carefully

Table 2.8: Survey of triboelectric energy harvesters focused on low-frequency human body energy harvesting

Reference	Energy Source	Power	Size	Triboelectric materials & mode [a]
Fan et al. 2012 [42]	Bending 0.33 Hz	3.3 V, 0.6 μA	4.5 cm × 1.2 cm × 345 μm	Kapton & PET; CS
Yang et al. 2013 [188]	Backpack	5.56 mW [b]	5 cm × 7.5 cm × 20 cm	PTFE nanowire & Al nanopores in rhombus structure; CS & LS
Zhong et al. 2013 [201]	Finger press	125 V, 33 μA	3.5 cm × 2.5 cm × 0.42 mm	PTFE & Ag; CS
Yang et al. 2013 [189]	Finger press	60 V, 3.5 μA	1 cm × 1 cm × 0.4 mm	Skin & micropyramid patterned PDMS; SE
Haque et al. 2016 [61]	Walking 0.9 Hz (shoe insole)	312.1 V, 1.14 μA	133 cm^2 × 2.11 mm	PUR & PDMS; CS
Haque et al. 2016 [60]	Stretching fabric	55 V, 0.19 μA	72 cm^2 × 0.13 mm	PDMS & PUR ; LS
Meng et a. 2013 [111]	Finger press	130 V, 3.75 μA	1.5 cm × 2.5 cm × 0.235 mm	microstructured PDMS; SE
Zhou et al. 2014 [206]	Stretching	25 V, 1.2 μA	11.2 cm × 11.2 cm × 0.820 mm	Nylon & polyester & Ag fiber woven fabric; FS & CS & LS
Zheng et al. 2014 [198]	Respiration 50 breaths/min (implanted)	3.73 V, 0.14 uA	1.2 cm × 1.2 cm × 0.5 mm	Kapton& PDMS & Al foil; CS
Pu et al. 2015 [133]	Stretching	50 V, 4 μA	5 cm × 5 cm [c]	Nickel & Parylene woven polyester fabric; CS
Yi et al. 2016 [192]	Stretching & bending	380 V, 3.2 μA [d]	7 cm × 3.8 cm × 1.06 cm	Sandpaper roughened carbon black & silicone; CS
Lai et al. 2016 [84]	Hand press 4 Hz	70 V, 3.8 μA	2.5 cm × 2.5 cm × 4.8 mm	Silicone rubber & Ag nanowire; SE
Kim et al. 2015 [74]	Compressive force 50 N	40 V, 10 μA	Diameter: 5 mm Length: 5 cm	Nanostructured PDMS & ZnO nanowire coated thread; CS
Niu et al. 2015 [121]	Walking (shoe)	1.044 mW	5.7 cm × 5.2 cm × 2.4 cm	Fluorinated ethylene propylene & Al foil; CS
Li et al. 2018 [89]	Respiration (implant)	0.12 μW	1.1 cm × 3 cm × 0.35 mm	PTFE & PET & Cu; LS
Ma et al. 2016 [104]	Heart beat (implant)	10 V, 4 μA	3 cm × 2 cm × 1 cm	PTFE & Al; CS
Zheng et al. 2016 [199]	Heart beat (implant)	14 V, 5 μA	5.6 cm × 3.5 cm × 1 mm [e]	PTFE & Al & PDMS; CS
Yao et al. 2018 [191]	Digestive system (gastric peristalsis 0.05 Hz)	40 μW	1.6 cm × 1.2 cm × 2.5 mm	Surface treated PTFE & PDMS & Cu; CS
Zheng et al. 2016 [197]	Respiration (implant)	40 V, 1 μA	2 cm × 3 cm × 0.5 mm	Biodegradable PLGA & PCL & PVA & PHB/V; CS
Liang et al. 2017 [96]	Finger press	1.47 V, 3.9 nA	15 cm^2 × 0.2 mm	Recycled PVA & sodium alginate (dissolves in water); CS
Pan et al. 2018 [128]	Compression force 50 N 5 Hz	500 V, 17 μA	4 cm × 4 cm × 6 mm	Biodegradable PLA nanofiber & nanostructured gelatin; CS
Wang et al. 2018 [175]	Compression force	1.4 V, 9.5 nA	1 cm × 2 cm [c]	Kapton & Chitosan biopolymers; CS
Ouyang et al. 2017 [127]	Wrist (radial artery)	1.52 V, 5.4 nA	2 cm × 1 cm × 0.8 mm	Kapton & Cu; CS
Shi et al. 2016 [154]	Finger bending 90°	2.5 V, 3.5 nA	3.5 cm × 11 cm [c]	PDMS & water; Liquid LS

[a]Modes are abbreviated: CS = contact-separation, SE = single-electrode, FS = free-standing triboelectric layer
LS = lateral-sliding,
[b]Derived from 3.18 mJ × 1.75 steps/sec (estimated from 3 mph walking speed)
[c]Thickness not reported
[d]Estimated from supplemental figures and reported area
[e]Approximated from figure

analyze the application space and choose one or more harvesting methods to best meet those goals. Indeed, many hybrid structures have emerged that combine multiple conversion techniques to leverage the advantages and mitigate the challenges associated with each. For example, electromagnetic-triboelectric structures can output both very high currents and voltages, but at the cost of more complicated fabrication and materials [194, 69]. Another popular hybrid is combining a self-induced, voltage-producing transduction method with electrostatics to offer a self-biasing solution for the electrostatic capacitors [144, 31, 83].

Recalling that two important considerations are small form factor and convenient integration with electronics, the electrostatic transduction method becomes very attractive. Most of the demonstrated scavenging devices require wires and connectors to reach rectifying and power conditioning circuits, which adds size and potential failure points, and decreases efficiency. Additional connectors and components also create assembly and packaging problems. In contrast, the simple capacitive structures and materials required for electrostatic energy harvesting allows it to be fabricated side-by-side with CMOS circuits. Using the various metal layers available in traditional, commoditized CMOS foundry processes gives us the platform to create an energy harvesting module on the same silicon die as its rectifying circuit, power electronics, and application specific circuits. The development, design, analysis, and performance of integrated electrostatic energy harvesters will be discussed in the following chapters.

Table 2.9: Comparison of piezoelectric, electromagnetic, electrostatic, and triboelectric conversion methods

Methods	Advantages	Disadvantages
Piezoelectric	No external voltage required [39] Large power density [39] High voltage output [39] Macro and micro fabrication [39]	Requires accurate impedance matching [82] Material fatigue [15] Not compatible with standard CMOS Wide range of efficiency depending on material
Electromagnetic	High output currents [82] Long life span [82] Macroscale robustness [114] No external voltage required	Very low output voltages [39] Limited miniaturization [39] Difficult to integrate with other fabrication processes [18] Expensive materials [82] Strong damping forces [114] Works better at high frequencies [15]
Electrostatic	High output voltage [82] Easy to miniaturize [82] Inexpensive [82] Integrates easily with CMOS and MEMS fabrication	External voltage required [39] Parasitics reduce efficiency [15] Electrets suffer charge decay [21]
Triboelectric	Very high voltages [25] Higher efficiency in low-frequency range [1] Inexpensive materials [182] Wide variety of materials [42] Flexible and biodegradable	Susceptible to humidity, stability, and surface damage [98] Lifetime reliability uncertain [25] Electrification mechanism still not fully understood [182] Not compatible with standard CMOS

Chapter 3

Electrostatic Energy Conversion Design

Electrostatic transduction provides an opportunity to fully integrate an energy harvesting module with CMOS electronics. The foundation of an electrostatic energy converter is a variable capacitor. This variable capacitor generally consists of two conductive electrodes with a dielectric in-between. These materials are readily available in commoditized CMOS foundries in the form of metal traces traditionally used for electrical routing and dielectric insulation. Capacitors have long been fabricated alongside advanced CMOS circuits; however, an obstacle arises when the application requires one of these electrodes to be mobile.

Most common electrostatic energy harvesting techniques require one of the capacitive electrodes to move relative to the other, therefore influencing the overlap area or distance between the two plates to create a variable capacitor. This would not be possible with general CMOS chips without post-processing steps such as a MEMS release etch, which adds complication, processing costs, and could damage the sensitive circuitry. Instead, we consider taking the "moving" component of the capacitor off-chip completely, and leverage finger and body capacitance to influence the capacitive nodes that remain on chip. Similar to how capacitive touch screens work, as a finger approaches two capacitive plates embedded in the device, it influences the electric field and charge distribution across the electrodes. This effective variable capacitance will be the driving force behind the electrostatic energy harvester. This chapter will investigate the theory behind this phenomenon and present a circuit architecture to rectify this energy into useful electrical energy. Simulations of the device will also be discussed.

3.1   Human Body and Finger Capacitance

It has long been known that the presence of a human (hand, finger, etc) modulates electric fields in electronics. In the 1920s, this concept birthed the invention of the Theremin, an electronic musical instrument that uses the changing distance from the player's hands to an
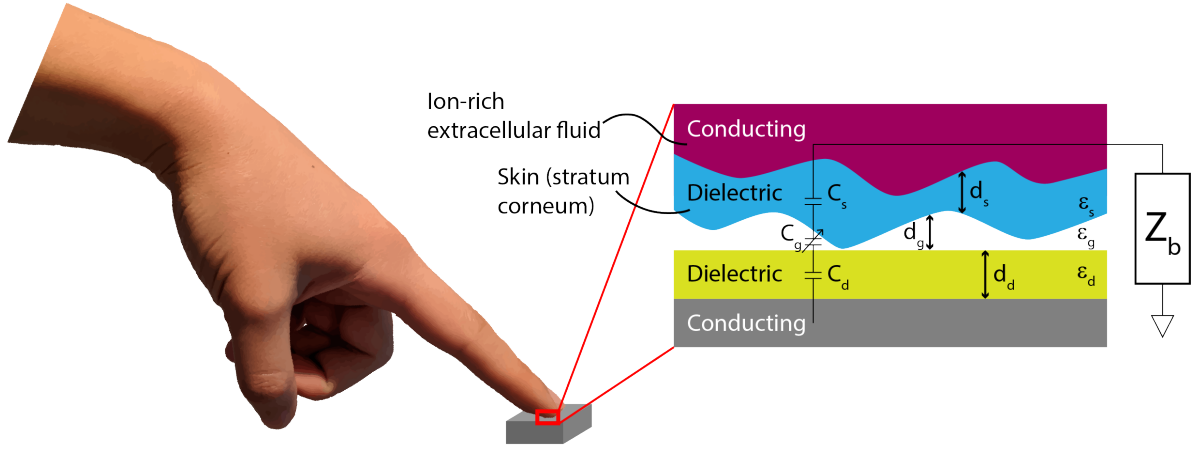
Figure 3.1: Finger on insulated electrode capacitive contact model.

antenna to tune the frequency of its notes [160]. As the performer's hands move through the instrument, it generates a variable capacitance in the system, which alters the frequency of the LC oscillator [48]. In the 1980s, as personal computing devices were emerging, researchers turned to this same finger capacitance effect as a way of creating touch sensitive devices, allowing the user to input data to these systems [87]. Now as devices continue to decrease in power consumption and increase in portability, this long-known phenomenon is applied to electrostatic energy harvesting.

Human skin consists of numerous layers of tissue, the outermost being the stratum corneum, which consists of cells that undergo the process of keratonization (or cornification) [38]. This outer layer of dead, dry, keratonin-filled cells is characterized by ridges and roughness that varies from person to person. In general, this skin qualifies as an insulator that encloses the ionic medium of the rest of the body [9]. This structure creates series capacitance with electrodes as seen in Figure 3.1. In addition to the capacitance of the skin, there are more complicated impedance pathways through the body (through capacitive cellular membrane structures, various degrees of ionic fluids, different impedance tissues, for example) [141] which are not discussed in detail in this thesis, but are lumped together into a single "body impedance" to ground.

Capacitive electrodes can be configured in many geometries and designs, but they generally fall into one of two categories: stacked electrodes and coplanar electrodes [109]. In the stacked mode, the two electrodes are manufactured as a stacked parallel-plate capacitor with dielectric in-between, therefore the electric field mainly exists inside the device. The finger makes contact with only the top active electrode through an insulating layer, and therefore adds a single gap capacitance and body impedance to ground. In the second mode, two
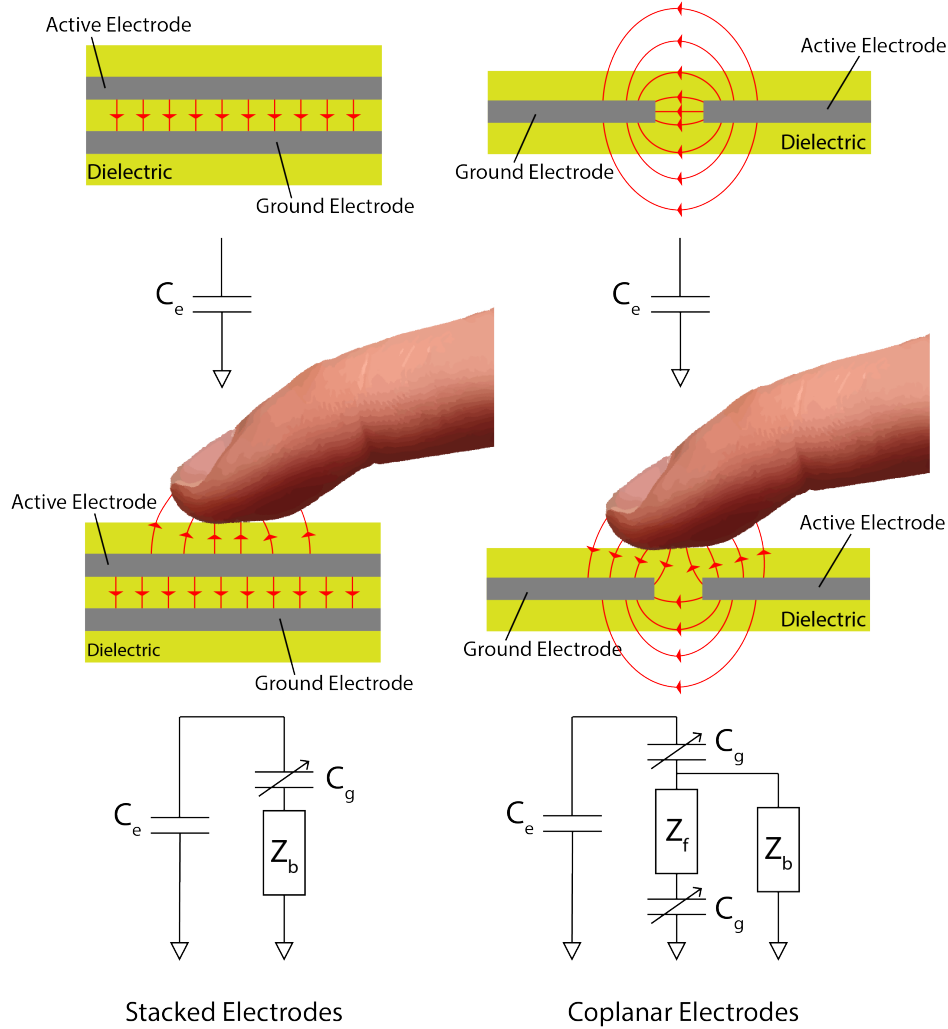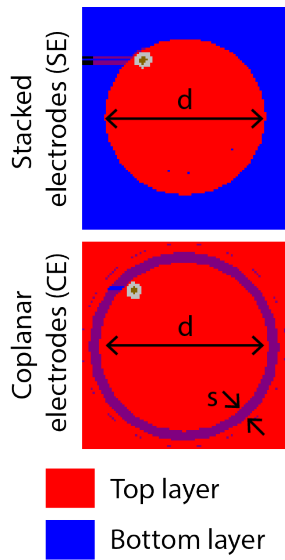
Figure 3.2: The effect of finger capacitance on two general electrode configurations: stacked electrode mode and coplanar electrode mode.

electrodes are fabricated side-by-side, and a significant amount of the electric field comes from the fringe field. The finger now makes contact to both the ground and active electrodes through an insulating layer. This adds the effect of two gap capacitances. Both of these modes are illustrated in Figure 3.2. Here C_e is the nominal capacitance between the electrodes, C_g is the capacitance of the gap between the finger and the electrodes, Z_f is the electrical impedance along the surface of the human finger, and Z_b is the impedance through the finger and into the body of the user.

In order to compare these two electrode configurations and understand the effect of a finger tap on the change in capacitance of fabricated electrodes, we designed a printed circuit

Mode	d [mm]	s [mm]	C_i [pF]	C_f [pF]	ΔC [pF]
SE	13.3	1.5	8.71	11.53	2.82
SE	11.3	1.5	7.85	10.89	3.04
SE	9.3	1.5	5.75	7.55	1.80
SE	7.3	1.5	5.36	6.85	1.49
SE	5.3	1.5	4.44	5.24	0.80
SE	3.3	1.5	4.04	4.35	0.31
CE	7.5	0.2	3.71	28.7	25.0
CE	7.5	1.0	3.44	31.1	27.7
CE	7.5	2.0	2.68	30.7	28.0
CE	11.5	0.2	4.31	57.6	53.3
CE	9.5	0.2	4.12	40.2	36.1
CE	7.5	0.2	3.71	28.7	25.0
CE	5.5	0.2	3.16	12.4	9.2

Table 3.1: Change in capacitance realized from a finger tap for varying size and space on PCB test structures.

board (PCB) with varying electrode sizes and spacings for both configurations. For the stacked electrode mode, we used the bottom layer of the PCB as a ground electrode, and the top layer as the active electrode. The dielectric in-between was FR-4, which had a dielectric constant of 4.4 and a thickness of 1.5 mm. The area of the active electrode was varied to determine how change in capacitance was affected by size. For the coplanar electrode mode, both electrodes were fabricated on the top metal layer. We used the same size active layers in both modes, and varied the space in-between the active and ground electrode. Because the thickness and properties of the top dielectric was an important variable to control, we drew solder relief masks over all the top layer electrodes so they were fully exposed. Upon receiving the PCB, we deposited 2 µm of parylene-C ($\varepsilon_p = 3.15$) over all the exposed electrodes to act as the top dielectric layer. Table 3.1 reports the change in capacitance measured for various dimensions.

The capacitance change observed from a finger tap on various electrode geometries ranged from 0.3 pF to 53.3 pF, depending on electrode configuration and size. The first six rows in Table 3.1 show stacked electrodes with the active electrode ranging in diameter from 13.3 mm to 3.3 mm. As expected, the change in capacitance consistently decreased with decreasing area of active electrode. The remaining eight rows demonstrate that the coplanar electrode configuration performed significantly better than the stacked electrodes. Again, we saw that an increase in active electrode diameter increases the change in capacitance. We also saw a weak positive relationship between spacing and change in capacitance. However, given a limited amount of space, it is better to maximize active electrode size at the expense of having a smaller gap. From these results we decided to pursue a coplanar electrode

configuration with small spacing between the electrodes. We also found that, due to the capacitive nature of the system, the effect of touch on capacitance was amplified by adding multiple capacitors in series. Although these results were not precisely representative of a variable finger capacitor in an integrated CMOS foundry process, which was our end goal, the trends in geometry should hold. Integrating these capacitors on-chip introduced new limitation on size, width, and spacing and used different electrode and dielectric materials. Still, these preliminary finger touch capacitance experiments demonstrated the ability to realize a change in capacitance from a finger tap. The next section discusses how to harvest useful electrical energy from this varying capacitance.

3.2 Electrostatic Charge-pump Circuit

The core of the electrostatic energy harvester was the change in capacitance that occurred when a finger approached a set of capacitive electrodes. In this section, we discuss an energy harvesting circuit which pumped generated charge onto an energy storage device. To understand the effect of the variable capacitance, recall some of the relevant equations from electrostatic conversion theory (Section 2.3):

$$Q = CV \tag{3.1}$$

$$\frac{dQ}{dt} = C\frac{dV}{dt} + V\frac{dC}{dt} \tag{3.2}$$

$$E = \frac{1}{2}CV^2 = \frac{1}{2}QV \tag{3.3}$$

Equation 3.1 defines the charge on a capacitor as a function of voltage and capacitance, equation 3.2 defines the current, or the change in charge over time , and equation 3.3 defines the total energy on a capacitor. We first consider a single standalone variable capacitor (Figure 3.3a) with an existing bias voltage across it. When the capacitance changes, then the voltage across the capacitor changes because the charge must remain the same. The resulting change in energy is summarized below, where subscripts i and f refer to the initial and final states:

$$Q_i = C_iV_i$$

$$Q_f = C_fV_f = Q_i = C_iV_i$$

$$V_f = \frac{C_i}{C_f}V_i$$

$$\Delta E = \frac{1}{2}C_fV_f^2 - \frac{1}{2}C_iV_i^2$$

$$\Delta E = \left(\frac{C_i}{C_f} - 1\right)E_i$$
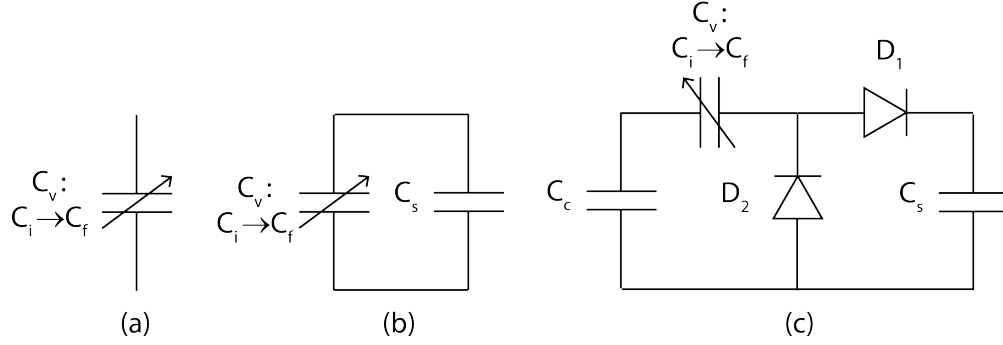
Figure 3.3: A variable capacitor in three configurations.

If this variable capacitance is now connected to an energy storage device, for example another static capacitor, C_s (Figure 3.3b), we can see the effect of a capacitance change on this system:

$$Q_i = C_i V_i + C_s V_i$$

$$Q_f = C_f V_f + C_s V_f$$

$$V_f = \frac{C_i + C_s}{C_f + C_s} V_i$$

$$\Delta E = \frac{1}{2} C_f V_f^2 + \frac{1}{2} C_s V_f^2 - \frac{1}{2} C_i V_i^2 - \frac{1}{2} C_s V_i^2$$

$$\Delta E = \frac{(C_i + C_s)(C_f + C_s)}{(C_f + C_s)^2} E_i$$

Although the charge in the whole system is still constant, there now exists a current, or dQ/dt, that moves charge between the two capacitors. Since the goal is to slowly charge up energy on the storage capacitor, we are particularly interested in the change in charge and energy on this element. We will refer to the charge and energy on the storage capacitor with the subscript $_s$.

$$Q_{s,i} = C_s V_i$$

$$Q_{s,f} = C_s V_f = C_s \frac{C_i + C_s}{C_f + C_s} V_i$$

$$\Delta Q_s = Q_{s,i} \left(\frac{C_i + C_s}{C_f + C_s} - 1 \right)$$

$$\Delta E_s = E_{s,i} \left(\frac{C_i + C_s}{C_f + C_s} \right)^2$$

Assuming an ideal system where the capacitors did not decay over time, this same amount of charge would be shuttled back and forth between the two capacitors with every finger tap.
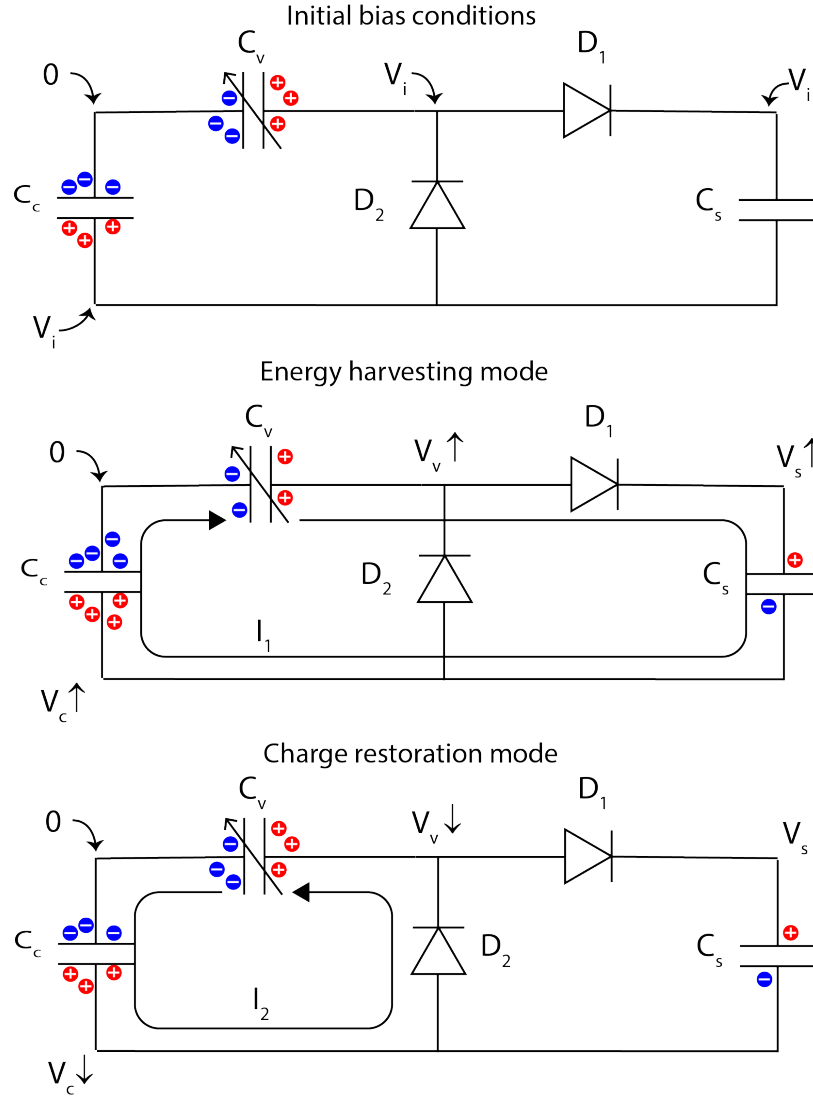
Figure 3.4: Electrostatic harvesting charge-pump circuit throughout a cycle of operation.

In order to charge up the storage device and keep the energy there, rectifying elements are needed. In addition, recalling that an electrostatic energy harvesting system requires an initial bias voltage, it will be important to ensure that this bias voltage is maintained and replenished when necessary. In order to achieve these two goals, we introduce two rectifying diodes, D_1 and D_2, as well as an initial capacitor charge supply, C_c, connected as shown in Figure 3.3c.

This charge-pump circuit can be analyzed in two phases of operation - an energy harvesting half-cycle and a restorative half-cycle - to correspond with the rising and falling edges

of the variable capacitor during a finger tap. Figure 3.4 illustrates the movement of charge throughout this cycle. During the energy harvesting mode, the voltage at the intermediate node between the variable capacitor and the diodes increases, which leads D_1 to turn on and conduct current in the direction of I_1. In restoration mode, the original charge is restored on the variable and initial charge capacitors following the current pathway of I_2 through diode D_2. The full cycle results in charge pumped onto the storage capacitor while maintaining the initial energy states of the initial charge and variable capacitors, C_c and C_v. This energy harvesting charge-pump circuit has also been used in applications for harvesting energy from ventricular wall motion [166], and scavenging energy from evaporation forces in synthetic leaves [14].

This charge-pumping harvesting circuit was simulated with Cadence Spectre Simulator and results are presented in Figures 3.5 and 3.6. The variable capacitor was modeled by a four-terminal voltage controlled capacitor element that varied linearly with control voltage, and simulated the change in capacitance from a tapping finger at 1 Hz. The diode was modeled after a commercially available off-the-shelf low-leakage diode (BAS116, Nexperia). Figure 3.5 illustrates how the variable capacitor influenced the voltage at the central node, V_v, which then forward biased either D_1 or D_2, depending on the edge of the capacitance change. This slowly shuttled charge onto the storage capacitor V_s, while maintaining the charge on the initial charged capacitor, V_c. Each finger tap added an additional 'step' to the staircase-like charge-up pathway of the storage capacitor. Due to parasitics in the system, the charge on the capacitors decayed over time, which was most apparent in the slow decline of the initial charge capacitor voltage. As with any electrostatic energy harvester, the system required periodic re-biasing. Finally, the total energy in the system E_{sys}, or the sum of the energies stored on all three capacitors defined as $E = \frac{1}{2}CV^2$, increased over time as the system harvested energy from the work done to modulate the variable capacitor.

Selecting appropriate capacitance values depends on the application and its requirements, including how quickly a high voltage must be reached and how often the system can be re-biased. Figure 3.6 demonstrates how the energy harvesting circuit performance can be affected by varying the parameters C_v, C_c, and C_s. Note that in these figures, one legend is presented in the V_s plots for each parameter, but this legend applies to all plots in that column. The first column looks at the effects of a changing variable capacitor, where the minimum capacitance value stayed constant at 1 pF, but the maximum value varied from 50 pF to 150 pF. This had the largest effect on the storage capacitor, which charged up faster with a larger change in capacitance. Ideally, we want the largest realizable change in capacitance, but this is limited by the area and size constraints of an application. The second column looks at varying the initial charge capacitor, C_c, between 100 nF and 10 µF. In an ideal circuit, this capacitance would not have any affect on the performance of the harvester. However, due to parasitics and resistive pathways to ground, the voltage on capacitors decayed over time leading them to require recharging. The largest possible capacitor here will increase the lifetime of the device between recharging, but will also require more energy to initially charge the capacitor to the same voltage. Finally, in the last column, the effects of the storage capacitor, C_s are presented over the range of 100pF to 10 nF.
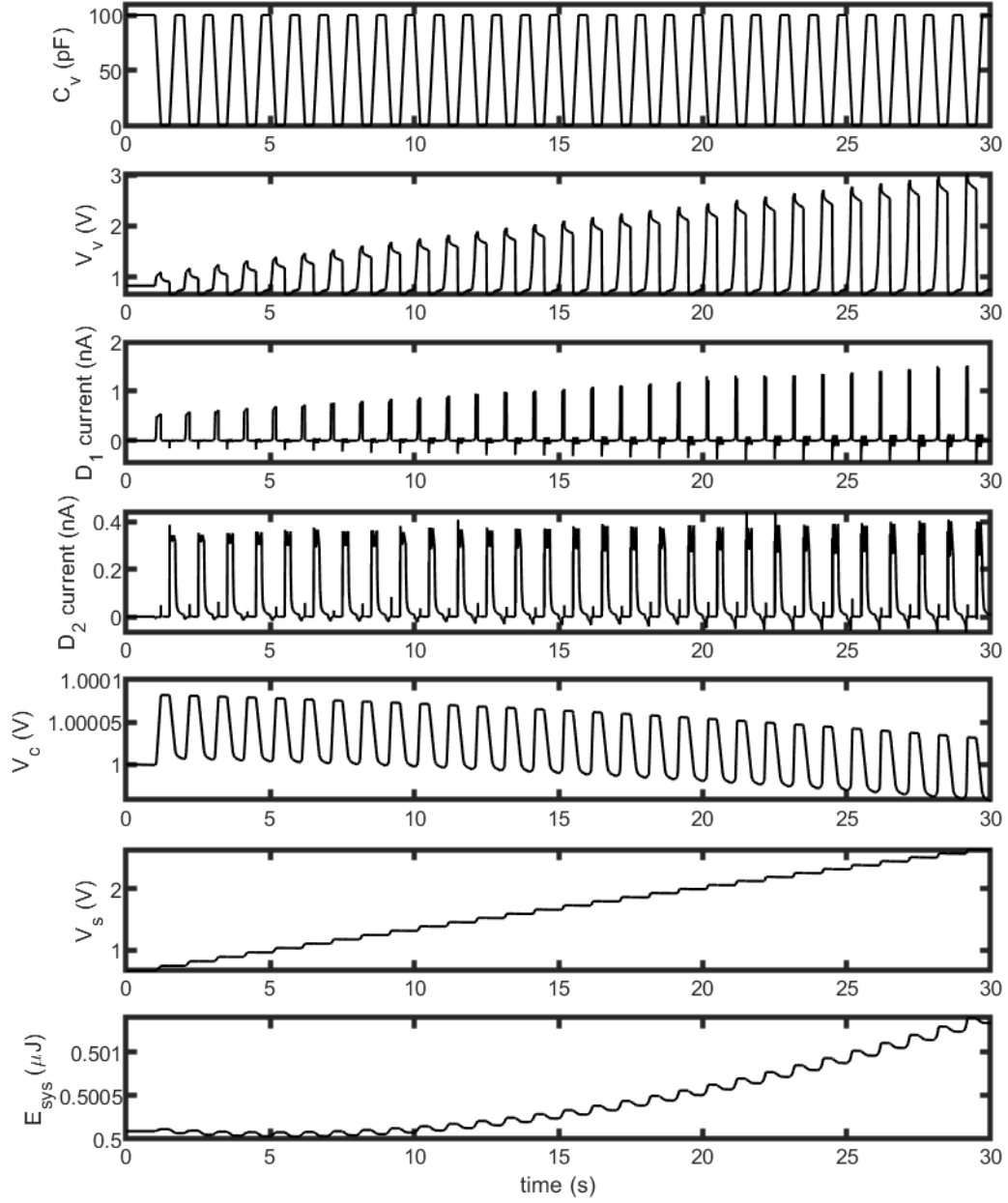
Figure 3.5: Charge-pumping harvesting circuit simulated results for a C_v ranging from 1 pF to 100 pF, $C_c = 1$ µF, $C_s = 1$ nF, and initial bias $V_i=1$.
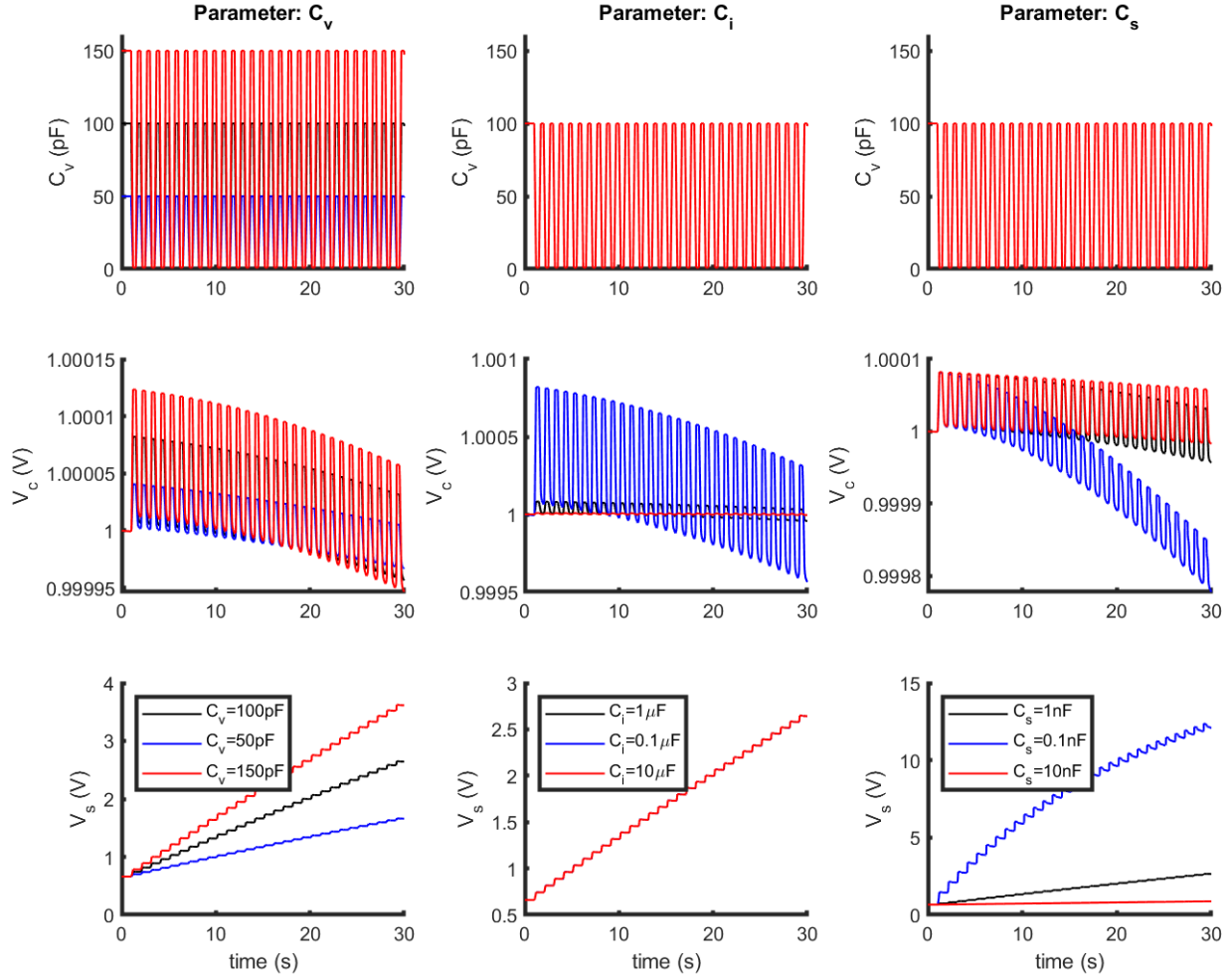
Figure 3.6: Charge-pumping harvesting circuit simulated results for varying C_v (left), varying C_c (middle), and varying C_s (right).

Since the same amount of charge pumped onto a smaller storage capacitor results in a larger voltage, reducing the size of this capacitor is the fastest way to harvest large voltages quickly. However, this effect also occurs when a load is connected and a small capacitor results in faster discharge times, possibly resulting in the voltage quickly dropping below useful values for electronics. As a result, this capacitor should be carefully selected so that a high enough voltage can be built up in a reasonable amount of taps, while storing enough charge so that it can power the load application for however long necessary. Similar to energy harvesters in general, there is not a one-size-fits-all solution and each element should be designed to fit the application's specific requirements.

In addition to mindfully selecting capacitors and diodes, incorporating a convenient bi-

asing scheme is also crucial. A couple design questions to consider here include:

(1) How often will the bias source be available?

(2) How long will it take to bias the system?

(3) What voltage is achievable?

Due to leakage in the system, the electrostatic capacitors will have to be occasionally re-biased. The biasing source should be available often enough to periodically bias the system throughout its lifetime. In addition, most biasing sources have limited bias currents and this affects how long it will take to recharge a system with a specified amount of capacitance. Finally, the voltage achievable affects how much energy can be harvested with each modulated capacitance. Three biasing solutions include periodically recharging with a battery or power supply, incorporating an electret, and integrating an additional harvesting module. The first option of recharging is the most inconvenient for the user and is particularly restrictive for users without reliable access to power. However, energy harvesting can be a useful feature for elongating the lifetime between recharging for devices which already have batteries. In testing our electrostatic energy harvester, this option was used to isolate the performance of the charge-pump circuit in the first PCB prototype. Recalling the goal of demonstrating a fully integrated single-silicon energy harvesting solution for electronics, electret materials cannot be fabricated with ASICs. As other researchers have discovered [144, 31, 83], integrating two harvesting techniques into a hybrid structure is effective in providing the initial bias on an electrostatic converter. Understanding the limitations of commoditized CMOS foundries, one ready-to-integrate harvester is the silicon p-n junction solar cell. Without process optimization and very limited space coupled with inconsistent access to strong solar radiation, on-chip solar cells in CMOS processes often perform suboptimally and generate open-circuit voltages below threshold voltages of electronics. Integrating a small on-chip solar cell will allow for the slow trickle charge biasing of our system when light is available, even at low-levels. The electrostatic energy harvester steps up this energy to useful voltages through the charge-pump circuit described here. In the next chapter, we will present a PCB prototype of the energy harvesting system before diving into the discussion of the application specific integrated circuit (ASIC) chip.

Chapter 4

An Off-the-Shelf Harvester Prototype

This chapter includes content adapted with permission from the following paper:

"Charge pumping with finger capacitance for body sensor energy harvesting" by A. Y. Zhou and M. M. Maharbiz [202]

A perennial obstacle to realizing the deployment of the billions of IoT devices expected in the coming years is power. As established in Chapter 2, one promising solution to power devices on and around the human body is energy harvesting from kinetic human motion. Specifically, finger gestures, such as tapping, is a natural means of communication with devices, and can also generate on-demand energy during use. Our goal is to produce a complete, operational energy harvesting system integrated with CMOS electronics. Before designing a custom ASIC for this purpose, a printed circuit board (PCB) prototype was fabricated with commercial off-the-shelf (COTS) components. The capacitive electrodes to sense the variable finger capacitance were fabricated directly on the PCB. This prototype also offers an alternative energy harvesting solution for users who may not have access to semiconductor foundries but would like to incorporate an electrostatic generator on their boards.

In this chapter, we discuss a system that transduced the kinetic energy of a human finger to electric energy through electrostatic charge pumping. Finger proximity altered the electric field between capacitive electrodes (metal traces) on a PCB, producing a change in capacitance, ΔC. This resulted in a current which was rectified through the energy scavenging circuit presented in Section 3.2. This system harvested 2 nJ per finger tap and, as an example application, powered a light emitting diode (LED).

4.1 System Materials and Design

Variable Capacitor Design and Theory

Similar to the finger capacitance test PCB board discussed in Section 3.1, the capacitive electrodes were fabricated on board using standard metal traces. Instead of using a circular
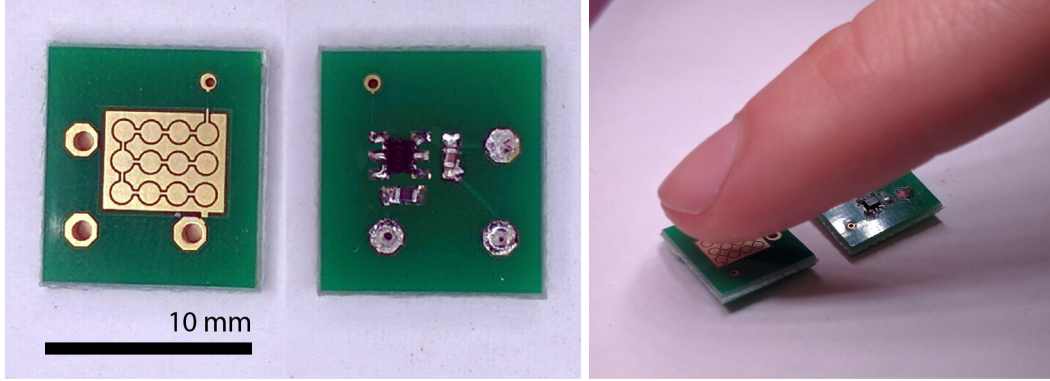
Figure 4.1: The front and back of an electrostatic energy harvesting PCB. On the front, a 6×5 mm^2 array of ENIG gold coated traces act as the variable capacitor electrodes. A finger approaching this grid interrupts the electric field and modulates the effective capacitance seen at the electrode nodes. The backside houses the electrical components of the energy harvesting circuit

button, we designed a meandering active electrode to increase finger capacitive effects. We fabricated this version with smaller than standard spacing (100 µm) between the electrodes to maximize active electrode area. This variable capacitor electrode consisted of a coplanar array of circular electrodes with 500 µm radius and 100 µm gap between the active and ground plates. Twelve of these capacitors were connected in parallel with 350 µm between each node, forming a 3×4 array. The entire sensor array measured 6×5 mm^2, comfortably fitting in the area under a pad of a finger. The electrodes were finished with ENIG gold to protect the copper from oxidizing and creating an additional dielectric layer. The electrodes were exposed without soldermask, and then coated with 2 µm of parylene-C in-house at the Berkeley Marvell NanoLab. The capacitors were fabricated on standard FR-4 circuit board material. The backside of the system housed the components that made up the electrostatic charge-pump circuit. Due to the required margins in fabrication and vias for wire connections to test equipment, the entire device measured 1×1 cm^2 (Figure 4.1).

Energy Scavenging Circuit

The energy scavenging circuit (Figure 4.2) applied in this PCB prototype was a modified version of the one presented in Section 3.2. The initial charge bias was introduced by manually connecting the system to a power supply through SW_1, and periodically recharging the initial charge capacitor, C_c. After the charge capacitor reached the desired initial voltage, the power supply was disconnected from the system. Then, as a finger tapped on the variable capacitor, C_v, it modulated the voltage at node V_1 which then conducted charge through diode D_1 or D_2 depending on which phase of the cycle the variable capacitor was
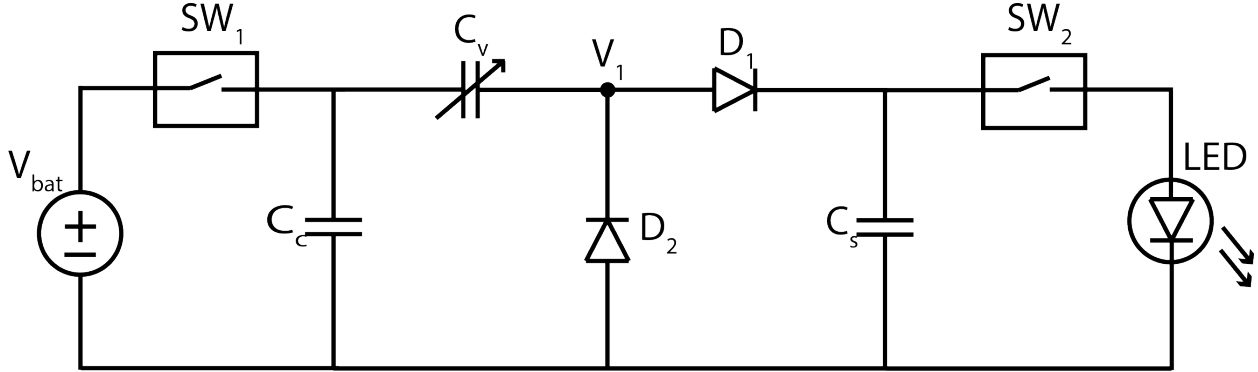
Figure 4.2: Schematic of energy harvesting circuit for the application of flashing an LED

moving through. Current through D_1 deposited charge on the storage capacitor C_s, which slowly accumulated this charge and built up its voltage. During this finger tapping charging period, no load was connected and we saw the effects of the energy harvesting circuit without compensating for a load current. As an example application, a push-button mechanical switch (SW_2) was connected to the storage capacitor, and when pushed dumped the charge across an LED and lit it up.

The components of this energy harvesting system were soldered onto the backside of the capacitive electrode traces. Two low-leakage rectifying diodes were mounted alongside two ceramic capacitors for the initial charge and storage capacitors. All components were commercially available and include two silicon low leakage diodes (Diodes Inc, BAS116V) and ceramic capacitors (TDK Corporation, C10-AC01-E3-KIT, $C_c = 1\ \mu F$ and $C_s = 10\ nF$).

Analysis of Devices

Simulations of the energy scavenging PCB were performed with Cadence Spectre Simulator. The ΔC of the electrode array was measured using a Hewlett Packard 4428A LCR meter. Voltages were measured by buffering the nodes of interest with an ultra-low input, externally powered current amplifier (Texas Instruments, LMC6001) and recorded with either an Agilent 34401A digital multimeter or a Keithley 2400 sourcemeter. For the application, an LED (Rohm Semiconductor, SML310LT) was connected to the circuit through a physical push-button switch (Mini Pushbutton Switch, Sparkfun). To determine power harvested from the scavenging circuit without interrupting the system with measurement devices, a silicon photodiode (OSI Optoelectronic, S-10C) was placed near the LED to measure the intensity of light emitted. The current of the photoreceptor was measured with a Keithley 2400 Sourcemeter.
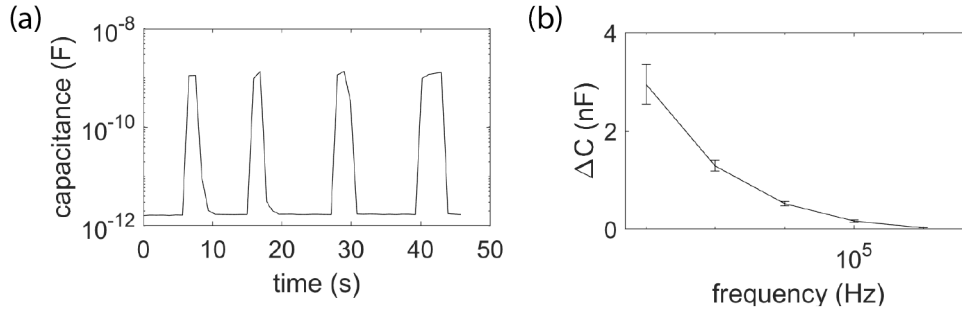
Figure 4.3: The effect of a finger tap on PCB capacitive electrodes as a function of time at 1 kHz (a), and frequency (b).

4.2 PCB Energy Harvester Performance

Finger effect on capacitance

The energy scavenged in our system was dependent on the ΔC realized by the variable capacitor, C_v. Figure 4.3a demonstrates the ΔC over time resulting from a slowly tapping finger sampled at 1 kHz. The capacitance increased from a nominal 1.7 pF to 1.5 nF. This 1000x increase in capacitance was consistent with measured finger capacitances on paper electrodes [109], and was 7-10x the variable capacitance reported from microfluidic-enabled energy harvesting [14, 190]. The ΔC varied with measurement frequency, as shown in Figure 4.3b. As frequency decreased, the capacitance increased non-linearly and the variation of capacitive readings also increased. Capacitance at low frequencies could not be precisely measured due to limitations of the LCR meter, but were extrapolated, resulting in a C_{max} of 6 nF at DC. This frequency dependence of the effect of finger proximity was expected as the charge re-distribution caused by a human finger is frequency dependent [186]. Most human biomechanic energy harvesting systems operate at relatively low frequencies [99] with respect to changes on the scavenging circuit.

Cadence Spectre Simulation Results

Using the finger capacitive effects discussed in the previous section, the expected performance of the energy harvesting circuit was simulated (Figure 4.4). Specifically, we modeled the variable capacitor with a $C_{max} = 2.9$ nF and a $C_{min} = 1.5$ pF. The rise and fall times were set to 1 second. The other components were defined as $C_c = 1$ µF, $C_s = 10$ nF, and $V_i = 5$ V. With each tap, the current through the variable capacitor was rectified by D_1 and charge was transferred to C_s, resulting in a step increase at V_{out}. The current passing through D_1 decreased with subsequent taps due to the charging of V_{out}, which decreased the forward bias voltage across the diode. This limited the voltage C_s could be charged to.
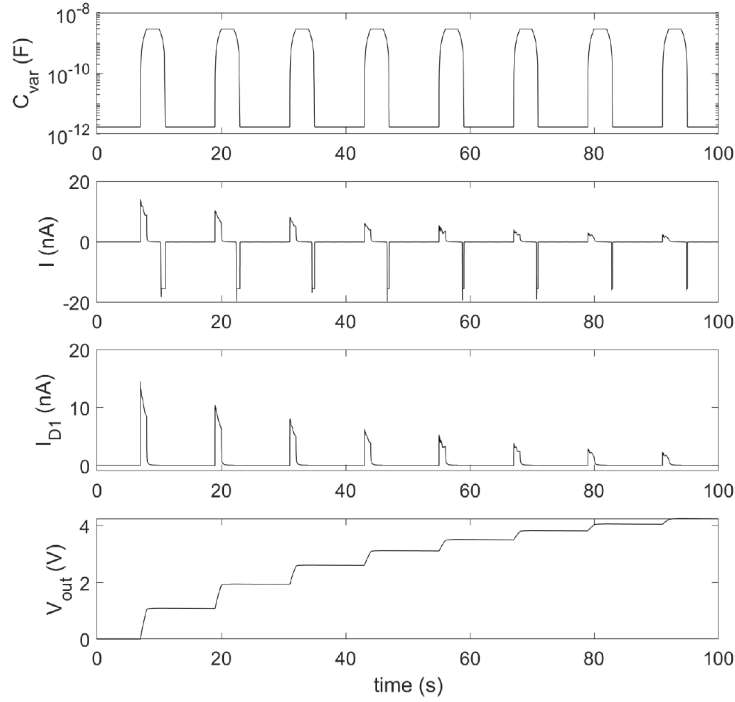
Figure 4.4: Simulation results for the energy scavenging circuit for the PCB prototype.

If more energy is required, the system could (a) pre-charge C_c to a higher V_i or (b) use a larger C_s. Option b enables larger energy storage at the same voltage, but also requires a longer time to charge up. These tradeoffs must be considered when designing an energy harvester for a specific application. In addition, it was shown that with the arrangement of diodes in the energy harvesting circuit, the negative ΔC does not discharge C_s. From these simulations, taps on a discharged storage capacitor resulted in 5 nJ of harvested energy.

Measured Energy Harvesting Results

An example of measured system operation is illustrated in Figure 4.5. Voltages at the nodes V_i and V_s were measured and plotted against their expected values. Each finger tap contributed to the staircase charging pattern of the storage capacitor. Unlike the simulations, there was much more variability in the energy harvested from each tap because human error made it difficult to identically reproduce the same ΔC. In addition, the measured V_{out} saturated at a maximum voltage below the simulated value, most likely due to losses in V_i. There was more rapid decay in the voltage across C_c, due to parallel resistances to ground not adequately represented in the simulation. Due to these losses and finger variability, the
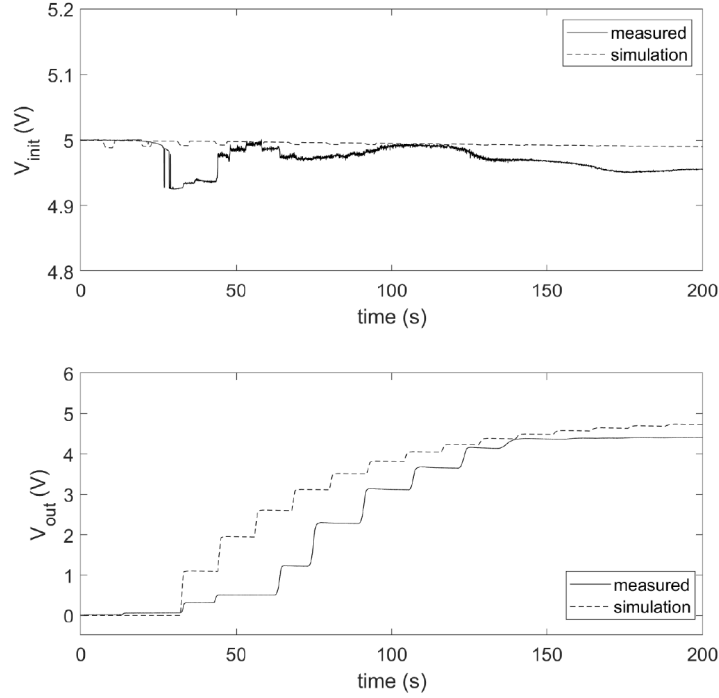
Figure 4.5: The measured and simulated voltages on the initial charge capacitor, V_{init}, and the ouput storage capacitor, V_{out}.

actual energy harvested was 2.0 ± 1.9 nJ per tap for the first eight taps, before it saturated at $V_{max}=4.3$ V.

4.3 Application: Powering an LED

As proof of concept for powering applications, we repeatedly powered a LED with the energy harvesting system. First, we connected the pushbotton switch (SW_2) and LED to the storage capacitor C_s. Using a multimeter, we measured the voltage profile on C_s (Figure 4.7a). Each tap pumped charge onto the storage capacitor, and after a series of taps, SW_2 was closed and charge was dumped onto the LED. During this time, the LED lit up and we saw the voltage on the storage capacitor decay until it reached 1.2 V. This cycle was repeated to power the LED six times. Later cycles required more taps to reach similar storage capacitor voltages because of decay in the initial charge capacitor.

In a separate experiment, we used an electrically isolated photodetector circuit to measure the power delivered to the LED to ensure there was no current injection or leakage into
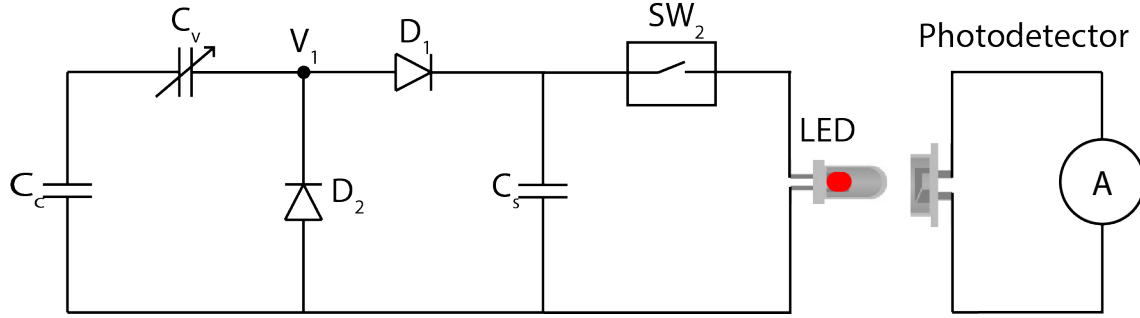
Figure 4.6: Experimental measurement circuit to indirectly determine the power delivered to an LED by measuring the current collected at a photodetector.

the system from the buffer or multimeter (Figure 4.6). This separate circuit consisted of a photodetector and ammeter, and experiments were performed in a dark box. The photocurrent generated by the photodetector was proprotional to the intensity on the incident light [115]; and that intensity was, to first order, proportional to how much power was drawn through the LED load [76]. We measured the current of the photodetector and extrapolated the intensity of the LED over a 500 second time frame (Figure 4.7b). Each spike seen in this figure represented one instance of the switch closing and the LED lighting up. The spikes decreased in both intensity and frequency over time due to decay of charge in the system. Light pollution through cracks in the dark box resulted in non-zero background intensity. During these 500 seconds, approximately 2.5x more useful power was harvested for the LED than initially present in the system at start-up (p<0.01). Figure 4.7c illustrates the power extracted normalized against the power initially input when charging V_i to 5 V (n=5). This demonstrated the system's ability to harvest energy from tactile motion to periodically power a load.

In this section, a PCB prototype of a finger capacitive energy scavenger capable of harvesting 2 nJ per finger tap was demonstrated. An LED was used to demonstrate operation and confirm that energy scavenging was occurring. Two additional components are needed to make this a stand-alone system: (a) a very small charge source to provide the initial voltage on the initial capacitor and (b) an electronic switch between the storage capacitor and the circuit to be powered. The charge could be provided with dielectric-trapped charge devices (electrets), or a small photovoltaic (which alone would be unable to power the system). This second option can be fabricated alongside integrated circuits. The system thus lends itself to monolithic integration with an ASIC or assembly as a mm-scale flexible system. The following chapters dive into the miniaturization of this system and a custom ASIC for energy harvesting.
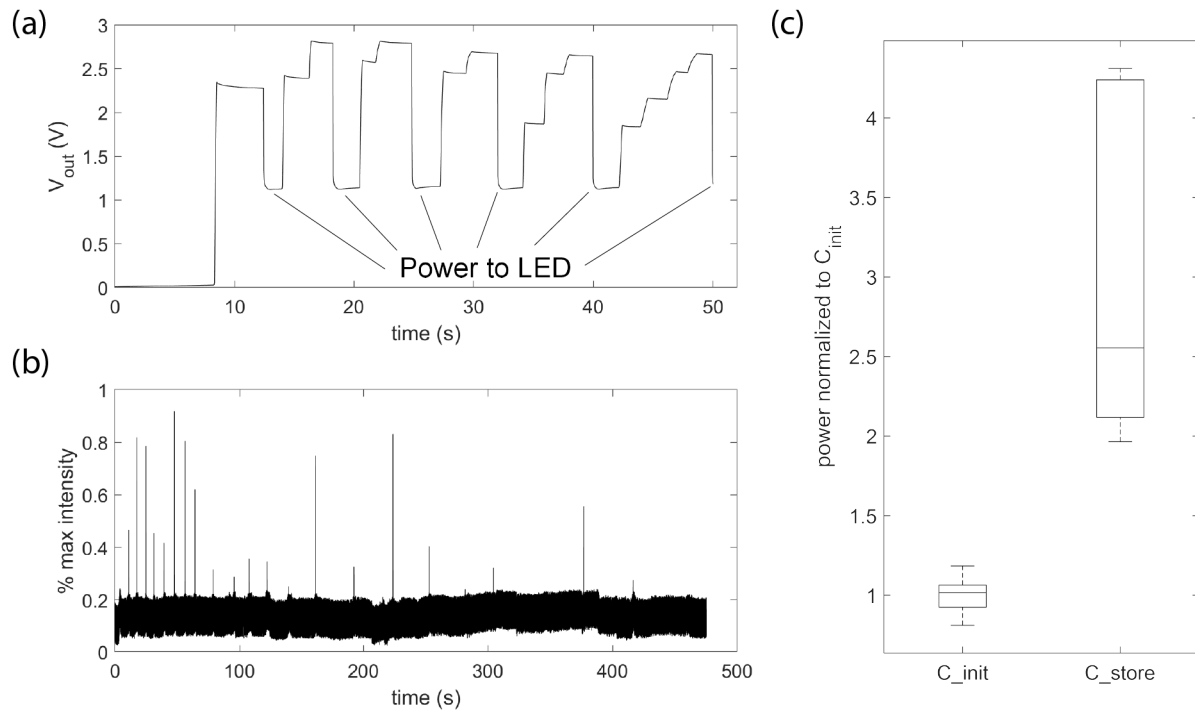
Figure 4.7: The PCB energy harvesting prototype delivering power to an LED. The voltage at the storage capacitor charged up with finger tapping, and discharged when the LED was connected (a). The intensity of the LED measured through an electrically isolated photodetector circuit (b), and this intensity corresponding to 2.5x additional power extracted from finger tap energy harvesting (c).

Chapter 5

Electrostatic Energy Harvesting ASIC

This chapter includes content adapted with permission from the following paper:

"Charge-pumping with finger capacitance in a custom electrostatic energy harvesting ASIC" by A. Y. Zhou and M. M. Maharbiz [203]

The growth of Internet-of-Things (IoT) systems and shrinking consumer electronics has generated a demand for battery-less power sources, and harvesting energy from human motion can be particularly useful for wearable sensors or interactive electronics. As discussed in Section 2.5, we focused on electrostatic energy conversion due the ease with which these systems can be manufactured and, importantly, co-fabricated with commoditized integrated circuits (ICs). Most other energy harvesters use piezoelectric, magnetic, or triboelectric materials which are not available in traditional, commoditized CMOS foundry processes. As a result, delivering power from these harvesters to power management and device electronics requires additional integration steps which can be costly and inconvenient. An important requirement of body energy harvesting is that the device is unobtrusive to natural motion, so additional wires and interconnects are undesirable as they can increase weight and size, while also reducing reliability and efficiency. Electrostatic harvesting requires only a variable capacitor which is readily incorporated into existing standard fabrication processes, allowing the energy harvesting module and electronics to be present on a single silicon die.

In this chapter, we leverage these advantages of electrostatic generators and present a custom application specific integrated circuit (ASIC) chip with built-in finger-capacitance energy harvesting capabilities on the same silicon die. As a finger approached the device, a change in capacitance was detected by two nodes of the ASIC. These changes fed into a rectifying charge-pump circuit which stored the energy on a capacitor. Once enough energy had been harvested and the capacitor reached the threshold voltage of a gating switch, downstream circuits were triggered and powered. We demonstrated switching on and powering a ring oscillator (RO) as a stand-in for generic blocks like a low power burst emitter or timing circuit.

Table 5.1: Key system dimensions

Parameter	Value
Total capacitive area	11.3 mm^2
Circuit active area	0.2 mm^2
Solar cell area	0.15mm^2
Bond pad area (single)	0.01mm^2
Total die volume	3.9mm^3

5.1   ASIC Overview

The ASIC, illustrated in Figure 5.1, consisted of five main components: (1) top level capacitive metal traces, (2) bond pads, (3) dielectric, (4) lower level metal interconnects, and (5) active area, which were fabricated on a bulk silicon substrate in a standard 0.18 µm CMOS process. The key dimensions of these components are listed in Table 5.1. The top level capacitive metal traces were fabricated in metal layers three through six, while the first two metal layers were reserved for routing between the active circuit components. The process included insulation between all the metal traces which also served as the dielectric for the finger-sensitive capacitor. As a finger approached the chip, it modulated the electric field between these metal traces, which created the transient changes in capacitance used to drive the energy harvester. The full implemented circuit is presented in Figure 5.2. A solar cell provided the initial biasing in the system, and this energy was amplified by the charge-pump circuit driven by the variable capacitor. Energy accumulated on the storage capacitor, C_s, until it reached the turn-on threshold of the switch, at which time a ring oscillator load was turned on and output a series of chirps. In the following sections we discuss the design and characterization of each component of this ASIC, and the system energy harvesting performance is discussed in Chapter 6.

5.2   Integrated Capacitor

The variable capacitor is pivotal to an effective electrostatic energy harvesting device. Because a capacitor is essentially two conductive electrodes with dielectric in between, we leveraged the top metal layers of a standard CMOS process to create the nodes for this variable capacitor. Learning from the trends in electrode geometries in the PCB test boards presented in Section 3.1, we strived to maximize active electrode area. However, integrating with commoditized CMOS processes had its limitations. For example, the reticle area for any process limited the absolute maximum size the lithography tools could pattern and etch, which in turn limited the maximum area of design for a single-chip device. Moreover, since pricing scaled with area, cost was often a limiting factor influencing the maximum area of the variable capacitor electrodes. In this specific case, our access to a 0.18 µm process was limited to a maximum chip size of 5 × 5 mm ^{2} of area, which was shared between three
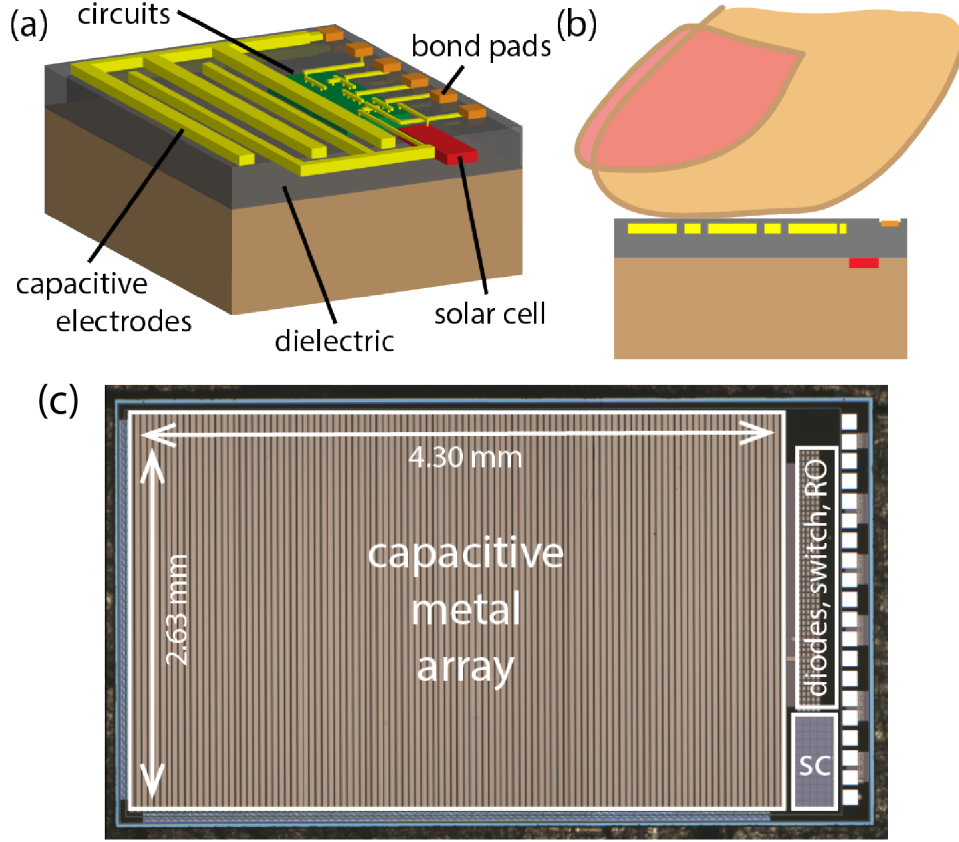
Figure 5.1: Custom ASIC with integrated electrostatic energy harvesting. (a) Model of the ASIC. (b) Representation of how a finger interacts with the cross-section of the ASIC during energy harvesting. (c) Chip die photo.

different research groups.

In terms of design limitations, each technology node also specifies its own line width and spacing rules which ensure lithography and etching are executed correctly. This delineated the minimum and maximum size of our electrode fingers as well as the gap between them. The thickness of metal layers and dielectrics were also defined for each process, which determined the thickness of the electrodes and the dielectric gap between multiple layers. Designing within these rules, we defined an interdigitated array of metals traces following the parameters in Table 5.2. This structure was designed in the top four metal layers (M3-M6), whereas the first two layers were reserved for connective routing for the circuits. All the metal layers of the capacitive traces were electrically connected together using contact vias and encased in the process's inter-level dielectric (Figure 5.3).

During operation, a finger tapped aperiodically on the ASIC and influenced the effective capacitance seen at these top level metal traces. These capacitance changes were measured
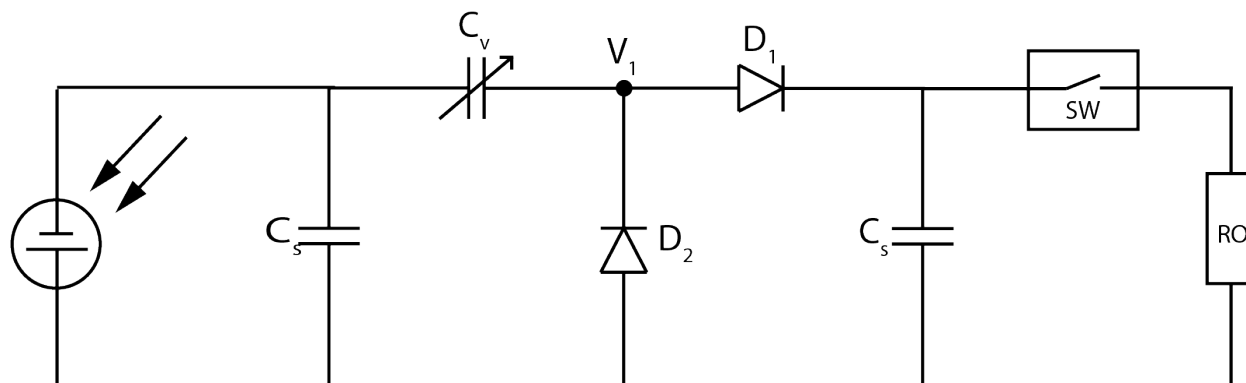
Figure 5.2: Energy harvesting rectifying charge-pump circuit with solar cell bias and ring oscillator load implemented on an ASIC.
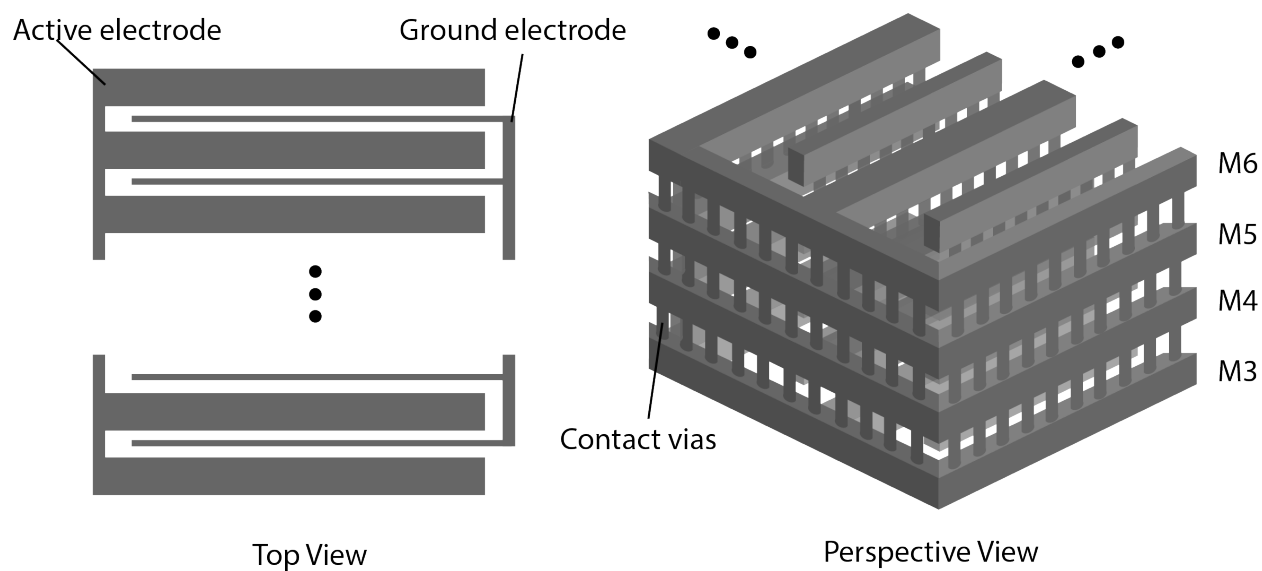
Figure 5.3: Top and perspective cartoon view of the integrated variable capacitor electrodes designed in the metal three through six layers of a CMOS process.

Table 5.2: Interdigitated variable capacitor electrode parameters

Parameter	Value
Total capacitive area	11.3 mm^2
Width of active fingers	35 μm
Width of ground fingers	2 μm
Length of fingers	2.6 mm
Gap between fingers	2 μm
# of fingers on ground electrode	104
# of fingers on sense electrode	105
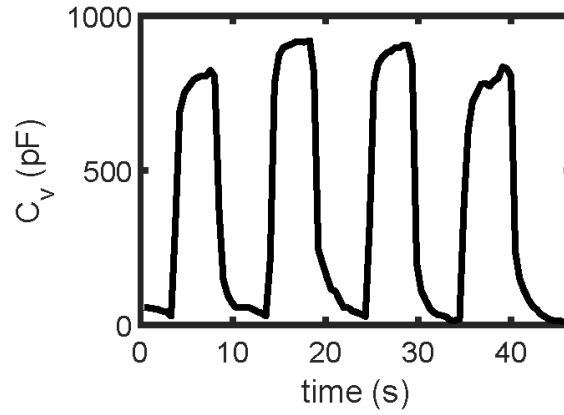
Figure 5.4: Capacitive response of integrated ASIC electrodes to a finger tap.

with an LCR meter (Keysight E4980a) and are shown in Figure 5.4. The nominal capacitance of the electrodes was 103 pF, and each finger tap resulted in an increase in capacitance to 825-920pF. As with any human interactive device, we saw a wide range of resulting capacitances since these changed with finger placement, timing, and operating conditions, such as dirt and sweat. For designing and analyzing our proof-of-concept system, the average value of C_{max}=870 pF was used in all simulations.

5.3 Integrated Solar Cell

A well-known disadvantge of electrostatic energy harvesting is the requirement for an external power supply to initially bias the entire system. Although there were various ways to address this challenge, including the addition of electrets, piezoelectrics, or triboelectrets, these solutions were not fully compatible with commoditized CMOS foundry processes. Instead, we introduced a very small integrated solar cell module that provided the initial bias voltage across the capacitors. In order for light to reach this p-n junction diode, we removed
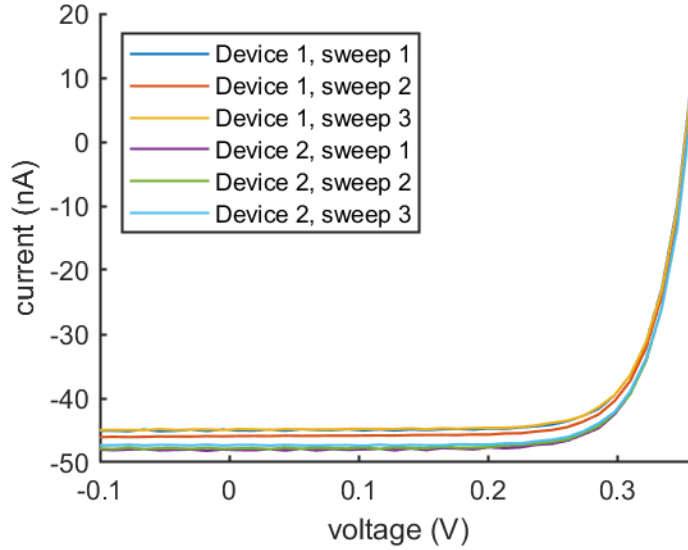
Figure 5.5: Integrated solar cell IV curves under indoor fluorescent lighting.

all metal (with the exception of contact traces) from above the area of the diode. The total solar cell area was 0.15 mm². Under indoor fluorescent lighting, which represented expected operating conditions, we characterized the solar cell with a short circuit current of approximately 47.5 nA and an open circuit voltage of 0.35 V (Figure 5.5. This solar cell provided charge for the initial bias in the system.

The initial charging of the energy harvesting system by this solar cell was simulated using the model of a current source and diode. As illustrated in Figure 5.6 the solar cell charged up the initial capacitor relatively quickly over 5 seconds. Due to the weakly forward biased diodes, the current through them was limited and the rest of the system took longer to charge up. An ideal system with ideal capacitors would be charged to the same voltage of the initial capacitor in approximately one minute. However, the parasitic resistances in parallel with the capacitors reduced this voltage. Although this initial bias was important to how much energy was harvested with each fingertap, even a small bias voltage was amplified through electrostatic harvesting to useful voltages on the storage capacitor.

5.4   Rectifying Diodes

After establishing initial charge across the variable capacitor, each tap created a small amount of charge movement. This charge fed into the rectifying charge-pump circuit presented in Figure 5.2. During a charging cycle, the voltage at V_1 increased; this turned diode D_1 on and pumped charge onto the storage capacitor C_s through a "clockwise" current
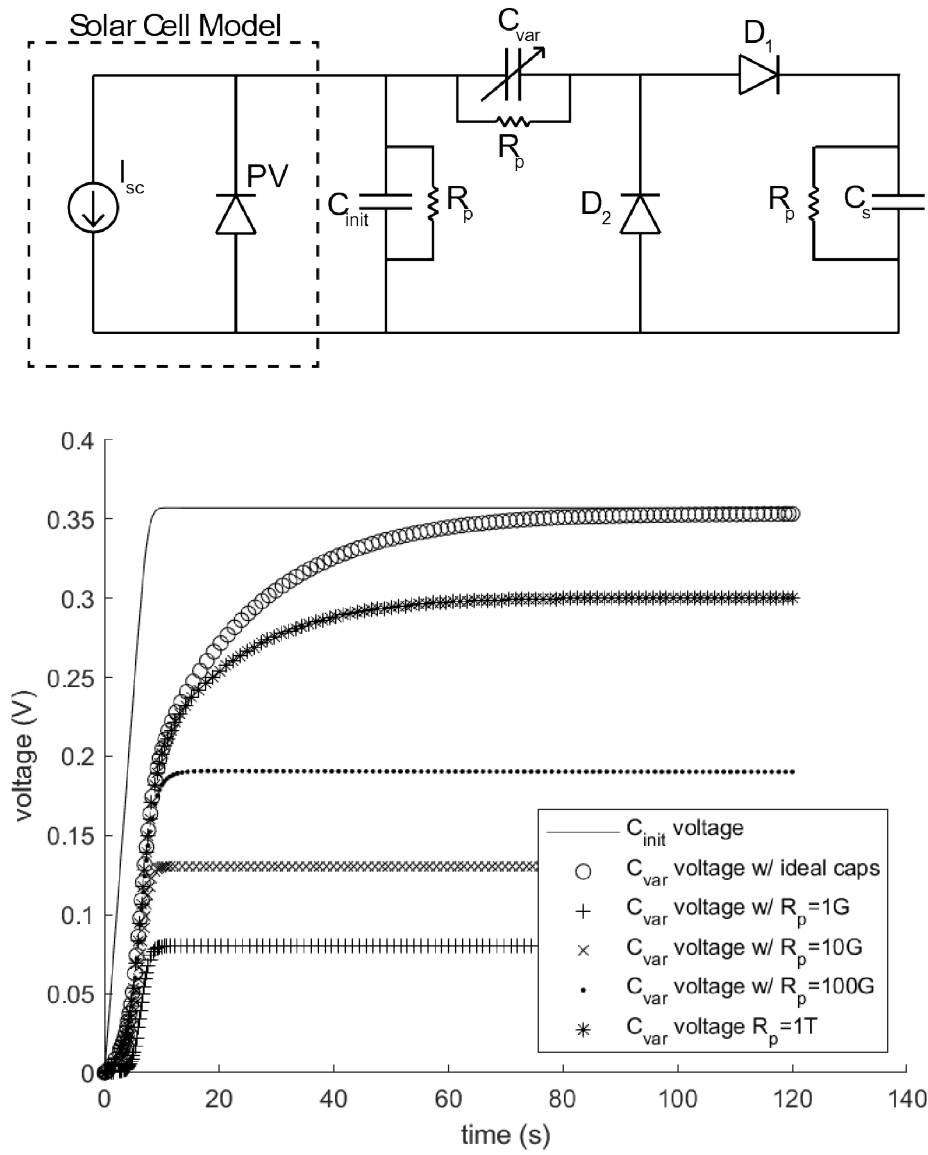
Figure 5.6: Simulation of integrated solar cell biasing the energy harvesting circuit.
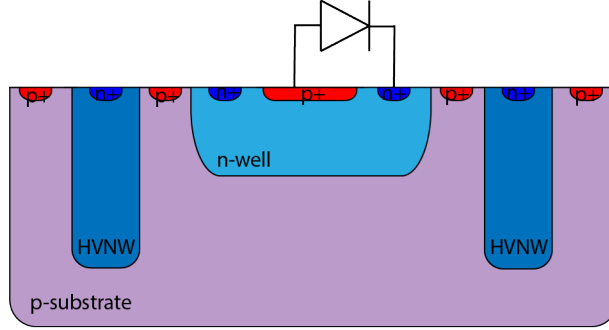
Figure 5.7: Diode isolation structure.

pathway. On the opposing edge of the variable capacitor, V_1 decreased; this restored the initial capacitor, C_c, and variable capacitor, C_v, to their original states via charge transferred through diode D_2 and a "counterclockwise" current pathway. To ensure minimum leakage in the rectifying circuit, both diodes were isolated with high-voltage (deep) n-wells (Figure 5.7). We used the standard high-voltage p-n diodes available in our technology node.

The simulation of the energy harvesting performance updated with these specific diode models and expected capacitance changes (from Section 5.2) are presented in Figure 5.8. These simulations were performed assuming a leisurely tapping speed of ~25 taps per minutes. As expected, charge was deposited on the storage capacitor on each finger tap, which increased the voltage on the storage capacitor in a stair-case like pattern. We expected the output voltage across the storage capacitor to reach 1.2 V after one minute of tapping. As a result, the total energy in the system, defined by the sum of all energies across the three capacitors ($E = 1/2CV^2$), reached 45 nJ.

5.5   Ring Oscillator

To demonstrate the energy harvester powering an on-chip circuit application, we implemented a diode-connected MOSFET switch connected to a 17-stage ring oscillator (RO). The switch was simulated to have a trigger voltage of 650mV. In order for the system to harvest enough energy to surpass this threshold without having to tap multiple times, we reduced the storage capacitor to C_s=10 pF. This allowed the system to recognize the energy harvested and trigger the RO once per tap, creating a self-powered touch sensor. Once the voltage threshold was surpassed, the RO ouput a chirp, the frequency of which depended on the storage capacitor voltage. Figure 5.9 presents the output frequency and power consumption of the RO as a function of voltage. With these calibration curves, we deduced the voltage on the storage capacitor and power consumption of the system from the measured RO outputs. This ensured no charge was lost or gained at the storage capacitor node due to connection to measurement equipment.
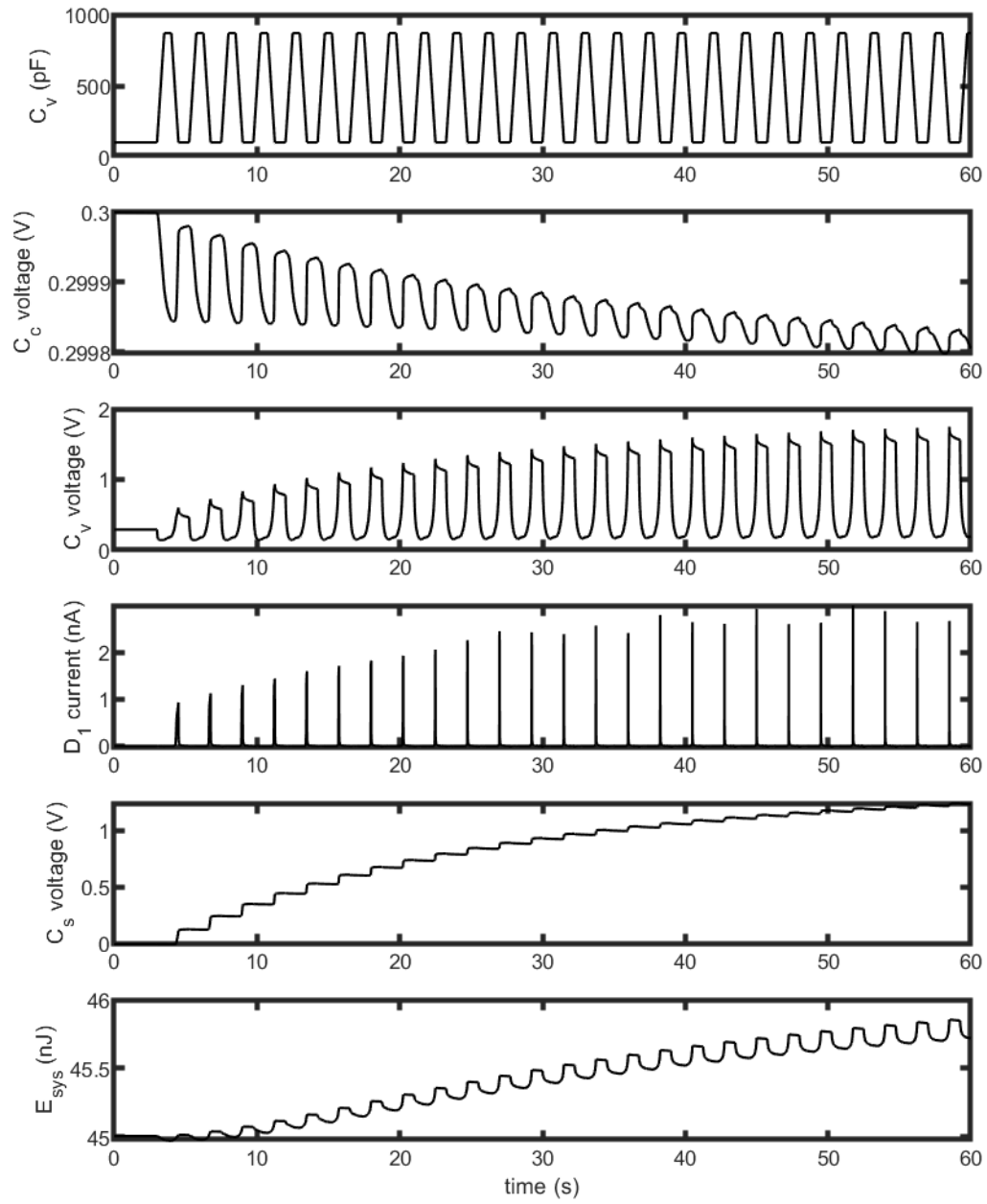
Figure 5.8: Custom electrostatic energy harvesting ASIC simulation results.
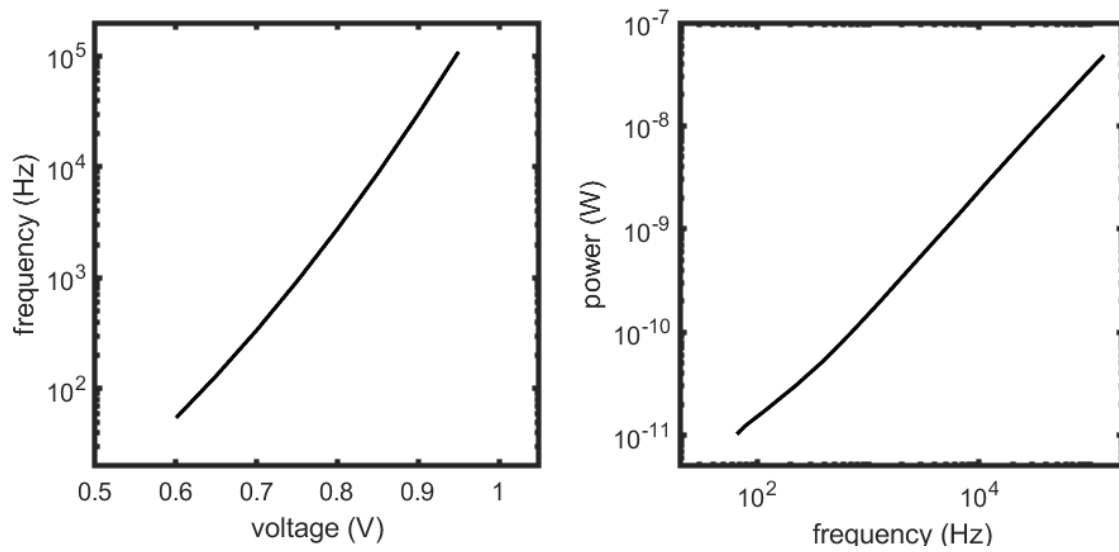
Figure 5.9: Ring oscillator calibration curves: frequency as a function of voltage and power as a function of frequency.

All of these components were fabricated on a single CMOS chip totaling a volume of 3.9 mm^3. The assembly and measured output performance during finger tap energy harvesting is discussed in the next chapter. Various system applications are also posited.

Chapter 6

Finger Motion Energy Harvesting System

This chapter includes content adapted with permission from the following papers:

"Charge-pumping with finger capacitance in a custom electrostatic energy harvesting ASIC" by A. Y. Zhou and M. M. Maharbiz [203]
"Electrostatic energy harvesting from human interactions with smart paper electronics" by A. Y. Zhou and M. M. Maharbiz [204]

A CMOS compatible energy harvesting alternative would allow for its integration alongside already established circuitry and electronics. As devices trend smaller, especially in wearable sensors and implants, this would be a convenient power solution which would further reduce size by eliminating additional ports, connectors, and wires to other battery or energy sources. The electrostatic energy harvesting ASIC presented in Chapter 5 harvested energy from a moving body by creating a change in capacitance across two electrodes. For interactive devices, a natural source of variable capacitance comes from finger movement, like a tapping gesture. This variable capacitance generated free charge which was pumped onto a storage capacitor through rectifying diodes. The previous chapter discussed the design and characterization of the components of this ASIC, including an integrated solar cell for initial biasing, variable capacitance electrodes, rectifying diodes, and an electronic load, including a switch and ring oscillator.

In this chapter, we discuss the assembly and performance of the electrostatic energy harvester in response to human motion. Although this integrated ASIC had numerous benefits including ease of miniaturization and fabrication beside CMOS circuits, there are other applications where more energy harvested is necessary. In these cases, the area of the CMOS fabrication masks can be limiting. To produce a larger change in capacitance, the capacitive electrodes were extended off-chip and integrated with conductive inks and fabrics. After presentation of the ASIC, we posit additional applications for this electrostatic energy harvesting system.
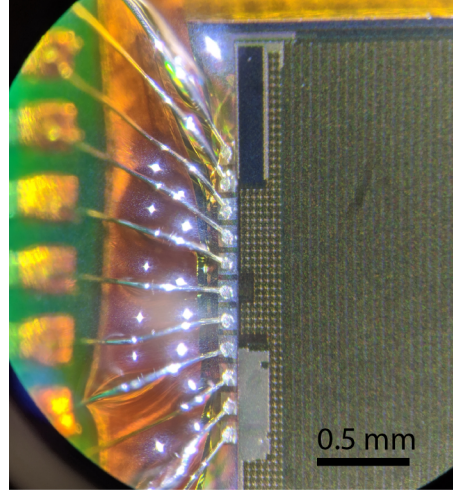
Figure 6.1: Epoxy applied to wirebonds.

6.1   General System Assembly

To assemble the device for characterization, the ASIC was wirebonded to a custom printed circuit board (PCB) with test leads out to a sourcemeter (Keithley 2400) for DC voltage measurement, and digital oscilloscope (National Instruments USB-5133) for ring oscillator output detection. The wirebonds were mechanically protected and electrically isolated with a low viscosity epoxy (EPO-TEK 353ND). Small amounts were applied at the PCB end of the wirebond and encouraged to spread in the direction of the chip manually with a needle. The surface tension of the epoxy aided it to wick up the length of the wirebond until it reached the bond pad. At the bond pad, the difference in hydrophobicity of the exposed metal pad versus the surrounding oxides encouraged the epoxy to ball at the bond pad without significant spreading on the surface of the chip. Figure 6.1 shows this epoxy, in amber, coating the wirebonds and not spreading over the chip. Future iterations of this device can use bumping assembly methods to avoid potential wirebond breakage and reduce area requirements. In any assembly process, it was important to avoid coating the ASIC with unwanted materials, which increased the distance between the finger and metal capacitive traces, reducing the effective change in capacitance. Figure 6.2 demonstrates the effect of thin films of dielectric over the capacitance. After recognizing the dramatic drop off in change in capacitance with the addition of any dielectric layer, we decided to forego this layer and ensured the insulating epoxy protected the wirebonds and bond pads from shorting during use.

In this system, both the initial charge capacitor and storage capacitor were incorporated as discrete, surface-mount components for flexibility of testing various values. This allowed for easier manipulation of these capacitor sizes to fit various applications in the character-
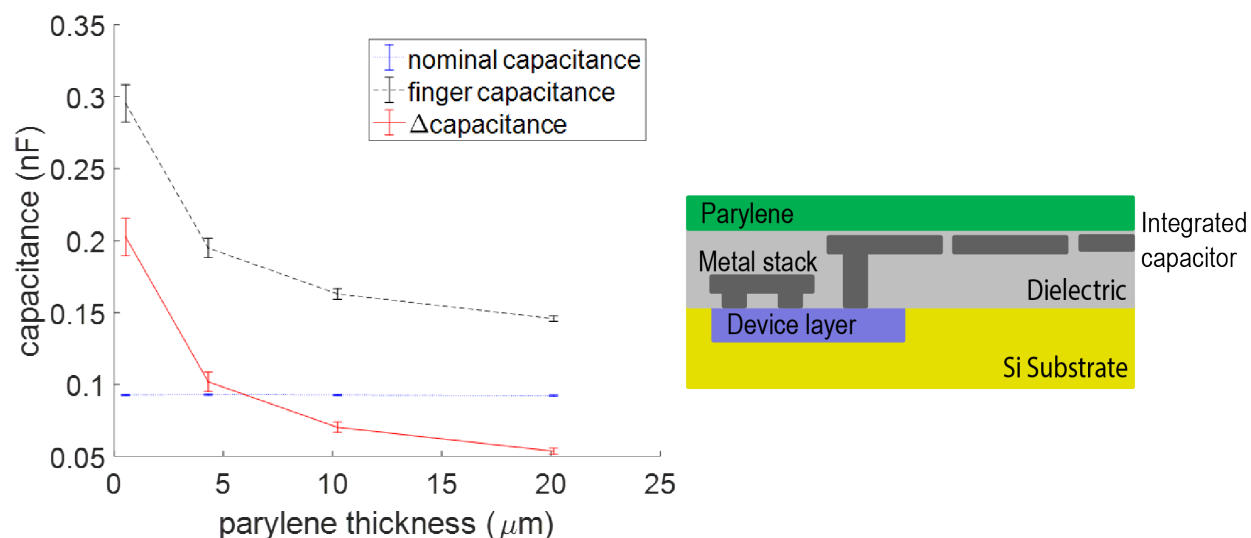
Figure 6.2: Additional films on top of ASIC reduces the effective change in capacitance sensed at the variable capacitor electrodes.
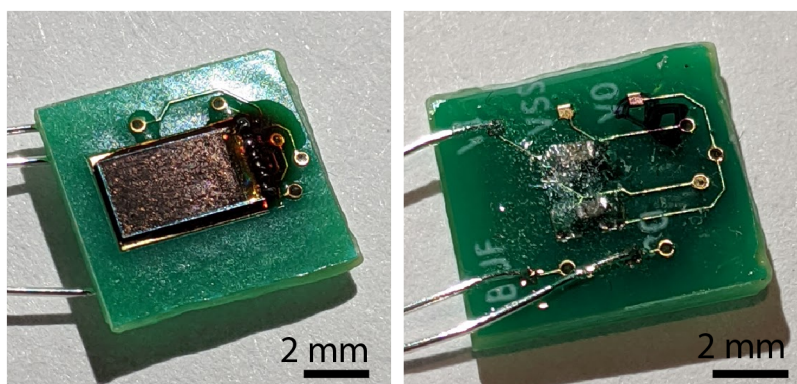
Figure 6.3: Fabricated chip wirebonded to a PCB ready for characterization.

ization and experimental phases, and reduced costs since a new chip did not have to be fabricated to fit each condition. For a fully integrated solution, smaller capacitors can be fabricated on chip. These discrete components were soldered to the backside of the PCB. All exposed metal on this component side of the PCB was insulated with UV curable epoxy (EPO-TEK OG116-31). Both the front and back of the PCB are pictured in Figure 6.3. Due to standard PCB manufacturing minimum area size requirements, the whole board area measured 8 mm × 8 mm, and had a standard FR-4 thickness of 62 mils.

6.2 Energy Harvested from Finger Tapping

We measured the energy harvested over a series of finger taps by tracking the voltage across the storage capacitor (C_s) with a voltmeter. During these experiments, the capacitor ($C_s = 1$ nF) was not connected to any application loads. We tapped the chip with a finger at a rate of ∼25 taps per min and saw a staircase-like increase of voltage on C_s (Figure 6.4). As expected with a human interactive device, we saw multiple energy harvesting pathways for each experimental measurement due to variations in tapping frequencies, finger placement, and finger conditions. Overall, we saw good agreement with the simulations. Initial taps showed a voltage increase on the storage capacitor of ∼0.12 V. Using the relationship $Q = CV$, this means 120 pC of charge was pumped onto the storage capacitor during a single tap. Since we know the energy of a storage capacitor is $E = \frac{1}{2}CV^2$, we solved for 7.2pJ of energy transferred to C_s on an initial tap. The energy transfer decreased upon successive taps because as the charge on C_s increased, the voltage differential across diode D_1 decreased, which decreased the current and charge transferred on each subsequent tap. After approximately 50 seconds of tapping at this frequency, C_s reached a total stored energy of 320 pJ at 0.8 V.

Given this data, we calculated approximate power and power density for this device. Using a leisurely tapping frequency of 25 taps per min, or 2.4 seconds per tap, we estimated the power the device delivered as

$$\Delta P_{max} = \frac{\Delta E}{\Delta t}$$

$$\Delta P_{max} = \frac{7.2pJ}{2.4s} = 3pW$$

This calculation considered the cycle time for a whole tap, but we saw that the majority of the charge was pumped onto the storage capacitor during the first 0.5-1 second of the tap, while the capacitance was changing. Therefore, we can increase our power delivered by increasing the frequency of tapping. However, there is a limit that is dictated by how quickly the system nodes can realize the capacitance change and the speed at which charge is shuttled. From our results we noted that this tapping frequency limit was ∼1 Hz, and the full capacitance change would not be realized at higher frequencies. We solved for power density using the chip die volume of 3.9 mm³, which resulted in 769 pW/cm³. Another way to increase power delivered by the device is by increasing the variable capacitor area. Because the finger capacitance is proportional to the total capacitive area of the electrodes, integrating the touch capacitor onto an ASIC chip limits the area, therefore limiting the maximum change in capacitance. There are methods to effectively extend these capacitive electrodes off-chip to other conductive mediums, which will be discussed later in Sections 6.4 and 6.5.

We also approximated the energy conversion efficiency of this system. We estimated the tip of a finger to be a 1 cm diameter sphere of water, so the weight of this sphere was 0.5 g. Assuming simple linear motion, we solved for the work exerted.

$$W = F \times d$$
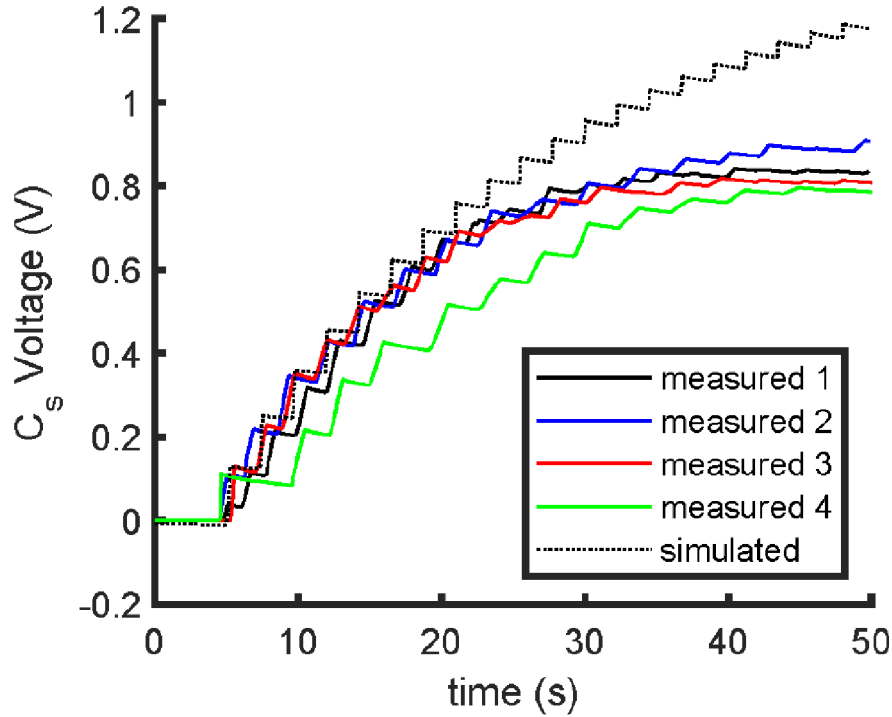
Figure 6.4: Four examples of the measured voltage (solid) and simulated voltage (dotted) on the storage capacitor during energy harvesting. Each tap pumps charge onto Cs creating a staircase-like curve.

$$F = ma$$
$$W = (0.5g)\left(9.8\frac{m}{s^2}\right)(1cm) = 49\mu J$$

Therefore the energy conversion efficiency was defined and calculated as

$$eff = \frac{E_{C_s}}{E_{tap}} \times 100\%$$

$$eff = \frac{7.2pJ}{49\mu J} \times 100\% = 1.5 \times 10^{-5}\%$$

We expected this efficiency to be very small because even though the finger traveled multiple millimeters through space in each tap, only the last couple tens to hundreds of microns did work and effected charge movement in the capacitive electrodes. Therefore, significant amounts of kinetic energy were not converted. Moreover, a small energy conversion efficiency such as this ensured that the energy harvesting system was not impeding the natural motion of the user. This emphasis on minimizing user effort is important for user adoption of any energy harvesting technology.

6.3 General Application: Powering Circuits

After validating operation and measuring available power, we tested the ability of the energy harvester to power an on-chip ring oscillator (RO). We connected the storage capacitor (C_s = 10 pF) to a diode-connected MOSFET, which acted as a switch and drew very little current at low voltages. Once enough charge was pumped onto C_s, so that the voltage exceeded the switch trigger level of 650 mV, the switch closed and powered the RO. The oscillator ran and drained energy from C_s until it switched off. When the ring oscillator first turned on, we saw an increase in frequency as the voltage on C_s continued to increased. As cycles got shorter, the power consumption of the ring oscillator increased. As the RO pulled more charge from the capacitor, the voltage on C_s fell, leading to a decrease in frequency. This push and pull between harvested charge from finger capacitance and current draw from the RO resulted in each finger tap creating a series of chirps. In order to record these chirps, we used an externally-powered buffer to drive the signal into an oscilloscope. The results of ten finger taps are shown in Figure 6.5 with subplots showing a zoomed-in view of a single tap, followed by a single chirp. The RO output frequency ranged from 80 Hz to 30 kHz. Using the RO calibration curves (Figure 5.9), this measured output implied the load in the system consumed between 37 pW and 9.4 nW of power. These frequencies also correspond to harvested C_s voltages of 625-890 mV. We saw that this trigger voltage was lower than our simulated 650 mV, which was due to a combination of process variation during chip fabrication and power draw from the electronic switch. A mechanical switch with zero open-circuit power consumption could replace this transistor to maximize the power delivered to the application. This system demonstrated a proof-of-concept for automatic activation of an electronic circuit upon integrated electrostatic energy harvesting.

In this section, we presented an integrated system combining electrostatic energy harvesting with electronics in a single standard CMOS fabrication process. This device harvested kinetic energy from a finger tap to power a ring oscillator. One potential use case of this system was integrating it with a bandaid (Figure 6.6 and using it to help power an impedance sensing system for wound healing. As with any electrostatic energy scavenger, harvesting was limited by resistive and capacitive parasitics. These losses can be reduced with use of more advanced fabrication technologies, such as dielectric trench isolation or native silicon isolation which were not available in our technology. Moreover, since harvested energy increased with area, this system was also constrained by area limitations of the CMOS fabrication process. However, the capacitive electrodes can be easily extended off-chip to various conductive mediums such as conductive fabrics and conductive inks, which will be discussed in the following sections.
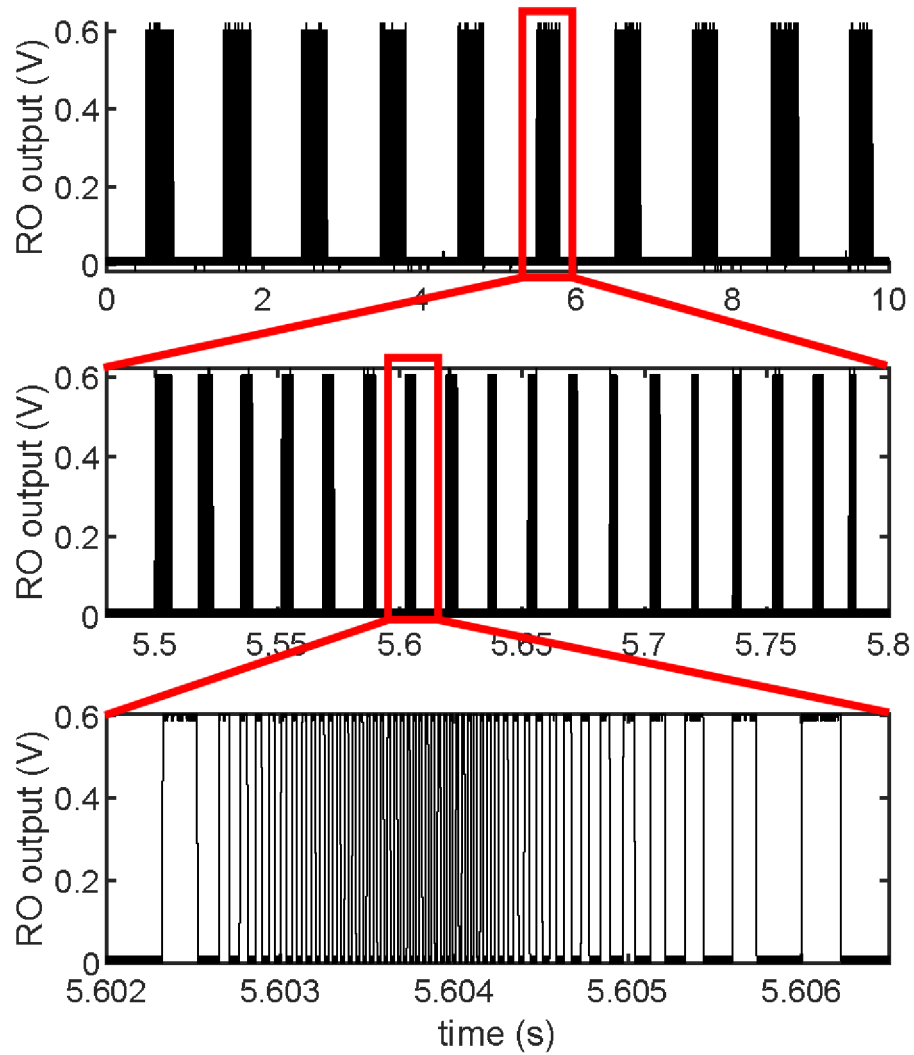
Figure 6.5: The RO output signal from being powered by charge-pumping with finger capacitance. Ten finger taps produces an activation of the RO (top). Each tap consists of a series of chirps (middle). Each chirp varies in frequency with modulating C_s voltage (bottom).
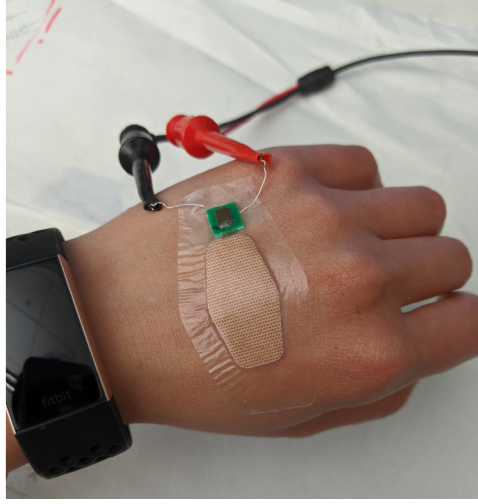
Figure 6.6: The energy harvesting ASIC incorporated with a bandaid as a potential use case.

6.4   Proposed Application: Harvesting from Conductive Fabrics

Electronic textiles is a growing field of research [49, 163]. It involves the integration of electronics on fabrics to create a class of smart fabrics. As electronics pervade everyday life, the goal of these smart fabrics is to create a platform where computing can be worn on the body as part of a casual outfit. These types of e-textiles could have applications in numerous fields including healthcare, military, sports, and consumer goods [49]. Indeed, there have been developments in using smart textiles for ECG monitoring [129], heart rate sensing [23], wound monitoring [123], and communications with wearable antennas [149]. Most traditional batteries are not suited for these applications due to their weight and bulkiness, in addition to their generally rigid structures which do not match well with stretchy, wearable fabrics. Although there have been many improvements for flexible and stretchable power sources for wearables [193], energy harvesting can again be a good alternative to provide power for electronic textiles. There have already been significant research into nanofabricated triboelectric fibers which can be integrated with fabrics (see Table 2.8). In this section, we offer electrostatic energy harvesting with conductive fabrics as an alternative energy harvesting system.

One of the limitations of integrating the entire energy harvesting system on an ASIC was the area restrictions of the capacitive electrodes. Here, we electrically connected the active capacitor node to a bond pad, which was then wirebonded off-chip and connected to a 20 cm × 20 cm sheet of conductive fabric (Knit Conductive Fabric - Silver, Adafruit 1167) with an alligator clip. The conductive fabric had a resistance of <1 Ω per foot. The fabric was insulated by depositing 2 μm of parylene-C. This reduced the elasticity of the fabric, and
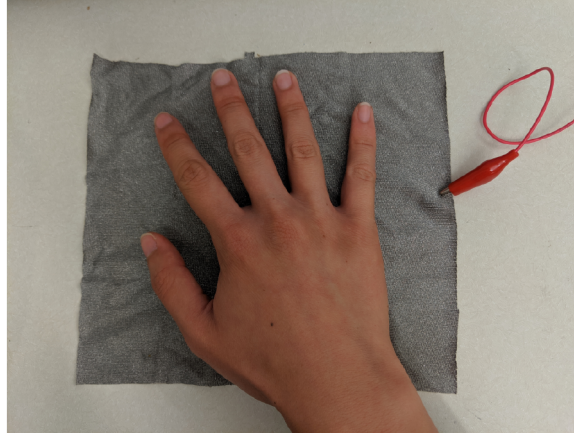
Figure 6.7: Conductive fabric tied to active electrode node on ASIC can operate as a variable capacitor with hand capacitance.

we would recommend alternative dielectric coating methods (like sprays and more elastic polymers) for wearable applications.

During operation, the user palmed the fabric with their whole hand and created a change in capacitance (Figure 6.7). Although only the active electrode was extended off-chip in the form of conductive fabric, the user was still connected to the ground electrode through their body capacitance. More complicated coplanar electrodes can be fabricated on textiles through processes such as weaving or screen printing various dielectric materials inbetween the conductive fabric. As a user palmed the fabric, the diodes rectified charge to the storage capacitor, and the voltage across this capacitor was buffered to a voltmeter. The performance of the conductive fabric energy harvester is presented in Figure 6.8. Since the area of the electrode was significantly larger and utilized the whole area of the hand, the change in capacitance was much larger. This led to more charge being pumped on the storage capacitor with each tap. We presented this charge up structure for two storage capacitor values. As expected, the voltage on the larger storage capacitance ($C_s = 1$ µF) increased much more slowly due to the relationship $Q = CV$. The smaller capacitor ($C_s = 100$ nF) charged up much more quickly, with initial taps building 350 mV per tap. This rapid charging caused the measured voltage to soon surpass the range of the buffer, causing it to flatten at 40 seconds. Using the equation for energy on a storage capacitor, this system harvested 6 nJ stored per tap. After forty seconds of tapping, the total energy stored by the fabric electrostatic energy harvesting system was 560 nJ and 117 nJ on a 100 nF and 1 µF storage capacitor, respectively.

This system illustrated how expanding the area of the variable capacitor electrodes increased the energy harvested of our system. The ASIC could still be leveraged with these fabrics since we believe it was small enough to be imperceptibly integrated onto a logo or tag, without affecting the comfort of the cloth. Moreover, demonstrating the various charge-up
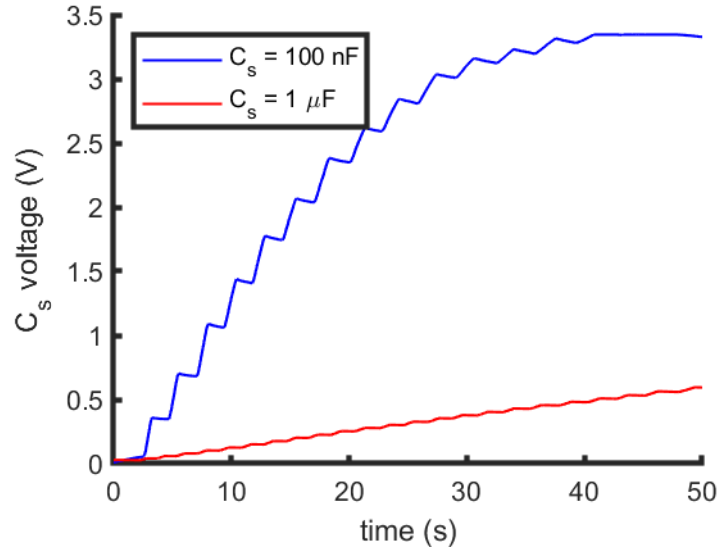
Figure 6.8: The measured voltage on a storage capacitor charging up with a hand palming conductive fabric for two storage capacitor values.

patterns for different capacitance sizes exemplified how these values should be designed to fit the applications' needs.

6.5 Proposed Application: Smart Paper Electronics

As smart devices permeate everyday life, there is an increasing number of consumer products with embedded electronics [108, 151]. This electrostatic energy harvesting system could be integrated with many of these smart objects to create an additional energy supply. Instead of relying solely on the integrated capacitive electrodes on the top metal layers of the ASIC, the variable capacitor nodes were routed to bond pads which can be electrically connected to any conductive material. There exist various types of conductive inks and paints which can be applied to many objects to extend the variable capacitor electrodes onto these items. Paper, in particular, is a target as an electronics substrate due to its low cost and wide availability [170, 156].

There is significant research into the concept of interactive paper, such as a paper Invite which turns into a musical instrument [155], paper-based capacitive touch pads [109, 93], paper embedded LED circuits [156], and paper-based computing through pop-up books [134]. Clinically, paper-based analytical devices (PADs) have attracted attention as an inexpensive, lightweight, and disposable alternative for diagnostics. Electrochemical PADs have been developed to detect HIV [196], diabetic ketoacidosis [173], and nucleic acids [32]. Although these technologies have developed paper-based, disposable diagnostic arrays, they

still require connecting to a separate potentiostat or glucometer to analyze the results. If we can combine these two technologies and add both electronics and electrochemistry to paper, we can conceive a full lab-on-paper system. One limitation of many of these systems is the requirement to be tethered to a power supply or battery, which undermines the portable and lightweight qualities of PADs. Harvesting energy from natural human gestures, such as tapping, enables the user to self-power these paper devices.

In this section, we demonstrate a method for self-powering interactive paper products with an electrostatic energy harvesting system. Conductive inks painted in various designs on paper acted as electrodes, creating a variable capacitor with the human body through finger tapping. This energy was transduced to electrical energy through the ASIC, resulting in a system that maintained the integrity of the lightweight and flexible feel of the paper substrate.

Designing Variable Capacitors on Paper

Electrostatic energy harvesting leverages a variable capacitance to pump charge onto an energy storage device. These electrodes can be defined by any type of conductive material with a dielectric in between. Traditionally, paints and inks are used with paper to convey information. Painting conductive ink on paper also creates flexible electrodes which can be easily incorporated into any paper product. Electrodes of various shapes and sizes were manufactured by laser cutting paper stencils (Universal Laser Systems VLS2.30) and hand-painting them onto standard printer paper with a nickel based conductive ink (MG Chemicals 841AR Nickel Super Shield Conductive Coating). Growing popularity of these conductive products [29] allowed for easily accessible and relatively cheap options for adding capacitive electrodes to materials like paper.

A large change in capacitance was important for a high-performing energy scavenging system. Commercially available conductive inks allowed for quick iterations of various electrode designs on common materials such as paper. Shapes and sizes were easily altered and reprinted, unlike previous systems where metal traces were defined on PCBs or integrated on-chip with CMOS devices. The five designs in Figure 6.9 were fabricated and Table 6.1 shows the change in capacitance as a finger, or palm for the larger design, approached the electrode.

As expected, larger designs like the diamond geometry resulted in a larger change in capacitance since there was more area in the palm of the hand. We also saw that designs with coplanar active and ground electrodes present on the paper (Diamond, Spiral) had a larger change in capacitance, about 100x, compared to the designs where only the active electrode was present (Square, Circle, Cal Bear). This was expected and corresponded well with our previous test structures on PCB (Section 3.1). For fingertip-sized active electrode designs which were more likely to appear in portable paper products like PADs, or in paper consumer goods, like children's books, we measured a 2-3x increase in capacitance. In addition, the Cal Bear electrode demonstrated that the electrode could be more complex than standard geometries and still be effective in creating a change in capacitance. The resolution
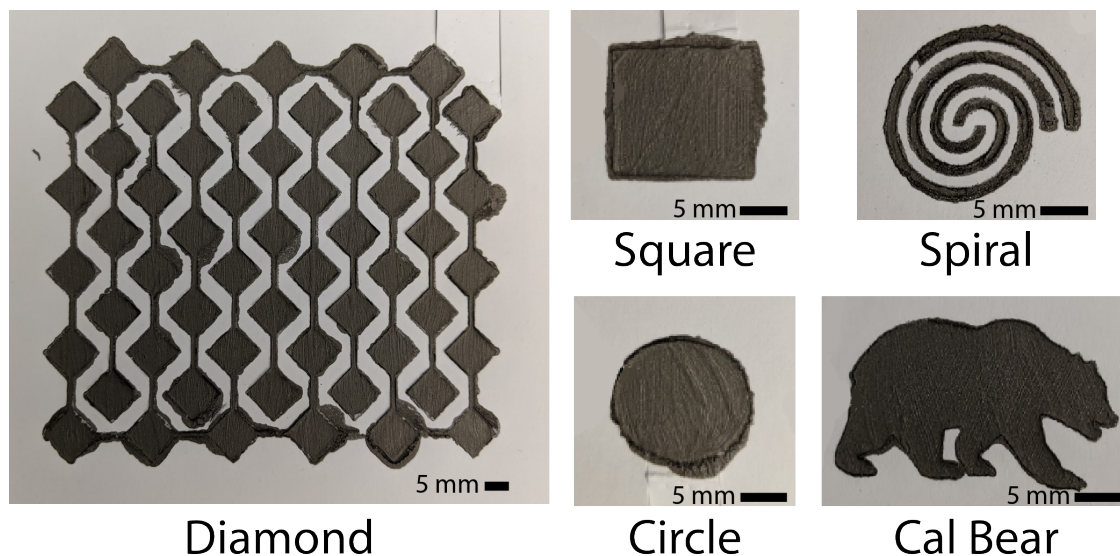
Figure 6.9: Painted conductive ink electrodes on paper. Designs of various shapes and sizes are easily prototyped.

Geometry	Size	Cmin	Cmax
Diamond	Square side = 9 mm Spacing = 4mm Total area = 86 x 95 mm	25 pF	3.2 nF
Square	Side = 15 mm	17 pF	37 pF
Circle	Radius = 15 mm	23 pF	48 pF
Spiral	Radius = 20 mm Line thickness = 1 mm Line spacing = 1.5 mm	11 pF	1.1 nF
Cal Bear	Tail to nose = 28 mm Height = 15 mm	13 pF	36 pF

Table 6.1: Change in capacitance for electrode geometries on paper.

and thickness of the paint layers in this prototype were variable due to being painted on manually with a brush. With different conductivities, this resulted in varying capacitances, even for similar sized electrodes. If necessary, the uniformity and resolution can be improved by screen printing or doctor blading, although these techniques may incur additional costs. It is also meaningful to note that these inks could be printed on other flexible substrates [112, 136], like polyethylene terephthalate (PET), which is used in wearable biosensors [47].
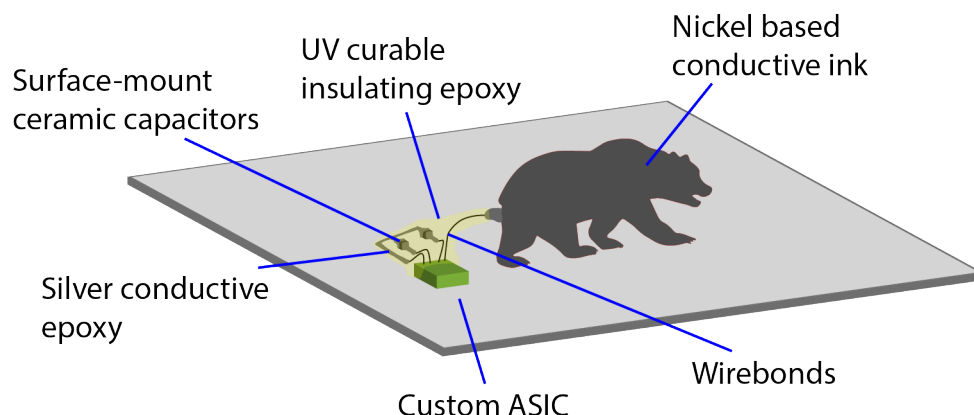
Figure 6.10: Cartoon schematic of full energy harvesting system for interactive paper.

Paper-Harvester Integration Assembly

In order to maintain the flexibility of paper and reduce the mass attached to paper, the ASIC was assembled directly onto the paper without a PCB. Figure 6.10 illustrates an overview of the system. The custom ASIC die was silver epoxy (EPO-TEK EJ2108) bonded to the paper, and wire bonds were attached with one end to the chip bond pad and the other end truncated and left floating. The ASIC end of the wirebonds were fortified with a UV curable epoxy (EPO-TEK OG116-31). Because the active electrode node was connected to the large on-paper electrode, and that was the point of contact with the finger, we were less concerned with depositing dielectric material over the chip itself. The opposite floating ends of the wirebonds were then manually attached to the paper with silver epoxy, followed by the surface mount capacitors. The capacitors in the harvesting circuit had values of C_c = 1 μF and C_s = 10 nF. The selection of a C_s value is dependent on the application and will offer tradeoffs between leakage and charging speed. All components were electrically connected with silver epoxy traces. Future iterations can use more elegant integration with printing conductive ink tracks followed by bump bonding or conductive potting for a smaller footprint and to avoid potential wirebond breakage. Two 10 mil silver wires (A-M Systems 787000) were attached to the circuit for output signals, and finally the chip was coated with the UV curable epoxy to ensure robustness.

To address the need of a source voltage to initially bias the capacitors, we again utilized the on-chip integrated solar cell. During these system experiments, a different version of the ASIC was used with fewer photodiodes in parallel, leading to an open circuit voltage of 0.34 V and a short circuit current of 19 nA. Using Spectre Circuit Simulations, we found that the system required approximately 20 seconds to charge up due to the capacitances in the system and the low bias voltage. This solar cell, in addition to the rectifying diodes and wirebond pads, resulted in an area requirement of 0.84 mm^2. This small footprint coupled with thin form factor (wafer thinned to < 300 μm thick) meant that this chip could be incorporated
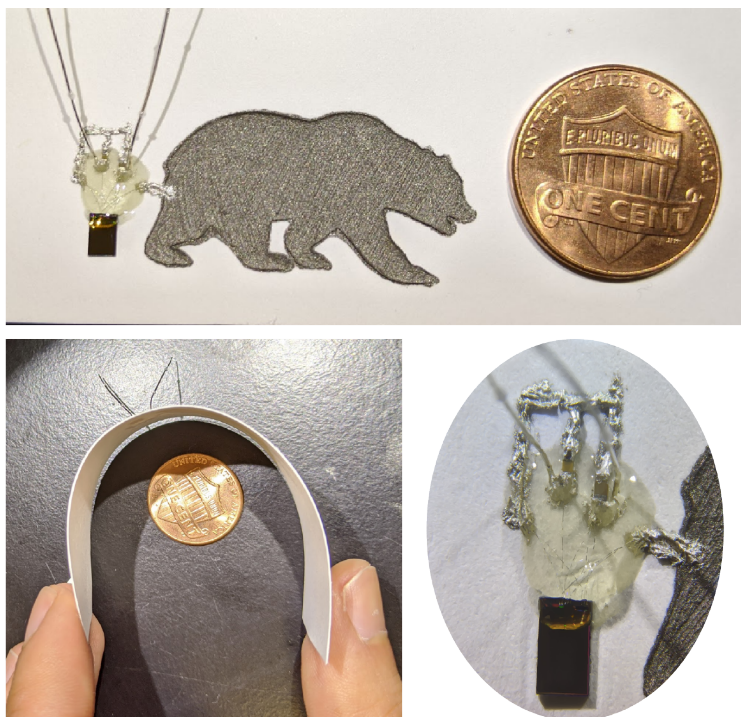
Figure 6.11: Electrostatic energy harvesting system on paper. The ASIC is assembled directly on paper maintaining its flexible and lightweight qualities. The harvesting system continues to work after bending.

almost imperceptibly on most paper products. Others interested in integrating this method of energy harvesting without access to foundry CMOS processes can use commercial-of-the-shelf (COTS) components, which will require a larger footprint, but can be similarly incorporated using conductive epoxies and inks.

Paper-Harvester Performance for paper-based devices

The Cal Bear electrode design was combined with the custom ASIC and energy harvesting circuity to create an operational energy harvesting system. Figure 6.11 shows the completed device, which measured 40 mm × 15 mm and added < 500 μm to the thickness of paper at the chip location. This system remained light and flexible, like paper. In fact, the system continued to harvest energy even after bending. This assembly can be further reduced in size by alternative integration techniques, like bump bonding instead of wirebonds, and additional wafer thinning.

As a finger approached the Cal Bear insignia, the change in capacitance drove the electrostatic harvesting circuit and pumped charge onto the storage capacitor. Figure 6.12 shows
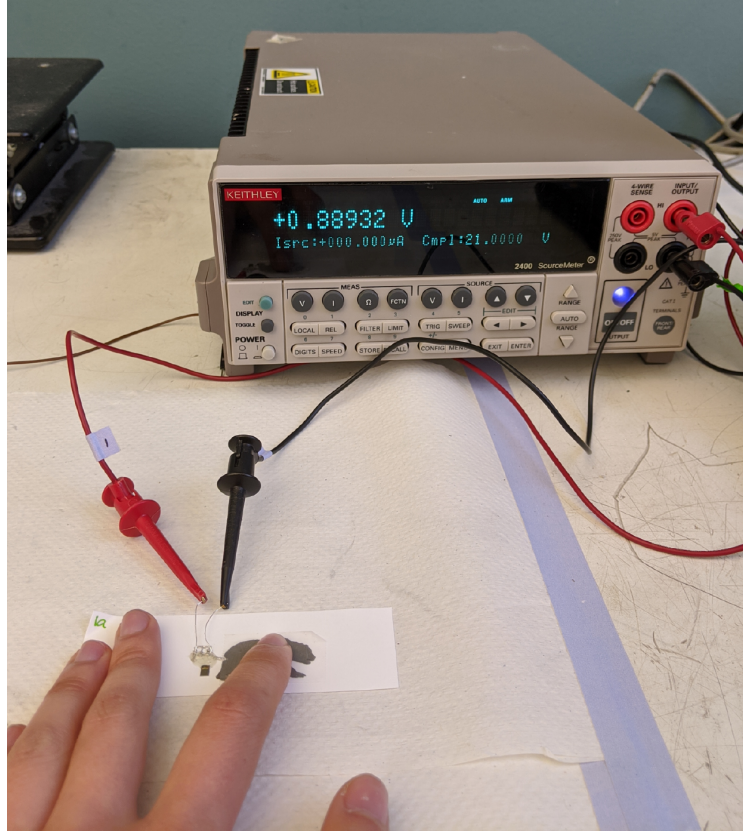
Figure 6.12: Test set-up to measure voltage across the storage capacitor.

the measurement setup system with the storage capacitor nodes directly connected to a sourcemeter in voltmeter mode. Figure 6.13 demonstrates four examples of how the voltage on the storage capacitor charged up with finger taps. Although each charging pattern was not perfectly repeatable due to dissimilar timings, placements of the finger, and conditions (sweat, dirt, etc), the system reached a consistent voltage of 1.3 V after approximately six taps. As the voltage approached the asymptote, the energy harvested per tap decreased because the voltage differential across D_1 decreased. This resulted in a total harvested energy of 8.5 nJ. It is important when applying this energy harvesting technology to consider worst-case scenarios because, as this data showed, energy harvested can differ from tap to tap and day to day, depending on varying finger and environmental conditions. We also saw a deviation from the ideal stair-case like structure of charge pumping due to a decrease in voltage between taps. This was because the voltage was not buffered into the voltmeter which led to a decay time constant of $\tau = R * C \approx 100M\Omega * 10nF = 1s$. We can extend this measured lifetime by increasing the storage capacitor size or adding a buffer.

In this section, we demonstrated a finger-tapping powered system for paper-based devices.
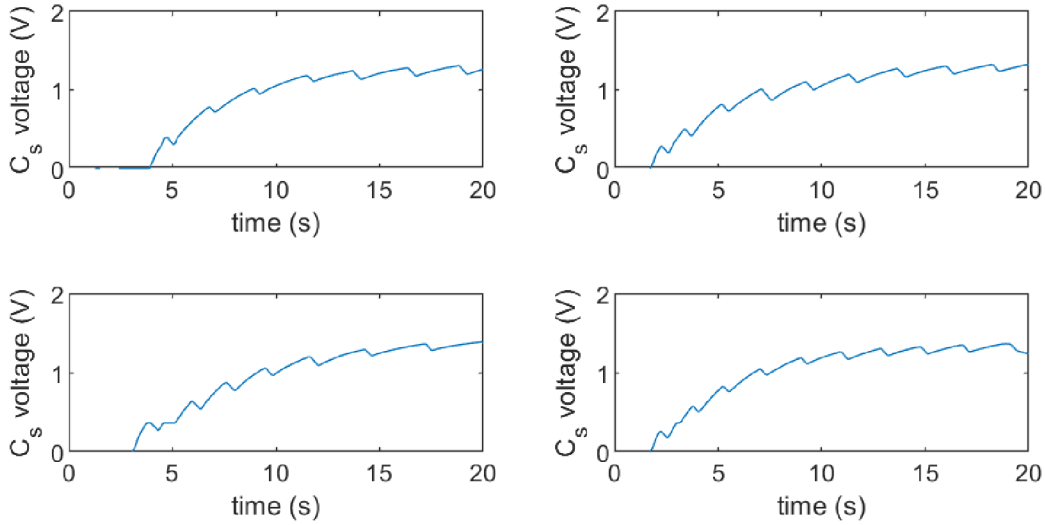
Figure 6.13: Four examples of how the storage capacitor voltage steps up with each finger tap on paper devices.

This technology allowed for tiny harvesting circuits to be integrated with conductive ink on paper, which maintained the thin, flexible, and lightweight qualities of the medium. Our system harvested 8.5 nJ at a voltage of 1.3 V. Given the size of the finger, the energy density was 50 pJ/mm^2. This is about 20x less than the 1 nJ/mm^2 energy density of a single layer of a piezoelectric polymer harvesting system [125]. Despite higher energy densities, there are applications where electrostatic harvesting is better suited. For example, piezoelectric polymers are generally more expensive ($10/g for P(VDF-TrFE) from PolyK Technologies vs. $0.22/g for conductive paint). Moreover, the poling required to functionalize the piezoelectric polymers in [125] require high voltages which is not always accessible. Currently, our device would be able to power simple circuits such as ring oscillators [107] and has the potential to harvest more energy with larger electrode designs.

In this chapter we presented a stand-alone electrostatic energy harvesting ASIC capable of powering a ring oscillator on the same die. This system was incorporated with other substrates through conductive mediums such as inks and fabrics.

Chapter 7

Conclusion

7.1   Summary

In this dissertation, we have described an energy harvester that was co-fabricated with commoditized integrated circuits. We discussed the theory and merits of four kinetic energy conversion methods - piezoelectric, electromagnetic, electrostatic, and triboelectric. In brief, piezoelectric and triboelectric transducers can achieve high built-in voltages using unique materials that exhibit piezoelectric and triboelectrific effects. Electrostatic transducers can also output relatively high voltages but rely on an externally applied bias voltage and changing capacitance to harvest energy. Electromagnetic transducers can output high currents and relatively low voltages using a changing magnetic field with respect to a conductive coil. With the goal of designing an integrated energy harvester, electrostatics was the most attractive option due to its compatibility with ICs.

To demonstrate the advantages of electrostatic transduction, we designed, fabricated, and tested an electrostatic energy harvesting ASIC. Without the need for incompatible piezoelectric, triboelectric, or electromagnetic materials, we incorporated capacitive metal electrodes directly into the top metal layers of a standard 0.18 µm TSMC fabrication technology. A finger tap modulated the effective capacitance seen at these electrode nodes, which drove a charge-pump circuit. In this way, the kinetic energy of finger tapping was transduced to electric energy to charge a circuit. The ASIC had a power harvesting density of 769 pW/cm^3 and, as proof-of-concept, powered a ring oscillator which output a series of chirps. With all components fabricated on the same silicon die, the need for interconnects, complex packaging, and additional fabrication was eliminated, which reduced size, weight, and costs for devices.

Additionally, we demonstrated this technology's versatility by extending the electrodes to conductive traces, fabrics, and inks. This is useful in applications where the CMOS die area is limiting, and the electrode area must be larger to increase energy harvested. Extending the electrodes off-chip with various conductive mediums expanded the active area and amplified the effect of body capacitance. The availability of these common conductive materials allows

for convenient integration with many existing electronic systems. We envision embedding a series of these energy scavenging motes into everyday objects, such as books, textiles, wearables, or other consumer goods, to create smart, interactive, self-powered devices.

7.2 Future Directions

The human body can be a very useful source of energy, if scavenged correctly. Kinetic energy harvesting of body motions can be supplied on-demand by the user, reducing their dependence on other power sources, such as solar radiation or chemical potentials of batteries. However, a number of technical challenges remain before the commercial deployment of electrostatic energy harvesting ASICs.

Human and Environmental Variability

The finger capacitance effects presented throughout this dissertation were performed by a single user on a lab benchtop or desk. Therefore, the results were specific to her unique finger, body capacitance, and environment. Similar to most devices which rely on user interaction, the variability of motion between humans leads to a difficult engineering problem. Even within a single user, these variables are constantly changing with both external conditions, such as sweat and dirt, and internal conditions, such as dehydration or edema (swelling caused by excess fluid). This creates uncertainty in the expected variable capacitance from the user, and can directly affect the energy harvested. This unpredictability is amplified when designing for multiple users, all with different shapes, weights, sizes, and body compositions. Additionally, the local environment of the user can effect the response of the energy harvester. For example, wearing nitrile gloves acted as an additional dielectric layer between the capacitive electrodes and the body capacitance, therefore reducing the change in capacitance. Leaning against a large conductive plate, such as a metal desk leg, acted as a ground node which enhanced the effect of the finger capacitance. To ensure consistent performance over a wide range of users, more research and testing must be conducted with many volunteers in routine environments. In general, conditions reducing the change in capacitance will be more difficult to resolve because less energy will be harvested and the user may have to repeat the harvesting motion multiple times. Conditions that result in larger than expected capacitive changes have the benefit of harvesting more energy, but power protection should be integrated to ensure the the circuits are not damanged by unexpected power spikes. The system should be designed with large margins of operation to ensure proper functionality for the general public.

Lifetime Reliability

The longest presented continuous use of the electrostatic energy harvesting ASIC was 50 seconds in Section 6.2. Experiments were repeated on the same ASIC chip multiple times

over the course of one week, which contributed to the variation between charge-up pathways, but no consistent trends were detected. However, visual inspection of the chip showed debris and particles (skin cells) deposited on the surface of the chip. A thick layer of this buildup would result in increased distance between the finger and electrode, which decreases the effect of finger capacitance. Because longevity is important to many interactive devices, it is necessary to better understand the effects of debris buildup over time on the ASIC. One solution could be to package the device in a thin-film protective layer, such as parylene, and request that the user periodically rinse and clean the device. Another consideration is the durability of the bare silicon die, which can be chipped and scratched over time. Using epoxy to build up a barrier around the chip can help prevent it from being physically damaged. Selecting a protection method and understanding the reasonable lifetime of the device will depend on the application and environment of the energy harvester.

Adaptation for Multiple Process Nodes

The TSMC 0.18 μm technology which was used to fabricate the electrostatic energy harvesting ASIC was first offered in 1998. Today, many commercial electronics are fabricated at much smaller nodes, such as the 65 nm, 28 nm, or the 5 nm process node which was released in 2019 [102]. Integrating the electrostatic harvester module with each process node will require adapting the capacitive electrodes to meet the different design rules of the technology. Some design rules which may affect electrode geometry are listed below:

- Number of metal layers

- Thickness of metal layers

- Thickness of dielectric

- Minimum and maximum metal width

- Minimum and maximum metal area

- Minimum spacing between metal

These rules will affect the number of layers that can be stacked for the electrodes, the width, thickness, and spacing of the electrodes, and the total area that can be dedicated to a capacitor plate. Therefore, both the nominal capacitance and the effect of finger capacitance will be different.

Enhancement of Energy Harvested

The ASIC presented in Section 6.2 delivers 3 pW of power (7.2 pJ of energy per tap) on a 1 nF storage capacitor. Given that many applications will require more power, we posit three ways of improving the energy scavenger including (1) increasing the bias voltage, (2) increasing the effective capacitance change, and (3) reducing the parasitic losses in the system. The initial bias voltage can be amplified by series connecting multiple photovoltaic solar cells. Although substrate leakage prevented the voltage from stacking for series connected solar cells in the current fabrication technology, an array of integrated silicon solar cells in a trench-isolated SOI CMOS process can output up to 140 V [142]. Different electrode geometries can also enhance the effect of finger capacitance. Section 3.1 compares the change in capacitance for a range of sizes and separation distances for a circular electrode. There are many different electrode configurations, such as diamond, spiral, and rectangular patterns in addition to the interdigitated comb shape used in the ASIC. Hu and Yang showed that these different geometries have significant effects on the sensitivity of capacitive sensors [63], which implies different capacitance changes. In addition, due to the multi-metal layers included in ASIC technologies, complex 3D structures beyond co-planar electrodes can be investigated. Finally, the substrate losses through our ASIC can also be reduced with more advanced fabrication technologies such as dielectric trenches or native silicon isolation which were not available in our technology. Integrating small initial and storage capacitors on chip can also reduce some resistive pathways and parasitic capacitances from the interconnects and PCBs.

Off-chip Harvesting Applications

Beyond a fully integrated energy harvesting ASIC, electrostatic energy harvesting can be integrated with various conductive materials. Sections 6.4 and 6.5 present two examples in the form of conductive fabrics and conductive inks on paper. Extending the electrostatic electrodes off-chip typically increases the capacitive area which results in larger capacitive changes and more harvested energy. These applications have similar challenges to the ASIC, including environmental variability and longevity. For example, the parylene insulation layer deposited on the fabric cracked and delaminated after mechanically stressing the fabric. Moreover, integrating off-chip electrodes requires more complex packaging and interconnects to the electronics. Although the wirebonding and conductive potting presented with the interactive paper devices (Section 6.5) is one solution, this method has a number of potential failure modes. With repeated bending of the paper, the wirebonds could break, the epoxy could chip, and conductive traces could be severed. One better solution is screen printing thin, flexible, conductive traces and bump bonding the ASIC directly onto the substrate. This method would also reduce the area required to assemble the ASIC. This is one example of many packaging considerations for deploying the electrostatic harvester with off-chip electrodes.

Closing Remarks

While more effort is required to understand these challenge areas, this work demonstrated the principle of a CMOS integrated electrostatic harvester. We believe this thesis represents an alternative to more common piezoelectric, triboelectric, and electromagnetic energy harvesting technologies. Our electrostatic technique provides unique advantages including fabrication alongside rectifying circuits and application electronics, removing the need for additional connectors and assembly. Finally, we believe focusing on small, aperiodic motions such as finger tapping, as opposed to walking or shaking hands, minimizes user effort and leverages actions already common for interacting with devices. We hope that further development in reducing power requirements of electronics coupled with this technology will enable the deployment of integrated electrostatic generators with everyday interactive electronics and wearables.

Bibliography

[1]   Abdelsalam Ahmed et al. "Integrated Triboelectric Nanogenerators in the Era of the Internet of Things". In: *Advanced Science* 6.24 (Dec. 2019), p. 1802230. ISSN: 21983844. DOI: `10.1002/advs.201802230`.

[2]   Jason Alexander, John Hardy, and Stephen Wattam. "Characterising the physicality of everyday buttons". In: *ITS 2014 - Proceedings of the 2014 ACM International Conference on Interactive Tabletops and Surfaces*. New York, New York, USA: Association for Computing Machinery, Inc, Nov. 2014, pp. 205–208. ISBN: 9781450325875. DOI: `10.1145/2669485.2669519`.

[3]   Luciana Algieri et al. "Flexible Piezoelectric Energy-Harvesting Exploiting Biocompatible AlN Thin Films Grown onto Spin-Coated Polyimide Layers". In: *ACS Applied Energy Materials* 1.10 (Oct. 2018), pp. 5203–5210. ISSN: 25740962. DOI: `10.1021/acsaem.8b00820`.

[4]   Shaban Almouahed et al. "Battery-free force sensor for instrumented knee implant". In: *2017 IEEE Healthcare Innovations and Point of Care Technologies, HI-POCT 2017*. Vol. 2017-Decem. Institute of Electrical and Electronics Engineers Inc., Dec. 2017, pp. 1–4. ISBN: 9781538613924. DOI: `10.1109/HIC.2017.8227570`.

[5]   Iman Aminzahed, Yue Zhang, and Milad Jabbari. "Energy harvesting from a five-story building and investigation of frequency effect on output power". In: *International Journal on Interactive Design and Manufacturing* 10.3 (Aug. 2016), pp. 301–308. ISSN: 19552505. DOI: `10.1007/s12008-016-0309-4`.

[6]   *Annual Update on Lithium-Ion Battery Technology*. Tech. rep. Inventus Power, 2016.

[7]   Y Arakawa, Y Suzuki, and N Kasagi. "Micro Seismic Power Generator Using Electret Polymer Film". In: *Fourth Internation Workshop on Micro and Nanotechnology for Power Generation and Energy Conversion Applications, PowerMEMS2004*. Kyoto, Japan, 2004.

[8]   Doron Aurbach et al. *Advances in understanding mechanisms underpinning lithium-air batteries*. Sept. 2016. DOI: `10.1038/nenergy.2016.128`.

[9]   Mehmet Ayyildiz et al. "Contact mechanics between the human finger and a touch-screen under electroadhesion". In: *Proceedings of the National Academy of Sciences of the United States of America* 115.50 (Dec. 2018), pp. 12668–12673. ISSN: 10916490. DOI: `10.1073/pnas.1811750115`.

[10]   Stephen P. Beeby and Terence O'Donnell. "Electromagnetic energy harvesting". In: *Energy Harvesting Technologies*. Springer US, 2009. ISBN: 9780387764634. DOI: `10.1007/978-0-387-76464-1_5`.

[11]   Steve Beeby et al. *Energy harvesting systems*. Ed. by Tom J. Kazmierski and Steve Beeby. Springer, 2014.

[12]   Mohd Fauzi Bin Ab Rahman and Swee Leong Kok. "Investigation of useful ambient vibration sources for the application of energy harvesting". In: *Proceedings - 2011 IEEE Student Conference on Research and Development, SCOReD 2011*. 2011, pp. 391–396. ISBN: 9781467301022. DOI: `10.1109/SCOReD.2011.6148771`.

[13]   A. Blyr. "Self-Discharge of LiMn[sub 2]O[sub 4]/C Li-Ion Cells in Their Discharged State". In: *Journal of The Electrochemical Society* 145.1 (1998), p. 194. ISSN: 00134651. DOI: `10.1149/1.1838235`. URL: `https://iopscience.iop.org/article/10.1149/1.1838235%20https://iopscience.iop.org/article/10.1149/1.1838235/meta`.

[14]   Ruba T. Borno, Joseph D. Steinmeyer, and Michel M. Maharbiz. "Charge-pumping in a synthetic leaf for harvesting energy from evaporation-driven flows". In: *Applied Physics Letters* 95.1 (July 2009), p. 013705. ISSN: 00036951. DOI: `10.1063/1.3157144`.

[15]   Ruba Talal Borno. "Transpiration as a mechanism for mechanical and electrical energy conversion". Doctor of Philsophy. University of Michigan, 2008.

[16]   V Bougrov and Y Goldberg. *Properties of Advanced Semiconductor Materials: GaN, AIN, InN, BN, SiC, SiGe*. Ed. by Michael E. Levinshtein, Sergey L. Rumyantsev, and Michael S. Shur. 2001.

[17]   Ling Bu et al. "Liquid encapsulated electrostatic energy harvester for low-frequency vibrations". In: *Journal of Intelligent Material Systems and Structures* 24.1 (Jan. 2013), pp. 61–69. ISSN: 1045-389X. DOI: `10.1177/1045389X12459590`.

[18]   Sravanthi Chalasani and James M. Conrad. "A survey of energy harvesting sources for embedded systems". In: *Conference Proceedings - IEEE SOUTHEASTCON*. 2008, pp. 442–447. ISBN: 9781424418848. DOI: `10.1109/SECON.2008.4494336`.

[19]   Salar Chamanian et al. "Wearable battery-less wireless sensor network with electromagnetic energy harvesting system". In: *Sensors and Actuators, A: Physical* 249 (Oct. 2016), pp. 77–84. ISSN: 09244247. DOI: `10.1016/j.sna.2016.07.020`.

[20]   Feifei Chen et al. "The electromechanical features of LiNbO3 crystal for potential high temperature piezoelectric applications". In: *Journal of Materiomics* 5.1 (Mar. 2019), pp. 73–80. ISSN: 23528486. DOI: `10.1016/j.jmat.2018.10.001`.

[21] Jun Chen and Zhong Lin Wang. *Reviving Vibration Energy Harvesting and Self-Powered Sensing by a Triboelectric Nanogenerator*. Nov. 2017. DOI: `10.1016/j.joule.2017.09.004`.

[22] Yan Chen and Armaghan Salehian. "Modeling, analysis and experimental validation of an electromagnetic energy harvesting unit". In: *ASME 2012 Conference on Smart Materials, Adaptive Structures and Intelligent Systems, SMASIS 2012*. Vol. 2. American Society of Mechanical Engineers Digital Collection, July 2012, pp. 793–802. ISBN: 9780791845103. DOI: `10.1115/SMASIS2012-8007`.

[23] F. Chiarugi et al. "Measurement of heart rate and respiratory rate using a textile-based wearable device in heart failure patients". In: *Computers in Cardiology*. Vol. 35. 2008, pp. 901–904. ISBN: 1424437067. DOI: `10.1109/CIC.2008.4749188`.

[24] Dong-Hoon Choi et al. "Liquid-based electrostatic energy harvester with high sensitivity to human physical motion". In: *Smart Materials and Structures* 20.12 (Nov. 2011), p. 125012. ISSN: 0964-1726. DOI: `10.1088/0964-1726/20/12/125012`.

[25] Young Man Choi, Moon Gu Lee, and Yongho Jeon. "Wearable Biomechanical Energy Harvesting Technologies". In: *Energies* 10.10 (Sept. 2017), p. 1483. ISSN: 1996-1073. DOI: `10.3390/en10101483`.

[26] Meysam T. Chorsi et al. "Piezoelectric Biomaterials for Sensors and Actuators". In: *Advanced Materials* 31.1 (Jan. 2019), p. 1802084. ISSN: 09359648. DOI: `10.1002/adma.201802084`.

[27] A. T. Collins, E. C. Lightowlers, and P. J. Dean. "Lattice vibration spectra of aluminum nitride". In: *Physical Review* 158.3 (June 1967), pp. 833–838. ISSN: 0031899X. DOI: `10.1103/PhysRev.158.833`.

[28] Louis Columbus. "2017 Roundup Of Internet Of Things Forecasts". In: *Forbes* (2017).

[29] *Conductive Ink Market Size & Share: Industry Report, 2024*. Tech. rep. San Francisco: Grand View Research, 2016.

[30] T. Vu-Cong, C. Jean-Mistral, and A. Sylvestre. "Autonomous dielectric elastomer generator using electret". In: *Electroactive Polymer Actuators and Devices (EAPAD) 2013*. Ed. by Yoseph Bar-Cohen. Vol. 8687. SPIE, Apr. 2013, 86870H. ISBN: 9780819494702. DOI: `10.1117/12.2008793`.

[31] Alexandru Cornogolub, Pierre-Jean Cottinet, and Lionel Petit. "Hybrid energy harvesting systems, using piezoelectric elements and dielectric polymers". In: *Smart Materials and Structures* 25.9 (Aug. 2016), p. 095048. ISSN: 0964-1726. DOI: `10.1088/0964-1726/25/9/095048`.

[32] Josephine C. Cunningham, Nicholas J. Brenes, and Richard M. Crooks. "Paper electrochemical device for detection of DNA and thrombin by target-induced conformational switching". In: *Analytical Chemistry* 86.12 (June 2014), pp. 6166–6170. ISSN: 15206882. DOI: `10.1021/ac501438y`.

[33] Alexander J. Curtis. "Dielectric properties of polyamides: polyhexamethylene adipamide and polyhexamethylene sebacamide". In: *Journal of Research of the National Bureau of Standards Section A: Physics and Chemistry* 65A.3 (May 1961), p. 185. ISSN: 0022-4332. DOI: 10.6028/jres.065a.022.

[34] Goncalo Da Cunha Rodrigues et al. "Strong piezoelectricity in single-layer graphene deposited on SiO2 grating substrates". In: *Nature Communications* 6.1 (June 2015), pp. 1–6. ISSN: 20411723. DOI: 10.1038/ncomms8572.

[35] Canan Dagdeviren et al. "Conformal piezoelectric energy harvesting and storage from motions of the heart, lung, and diaphragm". In: *Proceedings of the National Academy of Sciences of the United States of America* 111.5 (Feb. 2014), pp. 1927–1932. ISSN: 00278424. DOI: 10.1073/pnas.1317233111.

[36] Dan Dai and Jing Liu. "Hip-mounted electromagnetic generator to harvest energy from human motion". In: *Frontiers in Energy* 8.2 (Mar. 2014), pp. 173–181. ISSN: 20951698. DOI: 10.1007/s11708-014-0301-2.

[37] Aidin Delnavaz and Jeremie Voix. "Electromagnetic micro-power generator for energy harvesting from breathing". In: *IECON Proceedings (Industrial Electronics Conference)*. 2012, pp. 984–988. ISBN: 9781467324212. DOI: 10.1109/IECON.2012.6388587.

[38] Peter M. Elias. "Structure and function of the stratum corneum permeability barrier". In: *Drug Development Research* 13.2-3 (Jan. 1988), pp. 97–105. ISSN: 0272-4391. DOI: 10.1002/ddr.430130203.

[39] Alper Erturk and Daniel J. Inman. *Piezoelectric Energy Harvesting*. John Wiley & Sons, Ltd, 2011.

[40] R. A. Escalona-Villalpando et al. "Clean energy from human sweat using an enzymatic patch". In: *Journal of Power Sources* 412 (Feb. 2019), pp. 496–504. ISSN: 03787753. DOI: 10.1016/j.jpowsour.2018.11.076.

[41] Dave Evans. *The Internet of Things: How the Next Evolution of the Internet Is Changing Everything*. Tech. rep. 2011.

[42] Feng Ru Fan, Zhong Qun Tian, and Zhong Lin Wang. "Flexible triboelectric generator". In: *Nano Energy* 1.2 (Mar. 2012), pp. 328–334. ISSN: 22112855. DOI: 10.1016/j.nanoen.2012.01.004.

[43] Jingtian Fang, William G. Vandenberghe, and Massimo V. Fischetti. "Microscopic dielectric permittivities of graphene nanoribbons and graphene". In: *Physical Review B* 94.4 (July 2016), p. 045318. ISSN: 24699969. DOI: 10.1103/PhysRevB.94.045318.

[44] T. V. Galchev et al. "Harvesting traffic-induced vibrations for structural health monitoring of bridges". In: *Journal of Micromechanics and Microengineering* 21.10 (Sept. 2011). DOI: 10.1088/0960-1317.

[45] Tzeno Galchev et al. "A piezoelectric frequency-increased power generator for scavenging low-frequency ambient vibration". In: *Proceedings of the IEEE International Conference on Micro Electro Mechanical Systems (MEMS)*. 2010, pp. 1203–1206. ISBN: 9781424457649. DOI: 10.1109/MEMSYS.2010.5442428.

[46] Jinghui Gao et al. "Recent Progress on BaTiO3-Based Piezoelectric Ceramics for Actuator Applications". In: *Actuators* 6.3 (July 2017), p. 24. ISSN: 2076-0825. DOI: 10.3390/act6030024.

[47] Wei Gao et al. "Fully integrated wearable sensor arrays for multiplexed in situ perspiration analysis". In: *Nature* 529.7587 (Jan. 2016), pp. 509–514. ISSN: 14764687. DOI: 10.1038/nature16521.

[48] Louis E Garner. "For that different sound, Music a la Theremin". In: *Popular Electronics* 27.5 (1967), pp. 29–33.

[49] Mozhdeh Ghahremani Honarvar and Masoud Latifi. "Overview of wearable electronics and smart textiles". In: *The Journal of The Textile Institute* 108.4 (Apr. 2017), pp. 631–652. ISSN: 0040-5000. DOI: 10.1080/00405000.2016.1177870.

[50] John B. Goodenough and Youngsik Kim. "Challenges for rechargeable Li batteries". In: *Chemistry of Materials* 22.3 (Feb. 2010), pp. 587–603. ISSN: 08974756. DOI: 10.1021/cm901452z.

[51] Hiroyuki Goto et al. "Feasibility of using the automatic generating system for quartz watches as a leadless pacemaker power source". In: *Medical and Biological Engineering and Computing* 37.3 (1999), pp. 377–380. ISSN: 01400118. DOI: 10.1007/BF02513315.

[52] K. Goto et al. "An implantable power supply with an optically rechargeable lithium battery". In: *IEEE Transactions on Biomedical Engineering* 48.7 (2001), pp. 830–833. ISSN: 00189294. DOI: 10.1109/10.930908.

[53] Jonathan Granstrom et al. "Energy harvesting from a backpack instrumented with piezoelectric shoulder straps". In: *Smart Materials and Structures* 16.5 (Sept. 2007), p. 1810. ISSN: 0964-1726. DOI: 10.1088/0964-1726/16/5/036.

[54] Martin A. Green et al. "Solar cell efficiency tables (version 54)". In: *Progress in Photovoltaics: Research and Applications* 27.7 (July 2019), pp. 565–575. ISSN: 1099159X. DOI: 10.1002/pip.3171.

[55] Jayavardhana Gubbi et al. "Internet of Things (IoT): A vision, architectural elements, and future directions". In: *Future Generation Computer Systems* 29.7 (Sept. 2013), pp. 1645–1660. ISSN: 0167739X. DOI: 10.1016/j.future.2013.01.010. arXiv: 1207.0203.

[56] Francesco Guido et al. "AlN-based flexible piezoelectric skin for energy harvesting from human motion". In: *Microelectronic Engineering* 159 (June 2016), pp. 174–178. ISSN: 01679317. DOI: 10.1016/j.mee.2016.03.041.

[57] Nathaniel J. Guilar et al. "Integrated solar energy harvesting and storage". In: *IEEE Transactions on Very Large Scale Integration (VLSI) Systems* 17.5 (May 2009), pp. 627–637. ISSN: 10638210. DOI: 10.1109/TVLSI.2008.2006792.

[58] I. L. Guy, S. Muensit, and E. M. Goldys. "Extensional piezoelectric coefficients of gallium nitride and aluminum nitride". In: *Applied Physics Letters* 75.26 (Dec. 1999), pp. 4133–4135. ISSN: 00036951. DOI: 10.1063/1.125560.

[59] M. A. Halim et al. "Electromagnetic energy harvesting from swing-arm motion using rotational eccentric mass structure". In: *TRANSDUCERS 2017 - 19th International Conference on Solid-State Sensors, Actuators and Microsystems*. Institute of Electrical and Electronics Engineers Inc., July 2017, pp. 1863–1866. ISBN: 9781538627310. DOI: 10.1109/TRANSDUCERS.2017.7994434.

[60] Rubaiyet I Haque, Pierre-Andre Farine, and Danick Briand. "Electrically conductive fabric based stretchable triboelectric energy harvester - IOPscience". In: *Journal of Physics: Conference Seires* 773 (2016), p. 012005.

[61] Rubaiyet I Haque, Pierre-Andre Farine, and Danick Briand. "Fully casted soft power generating triboelectric shoe insole". In: *Journal of Physics: Conference Seires* 773 (2016), p. 012097.

[62] N. Heidrich et al. "Biocompatible AlN-based piezo energy harvesters for implants". In: *2011 16th International Solid-State Sensors, Actuators and Microsystems Conference, TRANSDUCERS'11.* 2011, pp. 1642–1644. ISBN: 9781457701573. DOI: 10.1109/TRANSDUCERS.2011.5969854.

[63] Xiaohui Hu and Wuqiang Yang. "Planar capacitive sensors - designs and applications". In: *Sensor Review* 30.1 (2010), pp. 24–39. DOI: https://doi.org/10.1108/02602281011010772.

[64] A. R. Hutson. "Piezoelectricity and conductivity in ZnO and CdS". In: *Physical Review Letters* 4.10 (May 1960), pp. 505–507. ISSN: 00319007. DOI: 10.1103/PhysRevLett.4.505.

[65] "Internet of Things Market Size, Growth: IoT Industry Report 2026". In: *Market Research Reports* (2019).

[66] Hrishikesh Jayakumar et al. "Powering the Internet of Things". In: *Proceedings of the International Symposium on Low Power Electronics and Design*. New York, New York, USA: Institute of Electrical and Electronics Engineers Inc., Oct. 2015, pp. 375–380. ISBN: 9781450329750. DOI: 10.1145/2627369.2631644. URL: http://dl.acm.org/citation.cfm?doid=2627369.2631644.

[67] Wenzhao Jia et al. "Epidermal biofuel cells: Energy harvesting from human perspiration". In: *Angewandte Chemie - International Edition* 52.28 (July 2013), pp. 7233–7236. ISSN: 14337851. DOI: 10.1002/anie.201302922.

[68] Wen Jiang et al. "Fully Bioabsorbable Natural-Materials-Based Triboelectric Nanogenerators". In: *Advanced Materials* 30.32 (Aug. 2018). ISSN: 15214095. DOI: 10.1002/adma.201801895.

[69] Long Jin et al. "Self-Powered Safety Helmet Based on Hybridized Nanogenerator for Emergency". In: *ACS Nano* 10.8 (Aug. 2016), pp. 7874–7881. ISSN: 1936086X. DOI: 10.1021/acsnano.6b03760.

[70] S. Kerzenmacher et al. "Energy harvesting by implantable abiotically catalyzed glucose fuel cells". In: *Journal of Power Sources* 182.1 (July 2008), pp. 1–17. ISSN: 03787753. DOI: 10.1016/j.jpowsour.2008.03.031.

[71] A. L. Kholkin, N. A. Pertsev, and A. V. Goltsev. "Piezoelectricity and crystal symmetry". In: *Piezoelectric and Acoustic Materials for Transducer Applications*. Springer US, 2008, pp. 17–38. ISBN: 9780387765389. DOI: 10.1007/978-0-387-76540-2_2.

[72] Dong Hyun Kim et al. "In Vivo Self-Powered Wireless Transmission Using Biocompatible Flexible Energy Harvesters". In: *Advanced Functional Materials* 27.25 (July 2017), p. 1700341. ISSN: 1616301X. DOI: 10.1002/adfm.201700341.

[73] Juwan Kim, Sung Jin Kim, and Dong Kwon Kim. "Energy harvesting from salinity gradient by reverse electrodialysis with anodic alumina nanopores". In: *Energy* 51 (Mar. 2013), pp. 413–421. ISSN: 03605442. DOI: 10.1016/j.energy.2013.01.019.

[74] Kyeong Nam Kim et al. "Highly Stretchable 2D Fabrics for Wearable Triboelectric Nanogenerator under Harsh Environments". In: *ACS Nano* 9.6 (June 2015), pp. 6394–6400. ISSN: 1936086X. DOI: 10.1021/acsnano.5b02010.

[75] Kyeong Nam Kim et al. "Surface dipole enhanced instantaneous charge pair generation in triboelectric nanogenerator". In: *Nano Energy* 26 (Aug. 2016), pp. 360–370. ISSN: 22112855. DOI: 10.1016/j.nanoen.2016.05.048.

[76] Sean King. "Luminous Intensity of an LED as a Function of Input Power". In: *ISB Journal of Physics* 2.2 (2008).

[77] Michail E. Kiziroglou, Cairan He, and Eric M. Yeatman. "Non-resonant electrostatic energy harvesting from a rolling mass". In: *Proc. 5th Int. Workshop on Wearable and Implantable Body Sensor Networks, BSN2008, in conjunction with the 5th Int. Summer School and Symp. on Medical Devices and Biosensors, ISSS-MDBS 2008*. 2008, pp. 318–321. ISBN: 9781424422531. DOI: 10.1109/ISSMDBS.2008.4575083.

[78] Gleb Kleyman et al. "Characterization of Triboelectric Charge Generation between PTFE and Nylon after Repeated Contacts". In: *Energy Harvesting and Systems* 4.4 (Apr. 2018), pp. 165–176. ISSN: 2329-8774. DOI: 10.1515/ehs-2018-0001.

[79] Naokazu Koizumi, Shinichi Yano, and Fukuju Tsuji. "Dielectric properties of polytetrafluoroethylene and tetrafluoroethylene-hexafluoropropylene copolymer". In: *Journal of Polymer Science Part C: Polymer Symposia* 23.2 (Mar. 1968), pp. 499–508. ISSN: 04492994. DOI: 10.1002/polc.5070230207.

[80] Xiangdong Kong et al. "Fault diagnosis and quantitative analysis of micro-short circuits for lithium-ion batteries in battery packs". In: *Journal of Power Sources* 395 (Aug. 2018), pp. 358–368. ISSN: 03787753. DOI: `10.1016/j.jpowsour.2018.05.097`.

[81] Yang Kuang and Meiling Zhu. "Characterisation of a knee-joint energy harvester powering a wireless communication sensing node". In: *Smart Materials and Structures* 25.5 (Apr. 2016), p. 055013. ISSN: 0964-1726. DOI: `10.1088/0964-1726/25/5/055013`.

[82] Sweta Kumari et al. "Energy harvesting via human body activities". In: *Smart Biosensors in Medical Care*. Elsevier, Jan. 2020, pp. 87–106. DOI: `10.1016/b978-0-12-820781-9.00005-x`.

[83] Clara Lagomarsini et al. "Hybrid piezoelectric–electrostatic generators for wearable energy harvesting applications". In: *Smart Materials and Structures* 28.3 (Feb. 2019), p. 035003. ISSN: 0964-1726. DOI: `10.1088/1361-665X/AAF34E`.

[84] Ying Chih Lai et al. "Electric Eel-Skin-Inspired Mechanically Durable and Super-Stretchable Nanogenerator for Deformable Power Source and Fully Autonomous Conformable Electronic-Skin Applications". In: *Advanced Materials* 28.45 (Dec. 2016), pp. 10024–10032. ISSN: 15214095. DOI: `10.1002/adma.201603527`.

[85] Minbaek Lee et al. "A hybrid piezoelectric structure for wearable nanogenerators". In: *Advanced Materials* 24.13 (Apr. 2012), pp. 1759–1764. ISSN: 15214095. DOI: `10.1002/adma.201200150`.

[86] Sangmin Lee et al. "Super-flexible nanogenerator for energy harvesting from gentle wind and as an active deformation sensor". In: *Advanced Functional Materials* 23.19 (May 2013), pp. 2445–2449. ISSN: 1616301X. DOI: `10.1002/adfm.201202867`.

[87] SK Lee, William Buxton, and K. C. Smith. "A multi-touch three dimensional touch-sensitive tablet". In: *ACM SIGCHI Bulletin* 16.4 (Apr. 1985), pp. 21–25. ISSN: 07366906. DOI: `10.1145/1165385.317461`.

[88] Huidong Li, Chuan Tian, and Z. Daniel Deng. "Energy harvesting from low frequency applications using piezoelectric materials". In: *Applied Physics Reviews* 1.4 (Dec. 2014), p. 041301. ISSN: 19319401. DOI: `10.1063/1.4900845`.

[89] Jun Li et al. "Implanted Battery-Free Direct-Current Micro-Power Supply from in Vivo Breath Energy Harvesting". In: *ACS Applied Materials and Interfaces* 10.49 (Dec. 2018), pp. 42030–42038. ISSN: 19448252. DOI: `10.1021/acsami.8b15619`.

[90] Ming Li et al. "Microbial fuel cell (MFC) power performance improvement through enhanced microbial electrogenicity". In: *Biotechnology Advances* 36.4 (July 2018), pp. 1316–1327. ISSN: 07349750. DOI: `10.1016/j.biotechadv.2018.04.010`.

[91] Ning Li et al. "Direct Powering a Real Cardiac Pacemaker by Natural Energy of a Heartbeat". In: *ACS Nano* 13.3 (Mar. 2019), pp. 2822–2830. ISSN: 1936086X. DOI: `10.1021/acsnano.8b08567`.

[92]   Qingguo Li, Veronica Naing, and J. Maxwell Donelan. "Development of a biomechanical energy harvester". In: *Journal of NeuroEngineering and Rehabilitation* 6.1 (Dec. 2009), p. 22. ISSN: 17430003. DOI: 10.1186/1743-0003-6-22.

[93]   Ruo Zhou Li et al. "Direct writing on paper of foldable capacitive touch pads with silver nanowire inks". In: *ACS Applied Materials and Interfaces* 6.23 (Dec. 2014), pp. 21721–21729. ISSN: 19448252. DOI: 10.1021/am506987w.

[94]   Shuguang Li, Jianping Yuan, and Hod Lipson. "Ambient wind energy harvesting using cross-flow fluttering". In: *Journal of Applied Physics* 109.2 (Jan. 2011), p. 026104. ISSN: 00218979. DOI: 10.1063/1.3525045.

[95]   Zhou Li et al. "Muscle-driven in vivo nanogenerator". In: *Advanced Materials* 22.23 (June 2010), pp. 2534–2537. ISSN: 09359648. DOI: 10.1002/adma.200904355.

[96]   Qijie Liang et al. "Recyclable and Green Triboelectric Nanogenerator". In: *Advanced Materials* 29.5 (Feb. 2017), p. 1604961. ISSN: 09359648. DOI: 10.1002/adma.201604961.

[97]   Yi-Chi Liao et al. "Button Simulation and Design via FDVV Models". In: Association for Computing Machinery (ACM), Apr. 2020, pp. 1–14. DOI: 10.1145/3313831.3376262. arXiv: 2001.04352.

[98]   Huicong Liu et al. "A comprehensive review on piezoelectric energy harvesting technology: Materials, mechanisms, and applications". In: *Applied Physics Reviews* 5.4 (Dec. 2018), p. 041306. ISSN: 19319401. DOI: 10.1063/1.5074184.

[99]   Huicong Liu et al. "A non-resonant rotational electromagnetic energy harvester for low-frequency and irregular human motion". In: *Applied Physics Letters* 113.20 (Nov. 2018), p. 203901. ISSN: 00036951. DOI: 10.1063/1.5053945.

[100] Huicong Liu et al. "Investigation of the nonlinear electromagnetic energy harvesters from hand shaking". In: *IEEE Sensors Journal* 15.4 (Apr. 2015), pp. 2356–2364. ISSN: 1530437X. DOI: 10.1109/JSEN.2014.2375354.

[101] Zhuo Liu et al. "Wearable and Implantable Triboelectric Nanogenerators". In: *Advanced Functional Materials* 29.20 (May 2019). ISSN: 16163028. DOI: 10.1002/adfm.201808820.

[102] *Logic Technology - Taiwan Semiconductor Manufacturing Company Limited*. URL: https://www.tsmc.com/english/dedicatedFoundry/technology/logic.htm.

[103] Y. Lu et al. "A nonlinear MEMS electrostatic kinetic energy harvester for human-powered biomedical devices". In: *Applied Physics Letters* 107.25 (2015), p. 253902. ISSN: 00036951. DOI: 10.1063/1.4937587.

[104] Ye Ma et al. "Self-Powered, One-Stop, and Multifunctional Implantable Triboelectric Active Sensor for Real-Time Biomedical Monitoring". In: *Nano Letters* 16.10 (Oct. 2016), pp. 6042–6051. ISSN: 15306992. DOI: 10.1021/acs.nanolett.6b01968.

[105]   Michele Magno et al. "Kinetic energy harvesting: Toward autonomous wearable sens-
        ing for Internet of Things". In: *2016 International Symposium on Power Electronics,
        Electrical Drives, Automation and Motion, SPEEDAM 2016*. Institute of Electrical
        and Electronics Engineers Inc., July 2016, pp. 248–254. ISBN: 9781509020676. DOI:
        `10.1109/SPEEDAM.2016.7525995`.

[106]   Loreto Mateu and Francesc Moll. "Review of energy harvesting techniques and appli-
        cations for microelectronics". In: *VLSI Circuits and Systems II*. Ed. by Jose F. Lopez
        et al. Vol. 5837. SPIE, June 2005, pp. 359–373. DOI: `10.1117/12.613046`.

[107]   Ryo Matsuzuka et al. "A 42 mV startup ring oscillator using gain-enhanced self-
        bias inverters for extremely low voltage energy harvesting". In: *Japanese Journal of
        Applied Physics* 59.SG (Feb. 2020), SGGL01. ISSN: 1347-4065. DOI: `10.7567/1347-
        4065/AB65D4`.

[108]   Friedemann Mattern. "From Smart Devices to Smart Everyday Objects". In: *Smart
        Objects Conference*. 2003, pp. 15–16.

[109]   Aaron D. Mazzeo et al. "Paper-based, capacitive touch pads". In: *Advanced Materials*
        24.21 (June 2012), pp. 2850–2856. ISSN: 09359648. DOI: `10.1002/adma.201200137`.

[110]   Thomas McKay et al. "Self-priming dielectric elastomer generators". In: *Smart Mate-
        rials and Structures* 19.5 (Apr. 2010), p. 055025. ISSN: 0964-1726. DOI: `10.1088/0964-
        1726/19/5/055025`.

[111]   Bo Meng et al. "A transparent single-friction-surface triboelectric generator and self-
        powered touch sensor". In: *Energy and Environmental Science* 6.11 (Nov. 2013),
        pp. 3235–3240. ISSN: 17545692. DOI: `10.1039/c3ee42311e`.

[112]   S. Merilampi, T. Laine-Ma, and P. Ruuskanen. "The characterization of electrically
        conductive silver ink patterns on flexible substrates". In: *Microelectronics Reliability*
        49.7 (July 2009), pp. 782–790. ISSN: 00262714. DOI: `10.1016/j.microrel.2009.04.
        004`.

[113]   P. Miao et al. "Mems inertial power generators for biomedical applications". In: *Mi-
        crosystem Technologies*. Vol. 12. 10-11. Springer, Sept. 2006, pp. 1079–1083. DOI:
        `10.1007/s00542-006-0152-9`.

[114]   Paul D. Mitcheson et al. "Energy harvesting from human and machine motion for
        wireless electronic devices". In: *Proceedings of the IEEE* 96.9 (2008), pp. 1457–1486.
        ISSN: 00189219. DOI: `10.1109/JPROC.2008.927494`.

[115]   Eiichi Miyazaki, Shin Itami, and Tsutomu Araki. "Using a light-emitting diode as a
        high-speed, wavelength selective photodetector". In: *Review of Scientific Instruments*
        69.11 (Nov. 1998), pp. 3751–3754. ISSN: 00346748. DOI: `10.1063/1.1149174`.

[116]   B. Muhthassim, X. K. Thian, and K. N. Hasan. "Energy Harvesting from Salinity
        Gradient". In: *4th International Conference on Civil and Environmental Engineering
        for Sustainability*. Vol. 140. IOP Publishing, Apr. 2017, p. 012045. DOI: `10.1088/
        1755-1315`.

[117] Koji Murakawa et al. "A wireless near-infrared energy system for medical implants: A less invasive method for supplying light power to implant devices". In: *IEEE Engineering in Medicine and Biology Magazine* 18.6 (Nov. 1999), pp. 70–72. ISSN: 07395175. DOI: 10.1109/51.805148.

[118] Jamal Al-Nabulsi et al. "Methods of energy generation from the human body: a literature review". In: *Journal of Medical Engineering & Technology* 43.4 (May 2019), pp. 255–272. ISSN: 0309-1902. DOI: 10.1080/03091902.2019.1658818. URL: https://www.tandfonline.com/doi/full/10.1080/03091902.2019.1658818.

[119] Aditya Nanda and M. Amin Karami. "Energy harvesting from arterial blood pressure for powering embedded micro sensors in human brain". In: *Journal of Applied Physics* 121.12 (Mar. 2017), p. 124506. ISSN: 10897550. DOI: 10.1063/1.4977842.

[120] Mehdi Niroomand and Hamid Reza Foroughi. "A rotary electromagnetic microgenerator for energy harvesting from human motions". In: *Journal of Applied Research and Technology* 14.4 (Aug. 2016), pp. 259–267. ISSN: 16656423. DOI: 10.1016/j.jart.2016.06.002.

[121] Simiao Niu et al. "A universal self-charging system driven by random biomechanical energy for sustainable operation of mobile electronics". In: *Nature Communications* 6.1 (Dec. 2015), pp. 1–8. ISSN: 20411723. DOI: 10.1038/ncomms9975.

[122] Simiao Niu et al. "Theoretical study of contact-mode triboelectric nanogenerators as an effective power source". In: *Energy and Environmental Science* 6.12 (Dec. 2013), pp. 3576–3583. ISSN: 17545692. DOI: 10.1039/c3ee42571a.

[123] Andreas Nocke et al. "Miniaturized textile-based multi-layer pH-sensor for wound monitoring applications". In: *Autex Research Journal* 12.1 (Mar. 2012), pp. 20–22. ISSN: 14709589. DOI: 10.2478/v10304-012-0004-x.

[124] Amin Nozariasbmarz et al. "Thermoelectric generators for wearable body heat harvesting: Material and device concurrent optimization". In: *Nano Energy* 67 (Jan. 2020), p. 104265. ISSN: 22112855. DOI: 10.1016/j.nanoen.2019.104265.

[125] Sharon Rosyln Oh et al. "Fabrication of piezoelectric polymer multilayers on flexible substrates for energy harvesting". In: *Smart Materials and Structures* 23.1 (Dec. 2014), p. 015013. ISSN: 0964-1726. DOI: 10.1088/0964-1726/23/1/015013.

[126] Poul Alberg Østergaard and Henrik Lund. "A renewable energy system in Frederikshavn using low-temperature geothermal energy for district heating". In: *Applied Energy* 88.2 (Feb. 2011), pp. 479–487. ISSN: 03062619. DOI: 10.1016/j.apenergy.2010.03.018.

[127] Han Ouyang et al. "Self-Powered Pulse Sensor for Antidiastole of Cardiovascular Disease". In: *Advanced Materials* 29.40 (Oct. 2017). ISSN: 15214095. DOI: 10.1002/adma.201703456.

[128] Ruizheng Pan et al. "Fully biodegradable triboelectric nanogenerators based on electrospun polylactic acid and nanostructured gelatin films". In: *Nano Energy* 45 (Mar. 2018), pp. 193–202. ISSN: 22112855. DOI: 10.1016/j.nanoen.2017.12.048.

[129] Danilo Pani, Andrea Achilli, and Annalisa Bonfiglio. "Survey on Textile Electrode Technologies for Electrocardiographic (ECG) Monitoring, from Metal Wires to Polymers". In: *Advanced Materials Technologies* 3.10 (Oct. 2018), p. 1800008. ISSN: 2365709X. DOI: 10.1002/admt.201800008.

[130] Joseph A. Paradiso and Thad Starner. "Energy scavenging for mobile and wireless electronics". In: *IEEE Pervasive Computing* 4.1 (Jan. 2005), pp. 18–27. ISSN: 15361268. DOI: 10.1109/MPRV.2005.9. URL: http://ieeexplore.ieee.org/document/1401839/.

[131] Kwi Il Park et al. "Piezoelectric BaTiO3 thin film nanogenerator on plastic substrates". In: *Nano Letters* 10.12 (Dec. 2010), pp. 4939–4943. ISSN: 15306984. DOI: 10.1021/nl102959k.

[132] Stephen R. Platt, Shane Farritor, and Hani Haider. "On Low-frequency electric power generation with PZT ceramics". In: *IEEE/ASME Transactions on Mechatronics* 10.2 (Apr. 2005), pp. 240–252. ISSN: 10834435. DOI: 10.1109/TMECH.2005.844704.

[133] Xiong Pu et al. "A self-charging power unit by integration of a textile triboelectric nanogenerator and a flexible lithium-ion battery for wearable electronics". In: *Advanced Materials* 27.15 (Apr. 2015), pp. 2472–2478. ISSN: 15214095. DOI: 10.1002/adma.201500311.

[134] Jie Qi and Leah Buechley. "Electronic popables: Exploring paper-based computing through an interactive pop-up book". In: *TEI'10 - Proceedings of the 4th International Conference on Tangible, Embedded, and Embodied Interaction.* New York, New York, USA: ACM Press, 2010, pp. 121–128. ISBN: 9781605588414. DOI: 10.1145/1709886.1709909.

[135] Feng Qian, Tian Bing Xu, and Lei Zuo. "Design, optimization, modeling and testing of a piezoelectric footwear energy harvester". In: *Energy Conversion and Management* 171 (Sept. 2018), pp. 1352–1364. ISSN: 01968904. DOI: 10.1016/j.enconman.2018.06.069.

[136] Hantang Qin et al. "Direct Printing of Capacitive Touch Sensors on Flexible Substrates by Additive E-Jet Printing With Silver Nanoinks". In: *Journal of Manufacturing Science and Engineering* 139 (June 2016). DOI: 10.1115/msec2016-8740.

[137] Yong Qin, Xudong Wang, and Zhong Lin Wang. "Microfibre-nanowire hybrid structure for energy scavenging". In: *Nature* 451.7180 (Feb. 2008), pp. 809–813. ISSN: 14764687. DOI: 10.1038/nature06601.

[138] Jan Rabaey. "Low Power Design Essentials". In: *Series on Integrated Circuits and Systems.* 2009. ISBN: 978-0-387-33398-4. DOI: 10.1007/978-0-387-71713-5.

[139] Arian Rahimi et al. "An electromagnetic energy harvesting system for low frequency applications with a passive interface ASIC in standard CMOS". In: *Sensors and Actuators, A: Physical*. Vol. 188. Elsevier, Dec. 2012, pp. 158–166. DOI: 10.1016/j.sna.2012.03.019.

[140] N. F.A.Abdul Rahman et al. "Design and development of thermoelectric generator kit from car engine heat". In: *Proceedings - 2016 IEEE Conference on Systems, Process and Control, ICSPC 2016*. Institute of Electrical and Electronics Engineers Inc., May 2017, pp. 47–52. ISBN: 9781509011810. DOI: 10.1109/SPC.2016.7920702.

[141] L. R. Rallison et al. "Errors in estimating peritoneal fluid by bioelectrical impedance analysis and total body electrical conductivity". In: *Journal of the American College of Nutrition* 12.1 (Feb. 1993), pp. 66–72. ISSN: 15411087. DOI: 10.1080/07315724.1993.10718285.

[142] Jan S Rentmeister, Kristofer Pister, and Jason T Stauth. "A 120-330V, sub-µA, Optically Powered Microrobotic Drive IC for DARPA SHRIMP". In: *GOMACTech*. 2020.

[143] Raziel Riemer and Amir Shapiro. "Biomechanical energy harvesting from human motion: Theory, state of the art, design guidelines, and future directions". In: *Journal of NeuroEngineering and Rehabilitation* 8.1 (Apr. 2011), p. 22. ISSN: 17430003. DOI: 10.1186/1743-0003-8-22.

[144] J. G. Rocha et al. "Energy harvesting from piezoelectric materials fully integrated in footwear". In: *IEEE Transactions on Industrial Electronics* 57.3 (Mar. 2010), pp. 813–819. ISSN: 02780046. DOI: 10.1109/TIE.2009.2028360.

[145] Edwar Romero, Robert O. Warrington, and Michael R. Neuman. "Body motion for powering biomedical devices". In: *Proceedings of the 31st Annual International Conference of the IEEE Engineering in Medicine and Biology Society: Engineering the Future of Biomedicine, EMBC 2009*. IEEE Computer Society, 2009, pp. 2752–2755. ISBN: 9781424432967. DOI: 10.1109/IEMBS.2009.5333329.

[146] Hanjun Ryu et al. "High-Performance Triboelectric Nanogenerators Based on Solid Polymer Electrolytes with Asymmetric Pairing of Ions". In: *Advanced Energy Materials* 7.17 (Sept. 2017), p. 1700289. ISSN: 16146832. DOI: 10.1002/aenm.201700289.

[147] C. R. Saha et al. "Electromagnetic generator for harvesting energy from human motion". In: *Sensors and Actuators, A: Physical* 147.1 (Sept. 2008), pp. 248–253. ISSN: 09244247. DOI: 10.1016/j.sna.2008.03.008.

[148] M Salauddin and Jae Y Park. "Design and experiment of human hand motion driven electromagnetic energy harvester using dual Halbach magnet array". In: *Smart Materials and Structures* 26.3 (Feb. 2017), p. 035011. ISSN: 0964-1726. DOI: 10.1088/1361-665X/AA573F.

[149] Pekka Salonen et al. "Effect of textile materials on wearable antenna performance: A case study of GPS antennas". In: *IEEE Antennas and Propagation Society, AP-S International Symposium (Digest)*. Vol. 1. Institute of Electrical and Electronics Engineers Inc., 2004, pp. 459–462. DOI: 10.1109/aps.2004.1329673.

[150] Farzanah Abdul Samad et al. "A Curved Electromagnetic Energy Harvesting System for Wearable Electronics". In: *IEEE Sensors Journal* 16.7 (Apr. 2016), pp. 1969–1974. ISSN: 1530437X. DOI: 10.1109/JSEN.2015.2500603.

[151] Albrecht Schmidt, Matthias Kranz, and Paul Holleis. "Interacting with the ubiquitous computer: Towards embedding interaction". In: *ACM International Conference Proceeding Series*. Vol. 121. New York, New York, USA: ACM Press, 2005, pp. 147–152. ISBN: 1595933042. DOI: 10.1145/1107548.1107588.

[152] Michael Shepertycky and Qingguo Li. "Generating Electricity during Walking with a Lower Limb-Driven Energy Harvester: Targeting a Minimum User Effort". In: *PLOS ONE* 10.6 (June 2015). Ed. by Kelvin E Jones, e0127635. ISSN: 1932-6203. DOI: 10.1371/journal.pone.0127635.

[153] Bojing Shi, Zhou Li, and Yubo Fan. "Implantable Energy-Harvesting Devices". In: *Advanced Materials* 30.44 (Nov. 2018), p. 1801511. ISSN: 09359648. DOI: 10.1002/adma.201801511.

[154] Qiongfeng Shi et al. "Self-powered liquid triboelectric microfluidic sensor for pressure sensing and finger motion monitoring applications". In: *Nano Energy* 30 (Dec. 2016), pp. 450–459. ISSN: 22112855. DOI: 10.1016/j.nanoen.2016.10.046.

[155] Michael Shorter, Jon Rogers, and John McGhee. "Enhancing everyday paper interactions with paper circuits". In: *Proceedings of the Conference on Designing Interactive Systems: Processes, Practices, Methods, and Techniques, DIS*. New York, New York, USA: Association for Computing Machinery, 2014, pp. 39–42. ISBN: 9781450329026. DOI: 10.1145/2598510.2598584.

[156] Adam C. Siegel et al. "Foldable Printed Circuit Boards on Paper Substrates". In: *Advanced Functional Materials* 20.1 (Jan. 2010), pp. 28–35. ISSN: 1616301X. DOI: 10.1002/adfm.200901363.

[157] Munindar P. Singh and Amit K. Chopra. "The Internet of Things and Multiagent Systems: Decentralized Intelligence in Distributed Computing". In: *Proceedings - International Conference on Distributed Computing Systems*. Institute of Electrical and Electronics Engineers Inc., July 2017, pp. 1738–1747. ISBN: 9781538617915. DOI: 10.1109/ICDCS.2017.304.

[158] Takao Someya, ed. *Stretchable Electronics*. Wiley-VCH, 2013.

[159] Ricardo E. Sousa, Carlos M. Costa, and Senentxu Lanceros-Méndez. "Advances and Future Challenges in Printed Batteries". In: *ChemSusChem* 8.21 (Nov. 2015), pp. 3539–3555. ISSN: 18645631. DOI: 10.1002/cssc.201500657.

[160] Theremin Leo Ssergejewitsch. *Method of and apparatus for the generation of sounds.* Dec. 1928.

[161] T. Starner. "Human-powered wearable computing". In: *IBM Systems Journal* 35.3-4 (1996), pp. 618–629. ISSN: 00188670. DOI: 10.1147/sj.353.0618.

[162] Thad Starner and Joseph A Paradiso. "Human Generated Power for Mobile Electronics". In: *Low Power Electronics Design.* 2005, pp. 45–1. URL: www.cpuscorecard.com;.

[163] Matteo Stoppa and Alessandro Chiolerio. "Wearable Electronics and Smart Textiles: A Critical Review". In: *Sensors* 14.7 (July 2014), pp. 11957–11992. ISSN: 1424-8220. DOI: 10.3390/s140711957. URL: http://www.mdpi.com/1424-8220/14/7/11957.

[164] Chengliang Sun et al. "PVDF microbelts for harvesting energy from respiration". In: *Energy and Environmental Science* 4.11 (Nov. 2011), pp. 4508–4512. ISSN: 17545692. DOI: 10.1039/c1ee02241e.

[165] Guo-Ming Sung et al. "Small-Area Radiofrequency-Energy-Harvesting Integrated Circuits for Powering Wireless Sensor Networks". In: *Sensors* 19.8 (Apr. 2019), p. 1754. ISSN: 1424-8220. DOI: 10.3390/s19081754.

[166] Ryoichi Tashiro et al. "Development of an electrostatic generator for a cardiac pacemaker that harnesses the ventricular wall motion". In: *Journal of Artificial Organs* 5.4 (2002), pp. 239–245. ISSN: 14347229. DOI: 10.1007/s100470200045.

[167] George W. Taylor et al. "The energy harvesting Eel: A small subsurface ocean/river power generator". In: *IEEE Journal of Oceanic Engineering* 26.4 (Oct. 2001), pp. 539–547. ISSN: 03649059. DOI: 10.1109/48.972090.

[168] Moritz Thielen et al. "Human body heat for powering wearable devices: From thermal energy to application". In: *Energy Conversion and Management* 131 (Jan. 2017), pp. 44–54. ISSN: 01968904. DOI: 10.1016/j.enconman.2016.11.005.

[169] Miao Tian et al. "A three-dimensional carbon nano-network for high performance lithium ion batteries". In: *Nano Energy* 11 (Jan. 2015), pp. 500–509. ISSN: 22112855. DOI: 10.1016/j.nanoen.2014.11.006.

[170] Daniel Tobjörk and Ronald Österbacka. "Paper Electronics". In: *Advanced Materials* 23.17 (May 2011), pp. 1935–1961. ISSN: 09359648. DOI: 10.1002/adma.201004692.

[171] T. Tsutsumino et al. "Seismic Power Generator Using High-Performance Polymer Electret". In: *19th IEEE International Conference on Micro Electro Mechanical Systems.* IEEE, 2006, pp. 98–101. ISBN: 0-7803-9475-5. DOI: 10.1109/MEMSYS.2006.1627745.

[172] L. Vincetti et al. "Broadband printed antenna for radiofrequency energy harvesting". In: *Proceedings of the 2012 International Conference on Electromagnetics in Advanced Applications, ICEAA'12.* 2012, pp. 814–816. ISBN: 9781467303354. DOI: 10.1109/ICEAA.2012.6328744.

[173] Chien Chung Wang et al. "A Paper-Based Pop-up Electrochemical Device for Analysis of Beta-Hydroxybutyrate". In: *Analytical Chemistry* 88.12 (June 2016), pp. 6326–6333. ISSN: 15206882. DOI: `10.1021/acs.analchem.6b00568`.

[174] Feng Wang and Xiangshi Ren. "Empirical evaluation for finger input properties in multi-touch interaction". In: *Proceedings of the Conference on Human Factors in Computing Systems*. New York, New York, USA: ACM Press, 2009, pp. 1063–1072. ISBN: 9781605582474. DOI: `10.1145/1518701.1518864`.

[175] Ruoxing Wang et al. "Engineered and Laser-Processed Chitosan Biopolymers for Sustainable and Biodegradable Triboelectric Power Generation". In: *Advanced Materials* 30.11 (Mar. 2018), p. 1706267. ISSN: 09359648. DOI: `10.1002/adma.201706267`.

[176] Zhong Lin Wang et al. *Triboelectric Nanogenerators*. Springer, 2016. ISBN: 978-3-319-40039-6.

[177] Alex S. Weddell et al. "A Survy of Multi-Source Energy Harvesting Systems". In: *Design, Automation & Test in Europe Conference & Exhibition (DATE), 2013*. New Jersey: IEEE Conference Publications, 2013, pp. 905–908. ISBN: 9781467350716. DOI: `10.7873/DATE.2013.190`.

[178] *Weight Of A Hand — What Things Weigh*. URL: `https://whatthingsweigh.com/how-much-does-a-hand-weigh/`.

[179] James Williamson et al. "Data sensing and analysis: Challenges for wearables". In: *20th Asia and South Pacific Design Automation Conference, ASP-DAC 2015*. Institute of Electrical and Electronics Engineers Inc., Mar. 2015, pp. 136–141. ISBN: 9781479977925. DOI: `10.1109/ASPDAC.2015.7058994`.

[180] David A Winters et al. "Biomechanical Walking Pattern Changes in the Fit and Healthy Elderly". In: *Physical Therapy* 70.6 (1990), pp. 340–347.

[181] Carole Jean Wu. "Architectural Thermal Energy Harvesting Opportunities for Sustainable Computing". In: *IEEE Computer Architecture Letters* 13.2 (July 2014), pp. 65–68. ISSN: 15566056. DOI: `10.1109/L-CA.2013.16`.

[182] Changsheng Wu et al. "Triboelectric Nanogenerator: A Foundation of the Energy for the New Era". In: *Advanced Energy Materials* 9.1 (Jan. 2019), p. 1802906. ISSN: 16146840. DOI: `10.1002/aenm.201802906`.

[183] Hui Wu et al. "Improving battery safety by early detection of internal shorting with a bifunctional separator". In: *Nature Communications* 5.1 (Oct. 2014), pp. 1–6. ISSN: 20411723. DOI: `10.1038/ncomms6193`.

[184] Longhan Xie and Mingjing Cai. "An In-Shoe Harvester with Motion Magnification for Scavenging Energy from Human Foot Strike". In: *IEEE/ASME Transactions on Mechatronics* 20.6 (Dec. 2015), pp. 3264–3268. ISSN: 10834435. DOI: `10.1109/TMECH.2015.2428618`.

[185]   Yi Xin et al. "Shoes-equipped piezoelectric transducer for energy harvesting: A brief review". In: *Ferroelectrics* 493.1 (Mar. 2016), pp. 12–24. ISSN: 0015-0193. DOI: 10.1080/00150193.2016.1123061.

[186]   T. Yamamoto and Y. Yamamoto. "Non-linear electrical properties of skin in the low frequency range". In: *Medical & Biological Engineering & Computing* 19.3 (May 1981), pp. 302–310. ISSN: 01400118. DOI: 10.1007/BF02442549.

[187]   Rusen Yang et al. "Converting biomechanical energy into electricity by a muscle-movement- driven nanogenerator". In: *Nano Letters* 9.3 (Mar. 2009), pp. 1201–1205. ISSN: 15306984. DOI: 10.1021/nl803904b.

[188]   Weiqing Yang et al. "Harvesting energy from the natural vibration of human walking". In: *ACS Nano* 7.12 (Dec. 2013), pp. 11317–11324. ISSN: 19360851. DOI: 10.1021/nn405175z.

[189]   Ya Yang et al. "Human skin based triboelectric nanogenerators for harvesting biomechanical energy and as self-powered active tactile sensor system". In: *ACS Nano* 7.10 (Oct. 2013), pp. 9213–9222. ISSN: 19360851. DOI: 10.1021/nn403838y.

[190]   Zhaochu Yang, Einar Halvorsen, and Tao Dong. "Power generation from conductive droplet sliding on electret film". In: *Applied Physics Letters* 100.21 (May 2012), p. 213905. ISSN: 00036951. DOI: 10.1063/1.4720517.

[191]   Guang Yao et al. "Effective weight control via an implanted self-powered vagus nerve stimulation device". In: *Nature Communications* 9.1 (Dec. 2018), pp. 1–10. ISSN: 20411723. DOI: 10.1038/s41467-018-07764-z.

[192]   Fang Yi et al. "Stretchable and Waterproof Self-Charging Power System for Harvesting Energy from Diverse Deformation and Powering Wearable Electronics". In: *ACS Nano* 10.7 (July 2016), pp. 6519–6525. ISSN: 1936086X. DOI: 10.1021/acsnano.6b03007.

[193]   Alla M. Zamarayeva et al. "Flexible and stretchable power sources for wearable electronics". In: *Science Advances* 3.6 (June 2017), e1602051. ISSN: 23752548. DOI: 10.1126/sciadv.1602051.

[194]   Kewei Zhang et al. "Hybridized Electromagnetic-Triboelectric Nanogenerator for Scavenging Biomechanical Energy for Sustainably Powering Wearable Electronics". In: *ACS Nano* 9.4 (Apr. 2015), pp. 3521–3529. ISSN: 1936086X. DOI: 10.1021/nn507455f.

[195]   Qian Zhang, Yufeng Wang, and Eun Sok Kim. "Power generation from human body motion through magnet and coil arrays with magnetic spring". In: *Journal of Applied Physics* 115.6 (Feb. 2014), p. 064908. ISSN: 10897550. DOI: 10.1063/1.4865792.

[196]   Chen Zhao and Xinyu Liu. "A portable paper-based microfluidic platform for multiplexed electrochemical detection of human immunodeficiency virus and hepatitis C virus antibodies in serum". In: *Biomicrofluidics* 10.2 (Mar. 2016), p. 024119. ISSN: 19321058. DOI: 10.1063/1.4945311.

[197] Qiang Zheng et al. "Biodegradable triboelectric nanogenerator as a life-time designed implantable power source". In: *Science Advances* 2.3 (Mar. 2016), e1501478. ISSN: 23752548. DOI: 10.1126/sciadv.1501478.

[198] Qiang Zheng et al. "In vivo powering of pacemaker by breathing-driven implanted triboelectric nanogenerator". In: *Advanced Materials* 26.33 (Sept. 2014), pp. 5851–5856. ISSN: 15214095. DOI: 10.1002/adma.201402064.

[199] Qiang Zheng et al. "In Vivo Self-Powered Wireless Cardiac Monitoring via Implantable Triboelectric Nanogenerator". In: *ACS Nano* 10.7 (July 2016), pp. 6510–6518. ISSN: 1936086X. DOI: 10.1021/acsnano.6b02693.

[200] Junwen Zhong et al. "Fiber-based generator for wearable electronics and mobile medication". In: *ACS Nano* 8.6 (June 2014), pp. 6273–6280. ISSN: 1936086X. DOI: 10.1021/nn501732z.

[201] Junwen Zhong et al. "Finger typing driven triboelectric nanogenerator and its use for instantaneously lighting up LEDs". In: *Nano Energy* 2.4 (July 2013), pp. 491–497. ISSN: 22112855. DOI: 10.1016/j.nanoen.2012.11.015.

[202] Alyssa Y. Zhou and Michel M. Maharbiz. "Charge pumping with finger capacitance for body sensor energy harvesting". In: *Proceedings of the Annual International Conference of the IEEE Engineering in Medicine and Biology Society, EMBS*. Institute of Electrical and Electronics Engineers Inc., Sept. 2017, pp. 775–778. ISBN: 9781509028092. DOI: 10.1109/EMBC.2017.8036939.

[203] Alyssa Y. Zhou and Michel M. Maharbiz. "Charge-pumping with finger capacitance in a custom electrostatic energy harvesting ASIC". In: *Applied Physics Letters* 117.3 (July 2020), p. 033902. ISSN: 0003-6951. DOI: 10.1063/5.0014008.

[204] Alyssa Y. Zhou and Michel M. Maharbiz. "Electrostatic Energy Harvesting from Human Interactions with Smart Paper Electronics". In: *Proceedings of the Annual International Conference of the IEEE Engineering in Medicine and Biology Society, EMBS*. 2020. (forthcoming).

[205] Maoying Zhou et al. "A review on heat and mechanical energy harvesting from human: Principles, prototypes and perspectives". In: *Renewable and Sustainable Energy Reviews* 82 (Feb. 2018), pp. 3582–3609. ISSN: 18790690. DOI: 10.1016/j.rser.2017.10.102.

[206] Tao Zhou et al. "Woven structured triboelectric nanogenerator for wearable devices". In: *ACS Applied Materials and Interfaces* 6.16 (2014), pp. 14695–14701. ISSN: 19448252. DOI: 10.1021/am504110u.

[207] Qingyuan Zhu, Mingjie Guan, and Yuanqin He. "Vibration energy harvesting in automobiles to power wireless sensors". In: *2012 IEEE International Conference on Information and Automation, ICIA 2012*. 2012, pp. 349–354. ISBN: 9781467322386. DOI: 10.1109/ICInfA.2012.6246873.